Norwegian University of Life Sciences

Master's Thesis 2023 45 ECTS

Faculty of Chemistry, Biotechnology and Food Science

Valorization of Monolignols through Enzymatic Bioconversions by Rational Design of Cytochrome P450 BM3

Caroline Gudrun Østvang Gundersen

Master of Biotechnology

ACKNOWLEDGEMENTS

This master's thesis was performed in the research group project NewCat at the Faculty of Chemistry, Biotechnology and Food Science (KBM), at the Norwegian University of Life Sciences (NMBU) under the supervision of Professor Morten Sørlie.

Firstly, I would like to say thank you to my supervisor Professor Morten Sørlie for including me in his research group. I have immense gratitude for all the help and resources you have provided me in my work. Thank you so much for the opportunity to write a thesis under your supervision within the field of protein chemistry.

I would also like to send a huge thank you to Dr. Gabriela Schröder and Dr. Kelsi Hall for designing the mutants employed in my study and helping me perform the site-directed mutagenesis. This thesis would not have been possible without your guidance. I would like to express some extra gratitude towards Dr. Gabriela Schröder who has helped me immensely through endless meetings and corrections always with much-needed encouragement. Words fall short when I try to express my gratitude to you. Your knowledge is highly admirable, and your kind heart is inspiring.

The biggest gratitude has to be expressed to my co-supervisor and Ph.D. candidate Marta Barros. You have not only sacrificed a large amount of your valuable time to help me in the laboratory, but you also deserve a great deal of credit for this thesis. Marta, you are my role model, and I deeply appreciate having had you as both a mentor and a friend throughout this period. Thank you so much!

Special thanks to my fellow master's students Synnøve Elisa Rønnekleiv, Manouck Oussoren, and Ingrid Rokke Elvebakken, as well as the Ph.D. students Rannei Skaali and Maja Mollatt for your help, kind words and uplifting spirit in the laboratory. You are all brilliant!

Finally, I would like to thank my friend Madeleine-Emilie Killingstad for proofreading my thesis. Thank you to my family for always believing in me, especially my mom Anita Østvang who always finds encouraging words in the hardest times. Also, a huge thanks to my boyfriend Martin Granheim for enduring weeks of hard work and always inspiring me with his kind heart and positive spirit. I could not have done this without your support and love.

Caroline Gudrun Østvang Gundersen
Ås, July 2023

SUMMARY

Lignin valorization is crucial to replace fossil fuels for a more sustainable future (Karunarathna & Smith, 2020). Reductive catalysis fractionation (RCF) produces phenolic monomers, termed monolignols, that can be valorized through enzymatic bioconversions. This study's main aim was to increase the value of three RCF monolignols: 4-propyl phenol (4-PP), 4-propyl guaiacol (4-PG), and 4-propyl syringol (4-PS), through oxyfunctionalization to value-added aromatic chemicals employing cytochrome P450 BM3 (CYPBM3) of *Bacillus megaterium.* Cytochrome P450 enzymes (CYPs) play critical roles in a wide range of biological processes by catalyzing diverse reactions (Munro *et al.*, 2002) and we sought to modulate the substrate specificity and selectivity of CYPBM3 by rational design.

Three mutants, M1 (Ala184Phe), M5 (Ala74Gly), and M7 (Ala328Leu), and CYPBM3wt were expressed and purified based on initial activity towards the monolignols and expression yields. Binding to monolignols was evaluated using absorbance shift assays, activity on monolignols was assessed *via* NADPH depletion assay, and oxidative regioselectivity was determined through mass spectrometry (MS) analysis. Binding shift assays indicated that M5 had improved binding to the bulkier monolignols (4-PG and 4-PS), while for M1 binding was only observed with the native palmitic acid substrate. CYPBM3wt binding was observed with all substrates, while M7 did not show any binding with any substrate potentially due to the introduction of steric hindrance in the active site. M5 showed the highest NADPH consumption rate with all three monolignols. M1 showed the lowest NADPH consumption rates with 4-PP and 4-PS. M7 showed the highest NADPH consumption rate with palmitic acid, exceeding the wild type, which could be the result of the uncoupling of electron donation from the reductase domain. 4-PP was the only monolignol showing product formation by identification by MS-analysis displaying hydroxylation in the meta- and ortho positions of the benzene ring. 4-PG also showed hydroxylation but in an unknown position. 4-PS had no product formation indicating uncoupling of electrons and non-productive binding.

The results of these analyses support the use of CYPBM3 for the oxyfunctionalization of lignin-derived monolignols. Further studies will be necessary to correlate substrate binding activity or uncoupling to better conclude which candidate had better activity. LC-MS should be employed for quantification of substrate disappearance and product formation to evaluate activity and specificity. Informed by this, a combination of mutations could also be generated for improved activity.

TABLE OF CONTENTS

ACKNOWLEDGEMENTS ..... **I**

SUMMARY ..... **II**

ABBREVIATIONS ..... **V**

1 INTRODUCTION **1**

1.1 The World of Lignin 1
1.1.1 Lignin Structure and Biosynthesis 2
1.1.2 Lignin Degradation 3

1.2 Cytochrome P450 6
1.2.1 CYP450 Structure 6
1.2.2 The CYP450 Reaction Mechanism 8
1.2.3 CYPBM3 9
1.2.4 Directed Evolution by Rational Design 10
1.2.5 Engineering BM3 toward Monolignol Activity 11

1.3 Objective of Thesis 14

2 MATERIALS **16**

2.1 Laboratory Equipment, Instruments, Columns, and Kits 16

2.2 Software for Analysis 19

2.3 Proteins, Enzymes, Primers, and Plasmids 20

2.4 Chemicals 21

3 METHODS **25**

3.1 Site-directed Mutagenesis 25
3.1.1 Building the Vector 25

3.2 Transformation of Chemically Competent Cells: *E. coli* TOP10 and *E. coli* BL21 29
3.2.1 *E. coli* TOP10 Transformation 29
3.2.2 Colony Study by Plasmid PCR 29
3.2.3 MiniPrep Plasmid Extraction 30
3.2.4 *E. coli* BL21 Transformation 31
3.2.5 Expression Test 31

3.3 Initial Screening Assays on Cell Lysate and Selection of Best Candidates 32
3.3.1 Protein Expression in 96 well-plates 32
3.3.2 NADPH Depletion Assay 33
3.3.3 Indole Oxidation 34
3.3.4 MS Analysis 34
3.3.5 Selection of Best Candidates 35

3.4 Expression and Purification of CYPBM3 36
3.4.1 Expression of CYPBM3 36
3.4.2 Purification of CYPBM3 Wild Type and Mutants 36
3.5 Characterization of Wild Type and Mutants' Activity on Monolignols 38
3.5.1 NADPH Depletion Assay 38
3.5.2 Binding Assay 38
3.5.3 MS Analysis 39
4 RESULTS 41
4.1 Site-directed Mutagenesis 41
4.1.1 Selected Mutations 41
4.2 Initial Screening Assays on Cell Lysate and Selection of Best Candidates 45
4.2.1 NADPH Depletion Assay 45
4.2.2 Indole Oxidation 47
4.2.3 MS Analysis. 47
4.2.4 Expression Quantification with ImageJ 49
4.3 Characterization of Wild Type and Mutants' Activity on Monolignols 53
4.3.1 NADPH Depletion Assay 53
4.3.2 Binding Assay 54
4.3.3 MS Analysis 59
5 DISCUSSION 62
5.1 Initial Screening on Cell Lysate 62
5.1.1 NADPH Depletion Assay with Cell Lysate 62
5.1.2 Indole Assay 63
5.1.3 MS Analysis 64
5.1.4 Expression Quantification with ImageJ 64
5.1.5 Chosen Candidates with Respective Mutations 65
5.2 Characterization of Wild Type and Mutants 66
5.2.1 NADPH Depletion Assay 66
5.2.2 Binding Assay 67
5.2.3 MS Analysis 69
6 CONCLUSION & FURTHER PERSPECTIVES 71
7 REFERENCES 72

ABBREVIATIONS

4-PP	4-propyl phenol
4-PG	4-propyl guaiacol (2-methoxy-4-propyl phenol)
4-PS	4-propyl syringol (2,6-dimethoxy-4-propyl phenol)
5-ALA	Aminolevulinic acid
ACN	Acetonitrile
AEX	Anion exchange chromatography
BSA	Body surface area
CV	Column volume
CYPBM3	Cytochrome P450 BM3
DNA	Deoxyribonucleic acid
E. coli	Escherichia coli
EDTA	Ethylenediaminetetraacetic acid
HPLC (LC-MS)	High-performance liquid chromatography
IEX	Ion exchange chromatography
IPTG	Isopropyl β-D-1-thiogalactopyranoside
LB	Luria-Bertani broth
mQ	Milli-Q water
NADPH	Nicotinamide adenine dinucleotide phosphate
PMSF	Phenylmethylsulfonyl fluoride
RCF	Reductive catalytic fractionation
TB	Terrific broth
UV	Ultraviolet

1 INTRODUCTION

1.1 The World of Lignin

Lignin is amongst the most abundant aromatic biopolymers on earth, second only to cellulose (Argyropoulos & Menachem, 1997). Compared to cellulose, lignin is considerably more resistant to biodegradation, changes in humidity, and balance of water. Whereas cellulose plays an important role in the paper-, textile- and pharmaceutical industries, lignin is seen as commercially less valuable due to the complicated process of lignin removal from plant biomass (Vanholme *et al.*, 2010). Despite its significance in the pulp and paper industry, the difficulties associated with lignin breakdown have contributed to researchers aiming to develop a form of lignin that is more susceptible to less costly and complex chemical degradation.

Besides its familiar role in plants, lignin has the prospective to be valorized as synthetic structural polymers and harnessed for valuable applications (Karunarathna & Smith, 2020). Using lignin to replace traditional high-cost materials is desirable to direct us toward a more sustainable world. This has been seen to be a challenge due to its complex three-dimensional structure (Figure 1.1) that makes depolymerization of the carbohydrate polymers in lignocellulosic biomass problematic and causes 98% of lignin waste to be used as low-cost fuel (Abdel-Hamid *et al.*, 2013; Karunarathna & Smith, 2020). Despite this, the remaining 2% has successfully been used to synthesize chemical compounds such as vanillin and polyols. With its abundant functional groups, lignin has great potential for chemical modification regarding achieving target properties (Karunarathna & Smith, 2020).

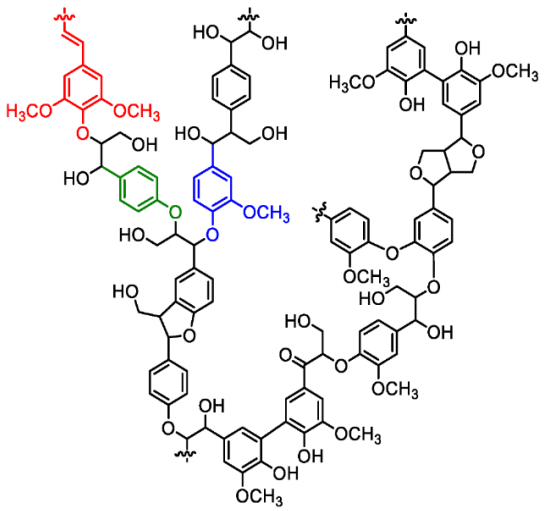

Figure 1.1: Structure of lignin with H, G, and S units. *The structure of lignin presented with its major monomeric units: Sinapyl (red), guaiacyl (blue), and p-hydroxyphenyl (green) (Karunarathna & Smith, 2020).*

1.1.1 Lignin Structure and Biosynthesis

Lignin is made up of the building blocks (also termed monolignols): *p*-coumaryl alcohol, coniferyl alcohol, and sinapyl alcohol (Abdel-Hamid *et al.*, 2013). The cinnamic acid (phenylpropanoid) derivatives: *p*-hydroxyphenyl (H), guaiacyl (G), and syringyl (S) are the corresponding monomeric units resulting from the monolignols (Figure 1.1; Figure 1.2).

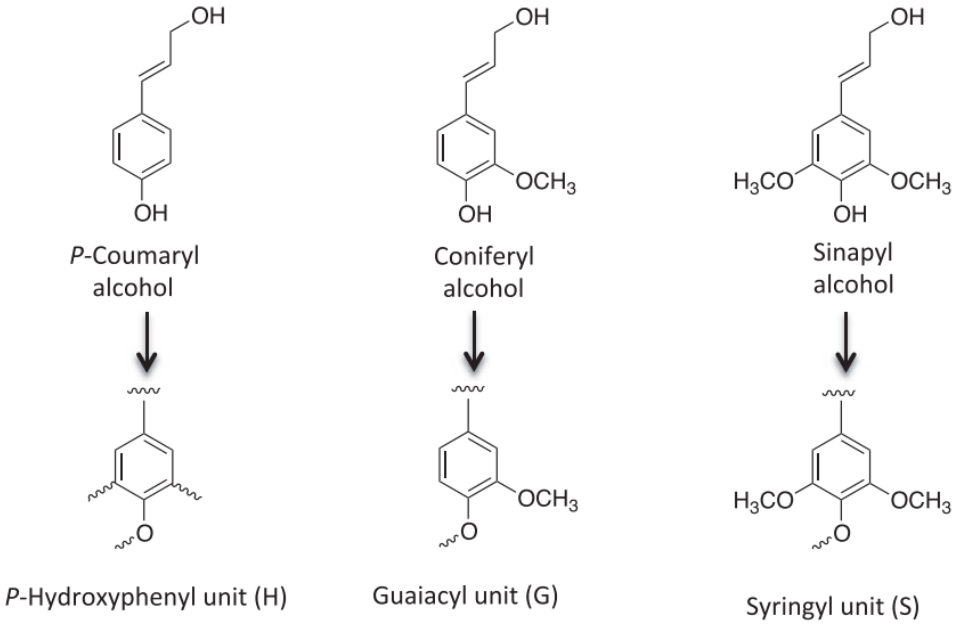

Figure 1.2: Monolignols with corresponding monomeric units. *This figure presents the structure of monolignols and their corresponding monomeric units (Abdel-Hamid et al., 2013).*

The amount of the three monolignols and their corresponding units in lignin varies between and within the plant species (Abdel-Hamid *et al.*, 2013). Hardwood plants contain more coniferyl- and sinapyl- alcohols, while grassy plants and similar species are rich in *p*-coumaryl alcohols (Karunarathna & Smith, 2020). These monolignols "derive from the general phenylpropanoid biosynthetic pathway" (del Río *et al.*, 2020).

The synthesis of monolignols is a multistep process involving several enzymes. More specifically, biosynthesis of the lignin building blocks begins with the deamination of phenylalanine, or tyrosine, and involves consecutive hydroxylation of the aromatic ring, accompanied by phenolic *O*-methylation and reduction of the side-chain carboxyl group to an alcohol (Takahama *et al.*, 1996; del Río *et al.*, 2020). The next step is the oxidation of the monolignols by peroxidases and/or laccases in the cell wall, where they form radicals that are polymerized by free-radical coupling mechanisms (Takahama *et al.*, 1996). This generates a succession of substructures within the phenolic polymer. Enzymatic dehydrogenation of the

monolignols *p*-coumaryl-, coniferyl-, and sinapyl alcohol produces the corresponding phenoxyl radicals as the initial step of lignin biosynthesis (Takahama *et al.*, 1996).

1.1.2 Lignin Degradation

The process where lignin is chemically separated from cellulose is called "delignification". The properties of the resulting phenolic polymer may vary depending on type of delignification, as well as which stage lignin was isolated (Argyropoulos & Menachem, 1997). During delignification, chemicals break down the lignin network and dissolve it as macromolecules in different sizes (Goring, 1977). The process of delignification has been important due to its commercial significance in the pulp industry.

Lignocellulosic biomass is the most abundant, economical, and highly renewable natural resource on earth (Qian, 2014). General depolymerization of lignin could in principle be the least complex method for the production of mentioned monolignols and their derivatives, as well as it would lower the cost of lignocellulose biorefinery (Sun *et al.,* 2019). It has been of great interest and importance to produce more valuable products from lignin such as pharmaceuticals and functional materials. Lignin degradation is the process where functional groups, side chains, and aromatic compounds are separated from the large polymer through oxidative reactions of carbon-carbon bonds or ether linkages (Zabel & Morrell, 2020). It can either be done chemically **(1)**, or enzymatically **(2)**. These two ways of lignin degradation are elaborated in the next paragraphs.

(1) Reductive Catalytic Fractionation

Monolignols are products from organic synthesis and cannot be derived directly from ordinary lignin depolymerization (Sun *et al.,* 2019). This type of synthesis is currently of prohibitive cost, and the goal of lignin degradation is (as mentioned) to lower the cost as well as the complexity of lignocellulose biorefinery. A solution could be the chemical approach with fractionation of the lignocellulosic biomass through reductive catalytic fractionation (RCF) (Renders *et al.*, 2019).

Reductive catalytic fractionation of lignocellulosic biomass refers to a biorefinery approach that integrates biomass fractionation with lignin depolymerization-stabilization, where the latter is enabled by a redox-active catalyst (Renders *et al.*, 2019). Utilizing RCF is not only beneficial to make lignin extraction less complicated. It also has the ability to amplify the total monomer

yield, as well as generate distinctive valuable products. RCF results in the production of lignin oil, a low-Mw (molecular weight) oil, which is composed of phenolic monomers in high yields.

The ingredients used to employ an RCF biorefinery are biomass (lignocellulose), an alcohol solvent or cyclic ether, and a heterogenous redox-active catalyst (Renders *et al.*, 2019). The three rudimentary steps of RFC are (i) extraction of lignin, (ii) depolymerization, and (iii) stabilization. Figure 1.3 shows a schematic representation of the three elementary steps in reductive catalytic fractionation.

The first step, extraction of lignin, does not require a redox-active catalyst and is exclusively dependent on the solvolytic conditions. The second step, depolymerization, is not as straightforward as the aforementioned steps and includes two routes: solvolytic depolymerization and catalytic hydrogenolysis. The third step of RCF, stabilization, is strongly influenced by the redox-active catalyst when stabilizing the unsaturated fragments.

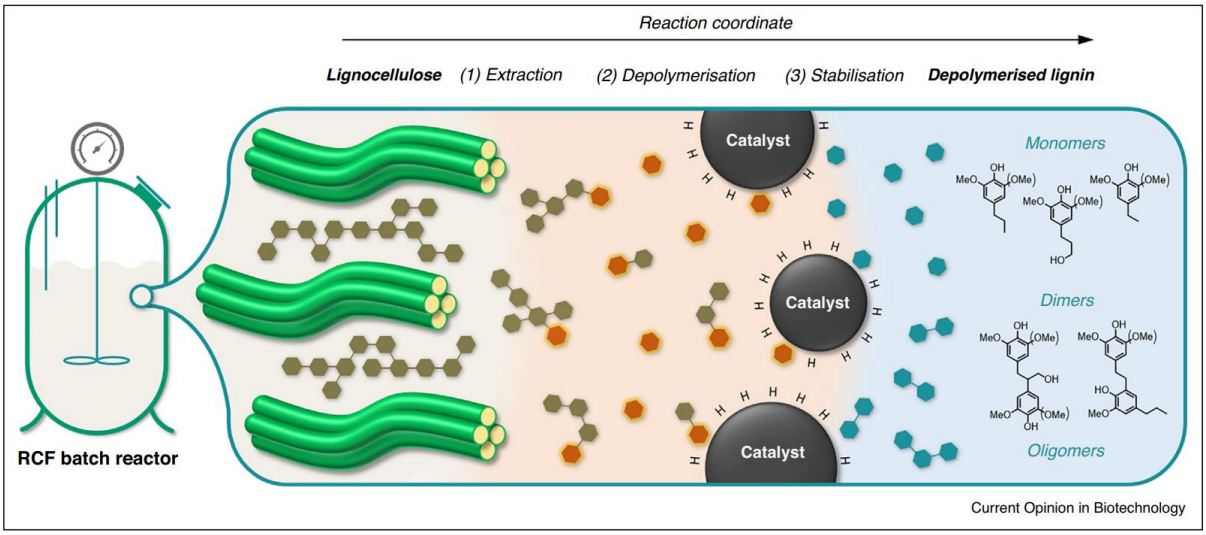

Figure 1.3: RCF presented in three elementary steps. *An overview of the main steps in reductive catalytic fractionation (Renders et al., 2019).*

The reaction process of RCF starts with raw material of the lignocellulosic biomass being transferred to a batch reactor together with the solvent (alcohol or cyclic ether), a hydrogen source, and the heterogenous redox-active catalyst (Arts *et al.*, 2021). The high-pressure batch reactor is heated to 160-250°C with a reaction time varying between 2-6 and 1-24 hours (Arts *et al.*, 2021; Renders *et al.*, 2019). Delignification is induced by solvolytic separation of lignin from the biomass and is followed by the ether and ester linkages between hemicellulose and lignin being cleaved (Arts *et al.*, 2021; Renders *et al.*, 2019). This releases lignin and activates the solubilization in the solvent. After solubilization, low-Mw intermediates (reactive) are

generated by catalytic depolymerization and solvolytic deconstruction of lignin fragments through the cleavage of inter-unit lignin bonds. Depolymerization is catalyzed with the help of a redox-active catalyst that catalyzes depolymerization to occur and reductively stabilizes the lignin fragments (Renders *et al*., 2019). This stabilization induces the newly generated blend of substituted aromatic molecules to be stable and also prevents condensation (Arts *et al.,* 2021).

The carbohydrate fraction largely retained during RCF results in delignified pulp, rich in carbohydrates (Arts *et al.,* 2021). The presence of hydrogen (H_2) is, even though both stabilization and depolymerization consume this element, optional as the solvent may be used as a hydrogen donor. RCF is able to yield the low-Mw, stable lignin oil composed of phenolic monomers, dimers, and oligomers after the solvent is filtrated and evaporated.

Some of the products that can be derived from this process are the monolignols: 4-propyl phenol (4-PP), 4-propyl guaiacol (4-PG), and 4-propyl syringol (4-PS) (Figure 1.4). As an example, RCF of lignocellulosic biomass with Ruthenium (Ru) catalysis under hydrogen pressure can produce a mix of the substrates 4-PG and 4-PS, with a total monomer yield representing more than 50 wt% of the original lignin content (Bomon *et al.,* 2021).

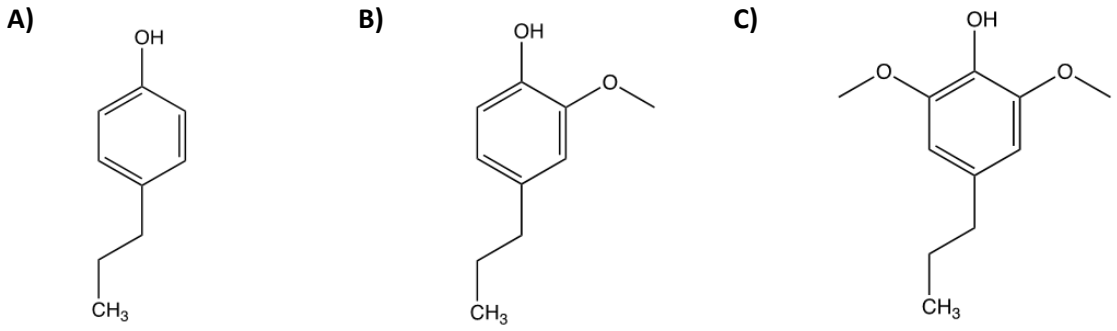

Figure 1.4: Monolignols derived from RCF. *Three of the products obtained from RCF are the monolignols 4-propyl phenol (A), 4-propyl guaiacol (B), and 4-propyl syringol (C).*

(2) Enzymatic Degradation of Lignin

In addition to delignification by chemical methods, enzymatic breakdown of lignin is also possible. Two major groups of enzymes are involved in this process: heme peroxidases and laccases (Abdel-Hamid *et al.,* 2013). Heme peroxidases are enzymes that utilize the reduction of hydrogen peroxide to catalyze numerous oxidative reactions with organic and inorganic substrates involving the intermediates Compound I [iron(IV)-oxo] as seen in Cytochrome c Peroxidase and Compound II [iron(IV)-hydroxo] as seen in Ascorbate Peroxidase (Figure 1.5) (Battistuzzi *et al.,* 2010; Moody & Raven, 2018). The catalytic cycle has three redox couples

(Compound I/Fe^{3+}, Compound I/Compound II, and Compound II/Fe^{3+}) which are formed as intermediate species with differing reduction potentials during the catalytic cycle. The oxidative power of these hemoproteins has been used for lignin degradation.

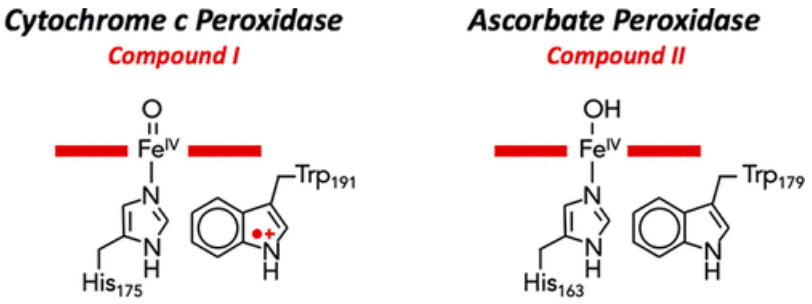

Figure 1.5: Compound I and Compound II. *This figure presents the high-valent intermediates that participate in the heme peroxidase oxidation of substrates (Moody & Raven, 2018).*

The second group of enzymes, laccases, display a broad substrate specificity when transforming lignin through depolymerization (Gianfreda *et al.*, 1999). The laccase active site contains four copper atoms (T1, T2, and two T3) arranged in two active sites. These are required for the catalyzation of one-electron oxidation and four-electron reduction of oxygen to water during lignin breakdown (Abdel-Hamid *et al.*, 2013).

1.2 Cytochrome P450

Cytochrome P450s (CYPs) are one of the largest groups of enzymes present in nature. CYPs are members of the monooxygenase superfamily (Eser *et al.*, 2021; Munro *et al.*, 2002). Enzymes in the CYP family contain an iron-heme group that plays a central role in enzyme reactivity and is needed to carry out oxidation reactions (Jung *et al.*, 2011; Eser *et al.*, 2021). In their reaction mechanism, CYPs use molecular oxygen and NADPH (pyridine nucleotide) as a hydride donor to affect the insertion of one oxygen atom into a substrate (Jung *et al.*, 2011). The activation of oxygen proceeds through a series of reduction and protonation steps to form the catalytically active Compound I species, a heme-Fe(IV) oxo cation radical is responsible for activation of the substrate by hydrogen atom abstraction (Schröder *et al.*, 2023).

1.2.1 CYP450 Structure

All CYPs share a common globular fold in which the active site core is composed of a four-helix bundle consisting of parallel helices denoted as D (yellow), L (orange), and I (dark purple)

which are presented in Figure 1.6, along with a single antiparallel helix (Denisov *et al.*, 2005). The heme active site is confined between the distal I-helix and proximal L-helix, which makes the I-helix of particular importance due to its proximity to the heme group. The heme iron is bound to a Cys-heme-ligand loop, and the conserved amino acid cysteine is bound through two hydrogen bonds with the adjacent amides and is seen as the "fifth" ligand to the heme group.

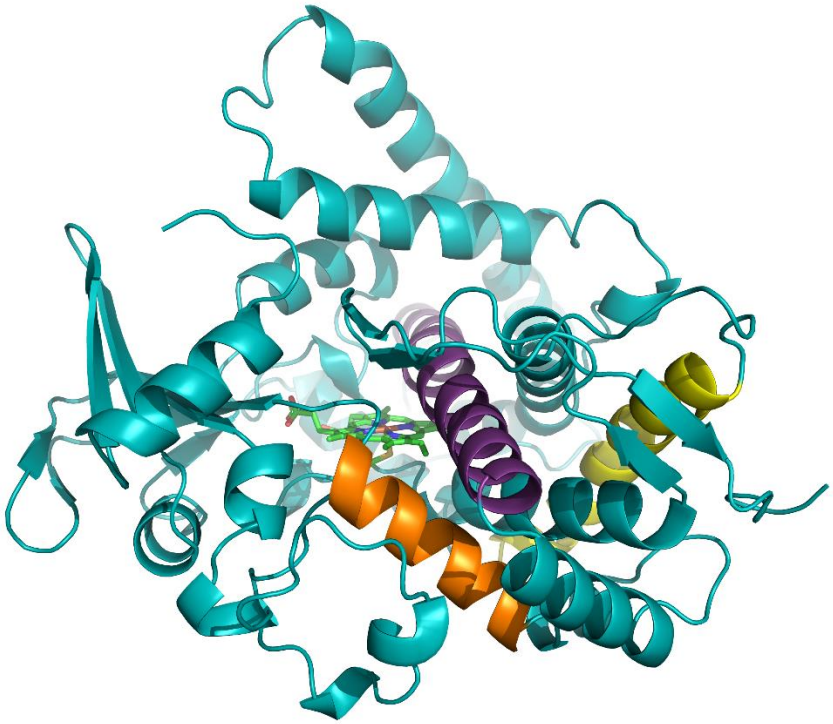

Figure 1.6: CYP450 structure. *This structure of CYP450 is presented in this figure. The three parallel helices composing the active site core are represented with their respective colors: I (dark purple), D (yellow), and L (orange) [PDB 1BVY] (Denisov et al., 2005).*

CYPs can be divided into various classes depending on their electron transport systems and redox partner protein interactions (Hannemann *et al.*, 2006). The classes range from I to X, with Class I, Class II, Class VII, and Class VIII being further discussed here as general examples. Class I encompass the majority of bacterial cytochrome P450 systems, in addition to the mitochondrial P450 systems found in eukaryotes. Both systems have a FAD-containing reductase and a ferredoxin in common. The reductase (FAD) transfer reduction equivalents in the form of electrons from, for example, NAD(P)H, while the ferredoxin contributes to the direct reduction of the enzyme (P450). The most prevalent cytochromes P450 in eukaryotes are Class II, exhibiting a wide range of catalytic reactions. Contrary to Class I, this class transfer electrons from NADPH via the redox centers FAD and FMN which belongs to two separated proteins. Class VII represents a groundbreaking category of soluble P450 systems,

distinguished by the fusion of a reductase domain at the C-terminus of the cytochrome P450. Notably, this reductase domain, typically unrelated to P450 systems, is derived from the phthalate dioxygenase reductase domain. The last class, Class VIII shares similarities with Class VII, with a fusion of the diflavin reductase (CPR) domain to the P450 domain. The enzymes belonging to this class are monooxygenases with CYPBM3 (CYP102A1) being amongst the most studied member due to its fused structure and solubility. CYPBM3 contains a heme domain which is, as mentioned, fused to the diflavin reductase domain, and the latter contains the cofactors FAD and FMN. Employing NADPH as an electron donor, these catalytic enzymes transfer electrons from FAD to FMN by reducing the protein. From FMN the electrons travel to the heme active site in the P450 domain in which the substrate is bound.

CYP450s have evolved great changes in their primary structure while maintaining the P450 fold and heme-binding site in their secondary structure, making it possible to tailor them for divergent redox partner interactions and substrate selectivity (Munro *et al.*, 2002). Due to their high stereo- and regioselectivity, these enzymes are considered to be exceptional biocatalysts (Schröder *et al.*, 2023). CYPBM3 from the soil bacterium *Bacillus megaterium* is seen to be a target in the progress of biocatalysis because of the two domains (heme and FMN/reductase domains) being fused and is with this a part of the CYP450 systems of Class VIII. This fusion makes the substrate specificity broader and ensures ease of application due to the expression of a single construct instead of requiring expression of multiple enzymes.

1.2.2 The CYP450 Reaction Mechanism

CYP450 uses NADH or NADPH to deliver electrons via either a flavoprotein or an iron-sulfur protein (Guengerich, 2018). The stoichiometry for these monooxygenases in which the cofactors NADH or NADPH are utilized is shown below:

$$\mathbf{NAD(P)H + O_2 + R \rightarrow NAD(P)^+ + RO + H_2O}$$

Here, R represents an organic substrate, and RO represents the oxidized reaction product.

The catalytic turnover of cytochrome P450 enzymes happens in several steps (Figure 1.7). First, the substrate binds to the heme active site, and the water molecule occupying the active site is displaced (Behrendorff, 2021). Then, the ferric (III) heme is reduced to the ferrous (II) state by electron transfer from the reductase domain. Molecular oxygen binds to the ferrous (II) iron and transfers a second electron to the resulting ferrous dioxy complex to form a ferric peroxy anion. Oxygen is activated by forming the ferric peroxy anion. This activation of oxygen makes

the P450 able to oxidize the substrate. The ultimate outcome of this sequential series of reactions culminates in the monooxygenation of the substrate, resulting in the formation of the product while simultaneously restoring the heme iron to its ferric state.

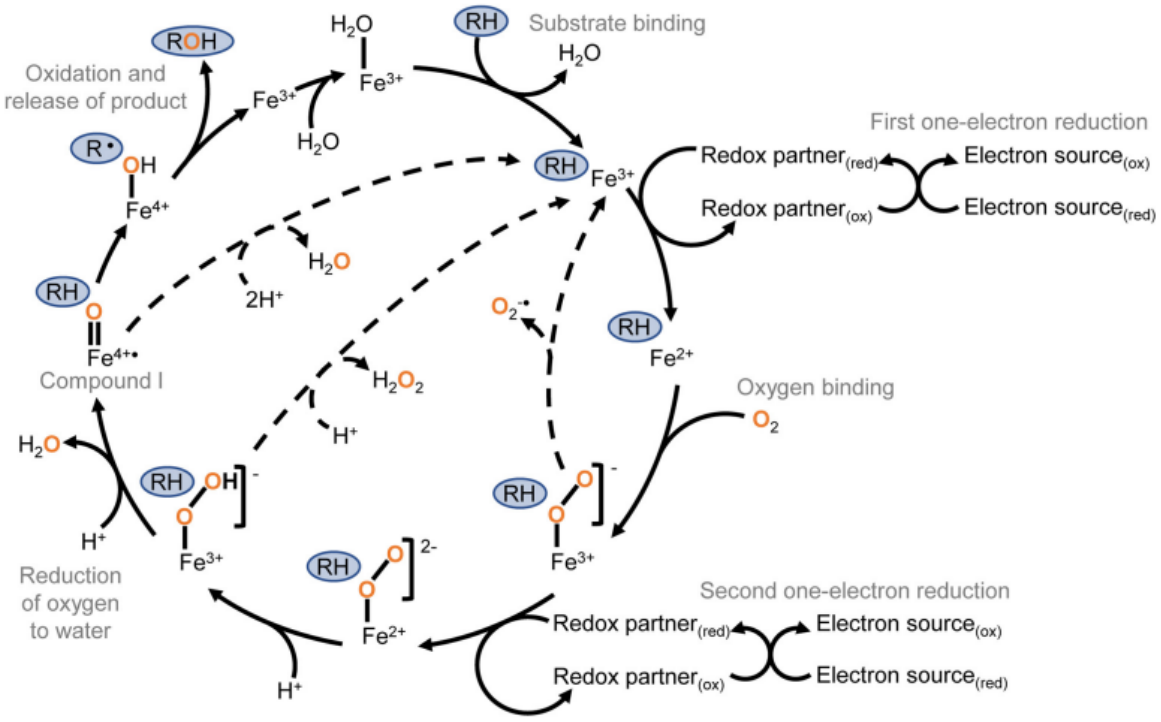

Figure 1.7: Catalytic turnover of cytochrome P450. *Substrate-binding activates several steps in the catalytic turnover of CYP450. This leads to the activation of oxygen which makes CYP450 able to oxidize the substrate bound. The stippled lines refer to uncoupling of electrons. The figure is adapted from a paper from 2021 by Behrendorff.*

As previously indicated, the initial electron in the catalytic cycle of CYP450 is acquired through the oxidation of NAD(P)H facilitated by a redox partner (Behrendorff, 2021). This redox partner may take the form of a diflavin reductase, which directly reduces the enzyme, or it may involve intermediate molecules such as ferredoxin or flavodoxin proteins. The first reduction can be achieved chemically typically using dithionite, but the second reduction can only be done enzymatically.

1.2.3 CYPBM3

CYPBM3, within the CYP450 superfamily, has been extensively studied due to its natural fusion with its reductase domain that has made it valuable for biocatalytic applications since it is not necessary to co-express redox-partner proteins (Urlacher *et al.*, 2012). CYPBM3 P450 has a crystal structure displaying two major domains as shown in Figure 1.8 called the heme domain (cyan) and the FMN domain/reductase domain (light magenta) (Sevrioukova *et al.*,

1999). The BM3-FMN complex shares a similar fold with the FMN domain of CPR (CPR-FMN) and flavodoxins. These are made up of a central five-stranded β-sheet (parallel) with four α-helices surrounding them. The peptide that heralds the heme-binding loop of the heme domain (in the FMN-binding domain) and the C helix (dark blue) interact with the residues from one of the four α-helices - α_1 (hot pink) and the outer FMN-binding loop (light yellow) faces the proximal face of the heme domain.

The two domains are bound together by two hydrogen bonds, one salt bridge, and a number of water-mediated contacts. The lack of more direct contact between the two domains in the 967 $Å^2$ area of the interface makes the interaction weak.

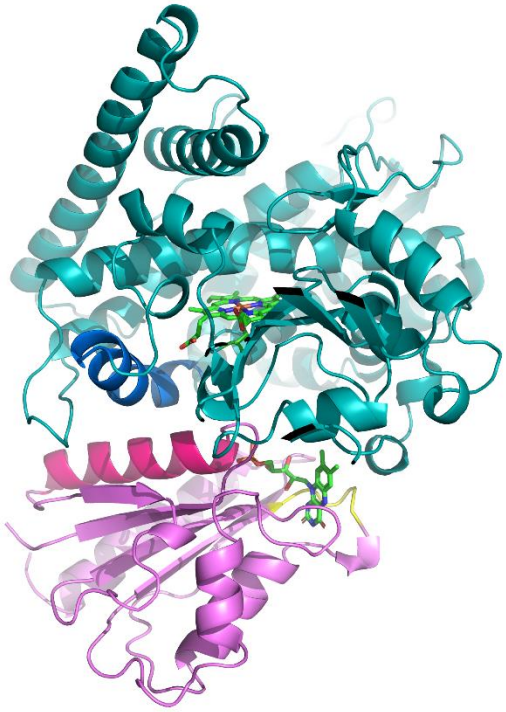

Figure 1.8: Cytochrome BM3 P450 structure. *The figure presents the two domains composing the CYPBM3 enzyme. The heme domain (cyan) is represented with the heme group (green), as well as the C helix (dark blue) interacting with the α_1 helix (hot pink) of the FMN reductive domain (light magenta) [PDB 1BVY] (Sevrioukova et al., 1999).*

1.2.4 Directed Evolution by Rational Design

To enhance CYP450 and its ability to react with more diverse substrates, directed evolution has been employed and played a central role in P450 engineering (Jung *et al.*, 2011). It is one of the most influential and extensive tools for protein engineering and has the aim to speed up the natural evolution process of biological systems and molecules through iterative rounds of library screening/selection, amongst other things (Wang *et al.*, 2021).

CYPBM3 P450 is the most published enzyme with high engineering abilities of the P450s (Urlacher & Girhard, 2012). A small number of amino acids in the enzymatic secondary structure of P450 are fully conserved, and they are therefore important key points for catalysis (Munro *et al.*, 2002). The fusion of the heme domain and the diflavin reductase domain in BM3 makes it an easy-going and preferable system for engineering (Urlacher & Girhard, 2012). Employing directed evolution demands a large enzyme library, while rational design allows a smaller collection of mutants to get successful results. Rational protein design is the first step of directed evolution, and the terms are therefore often used together. Directed evolution by rational design on CYP450 has resulted in many mutants that possess an expanded range of substrate selectivity and specificities that are important in the use of non-native substrate functionalization (Jung *et al.*, 2011). This may suggest that this enzyme can have the ability to react with new, aromatic substrates, such as the monolignols derived from RCF (Figure 1.4).

New studies have discovered that CYP450s can react with bulky aromatic structures in addition to reacting with substrates with simple structures (Eser *et al.*, 2021). In a specific study, mutagenesis was performed on two positions: Phe87 and Ala328 (Urlacher & Girhard, 2012). Here, the mutants showed either a higher or similar activity to the CYPBM3wt. To expand the substrate scope of CYP450, directed evolution by rational design has been employed as a strategy (Schröder *et al.*, 2023). Iterative saturation mutagenesis and site-directed mutagenesis have particularly contributed to the expansion of both chemical functionality and substrate specificity in these enzymes, where the latter has been especially important for this study.

1.2.5 Engineering BM3 toward Monolignol Activity

In this study, site-specific mutagenesis by rational design will be employed to make several mutants with the ability to affect the substrate specificity of CYPBM3 P450. Site-specific mutagenesis, or site-directed mutagenesis, is used to make alterations in specific, targeted positions to (in this case) study changes in protein activity (Kunkel, 1985). Some of the mutations made in this study were inspired by the results from the studies mentioned in this paragraph. CYPBM3 is a very efficient and broad-ranging catalyst and for this reason, it was chosen to be employed in biocatalysis of the chosen monolignols.

Monolignols are substituted benzene rings, and previous studies have demonstrated the capability of CYPs to engage with substrates that possess a similar substituted benzene ring configuration (Munday *et al.*, 2017). These enzymes are ideal catalysts because of their stereo- and regioselectivity, as well as their ability to function under mild conditions. The goal of this

study was to oxyfunctionalize monolignols for downstream applications. Figure 1.9 presents the chosen monolignols and their desired oxyfunctionalization sites.

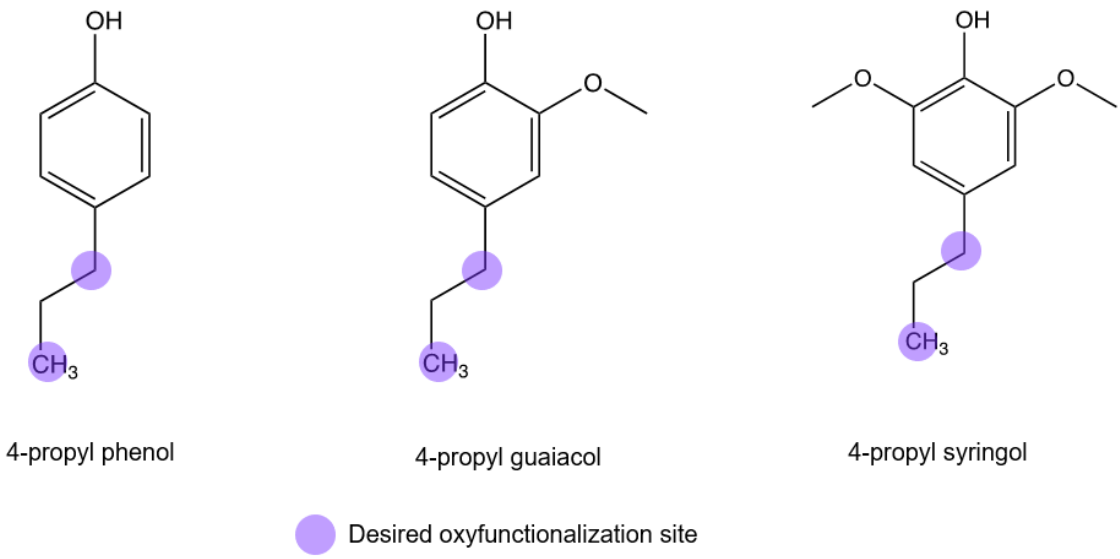

Figure 1.9: Chosen substrates with targeted oxyfunctionalization sites. *The monolignols 4-PP, 4-PGl, and 4-PS are substituted benzene rings and may have the ability to be oxidized by CYPBM3 as shown in studies with other substituted benzene rings.*

Previous studies have provided precedence that BM3 can be engineered to have activity on substituted benzene rings. The mutations carried out in this study were derived from prior research where specific sites demonstrated successful applications. These sites served as a precedent for the current study, suggesting that if these mutations effectively altered the regioselectivity of substrates with a comparable chemical structure, a similar outcome might be achievable with the selected monolignols.

The key residues of the CYPBM3 enzyme are the residues surrounding the active heme-binding site, and these are most prone to mutagenesis in studies (Figure 1.10). They are involved in affecting the entrance channel and hydrophobic binding pocket, opening the active site, or attributing to conformational change and destabilizing open conformation, amongst other things. These residues have been a target for direct evolution studies on CYP450 for several years as discussed below.

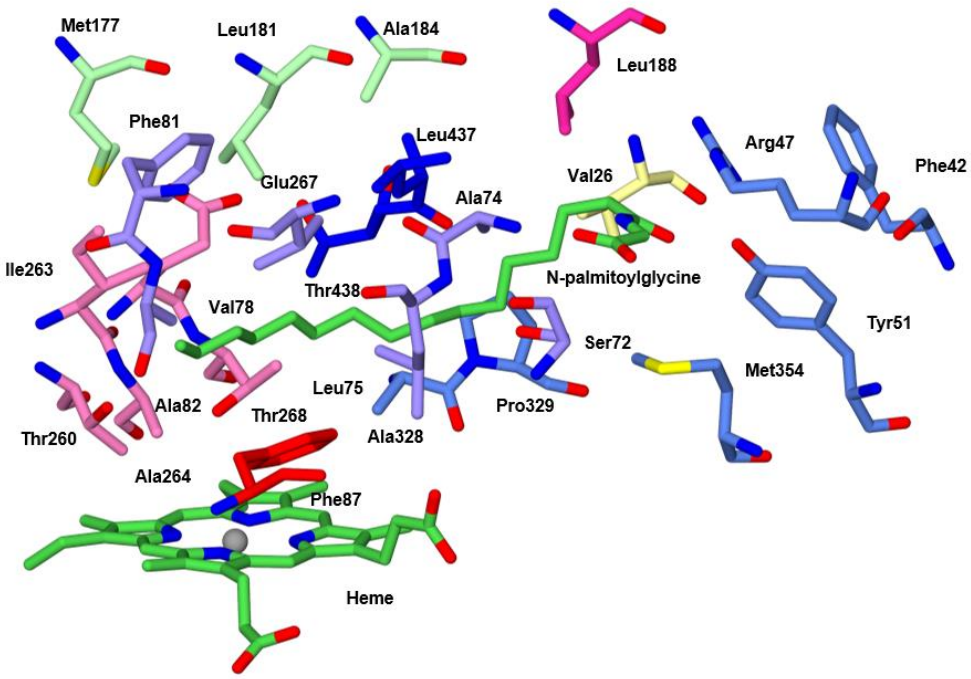

Figure 1.10: P450BM3 key residues. *The key residues that are prone to undergo mutagenesis and alter the substrate specificity of CYPBM3 P450 [PDB 1JPZ].*

The native CYBM3 P450 enzyme has a long and narrow entrance channel leading into its binding site. This indicates that long-chain fatty acids are the most suitable substrates for binding, but in 2001, Li *et al.* replaced the Phe87 residue with Ala, increasing the hydroxylation of propylbenzene considerably compared to the CYPBM3 wild type. The same mutation (Phe87Ala) could also have an impact on the big, aromatic compound methyl 2-methoxy-3-methylbenzoate and this substrate's ability to enter the narrow entrance channel of the active binding site. The same year a study presented results of a triple CYPBM3 mutant (Phe78Val, Leu188Gln, Ala74Gly) that had the ability to hydroxylate alkanes, cycloalkanes, arenes, such as the compound α-Ionone (Appel *et al.*, 2001). Another successful study was done by Tsotsou *et al.* 2012, where they managed to make a CYP450 mutant that showed new catalytic abilities towards diclofenac, tolbutamide, and ibuprofen by employing random mutagenesis.

In 2017, Munday *et al.* found that active-site mutations such as Ala330Pro would have an impact on the regioselectivity of the oxidation of substituted benzenes, such as 2-methylstyrene when using the CYPBM3 enzyme as catalyst. Two years later, Klaus and his crew detected that the amino acids in position 437 could have a high effect on 3-methylanisole in terms of the substrate binding to the heme group (Klaus *et al.*, 2019). In the same study, they also found out that hydrophobic amino acids (such as Ala and Leu) in position 328 were a so-called "hotspot" for CYP450 substrate selectivity and specificity because of their location in relation to the heme

active site. Limonene is a compound where this type of mutation had success. The double substitution R47L/Y51F of the hydrophobic amino acids that lies close to the substrate entrance channel, was shown to increase the oxidation activity considerably (Carmichael & Wong, 2001). In this study, the team used polycyclic aromatic hydrocarbons, but the same success was seen with the substrate 1-ethyl-2-methylbenzene.

These aromatic compounds, together with their targeted oxyfunctionalization sites are presented in Figure 1.11.

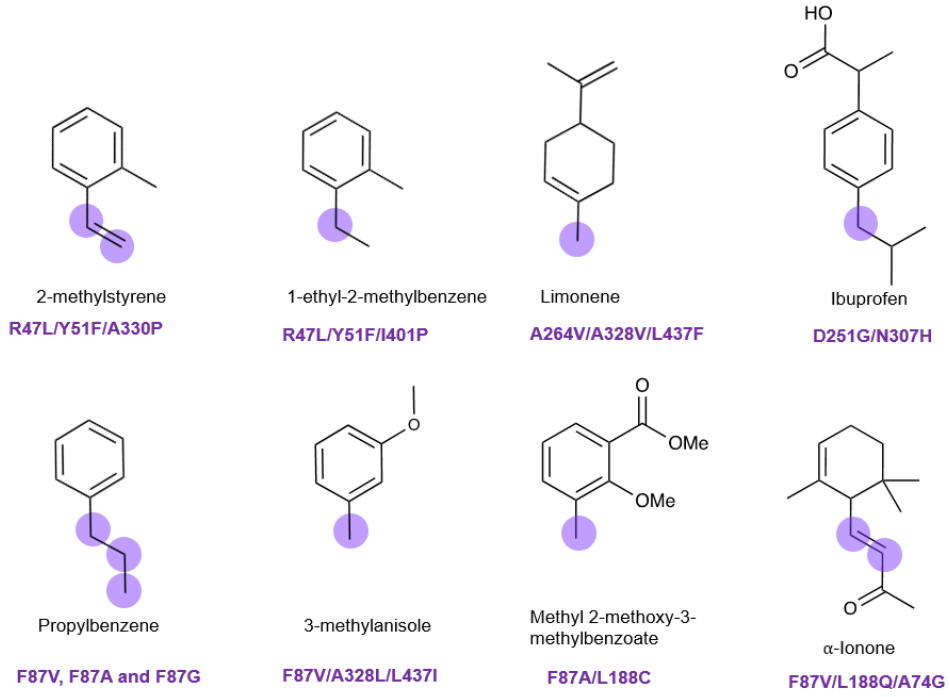

Figure 1.11: Chosen substrates with targeted oxyfunctionalization sites. *Successful studies on a selection of substrates done by direct evolution on CYPBM3. The substrates are presented with their targeted sites and respective mutations.*

1.3 Objective of Thesis

CYPs have through many years of research shown a high capacity for accepting new substrates, and an enzymatic hydroxylation by the CYPBM3 P450 of the desired derived monolignols may create value-added aromatic compounds, such as suggested in Figure 1.12 (Jung *et al.*, 2011; Jeffreys *et al.*, 2018). Using directed evolution coupled with rational design to enhance substrate selectivity and specificity, CYPs have the potential to use the monolignols as substrates in an enzymatic reaction.

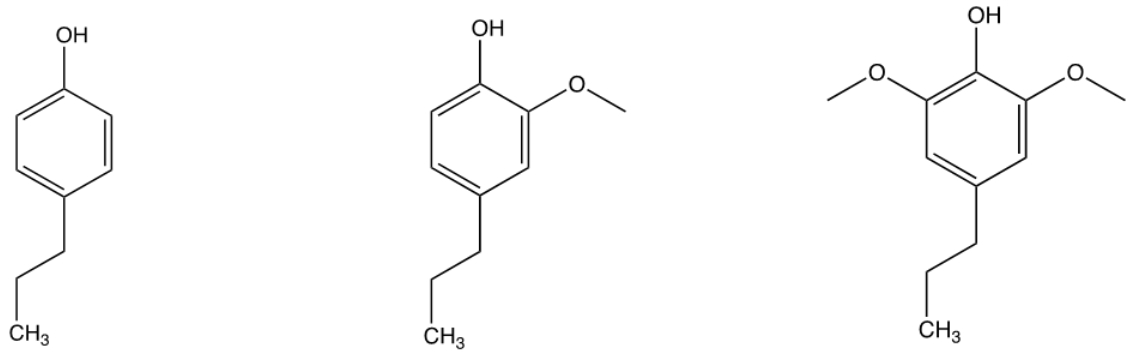

Figure 1.12: Desired substrates for selective hydroxylation by CYPBM3. *These substrates will be used for an enzymatic reaction with BM3.*

The main aim of this research is to convert derived monolignols to value-added aromatic chemicals using cytochrome P450 BM3 (CYPBM3) by rational design. This objective was followed by these sub-goals:

- ✓ Producing mutants inspired by recent successful studies, and expressing the mutants and CYPBM3 P450 wild type in *E. coli*
- ✓ Examine the initial activity of the monolignols with cell lysate, and employ mass spectrometry (MS) to check for product formation
- ✓ Purifying a selection of mutants for further analysis, and characterizing the activity of these candidates
- ✓ Examine reactions of monolignols with pure CYPBM3 P450 mutants and wild type with MS analysis for final product formation

This study provides a foundation for further research on CYPBM3 P450's biocatalysis of lignin-derived monolignols to achieve target properties and more valuable products in future lignin industry.

2 MATERIALS

2.1 Laboratory Equipment, Instruments, Columns, and Kits

Table 2.1. Instruments. All the instruments operated in this thesis's experimental work are included, along with application and supplier.

INSTRUMENT	APPLICATION	SUPPLIER
ÄKTA go protein purification system	AEX (Anion Exchange Chromatography)	Cytiva
Fraction collector F9-R	Collecting fractions in protein purification	Cytiva
NanoDrop™ One	Measurement of absorbance	Thermo Fisher Scientific
NanoPhotometer® C40	Measurement of absorbance	Implen
Thermo LTQ Velos Pro MS/MS	Mass spectrometry analysis	
Varioskan LUX Multimode Microplate Reader	○ Bradford protein assay ○ NADPH depletion assay	Thermo Fisher Scientific
UltiMate 3000 HPLC and UHPLC Systems	Collecting samples in MS	Thermo Fisher Scientific

Table 2.2. Laboratory equipment. This table contains the laboratory equipment used in the experiments performed in this master thesis. Specifications of the equipment and supplier are also included.

EQUIPMENT	SPECIFICATION	SUPPLIER
Autoclave tape	Sterilization indicator tape, 12 mm	Merck
Automatic pipettes	Single and multichannel pipettes	Thermo Fisher Scientific
Centrifugal bottles and tubes	Fisher Scientific™ LabServ Blue Flat Top Cap Conical Tubes (Falcon tubes) ○ 15 mL ○ 50 mL Nalgene™ High-Speed/Super-Speed Centrifuge Tubes/Bottles (with Sealing Cap/Closure) ○ 50 mL ○ 1 L	Thermo Fisher Scientific/Fisher Scientific

Centrifugal filter	Merck Amicon™ Ultra-15 Centrifugal Filter Units (15 mL)	Thermo Fisher Scientific/Fisher Scientific (Merck)
Centrifuge rotors	○ Eppendorf F-35-6-30 Rotor for 5430/5430R ○ Eppendorf FA-45-30-11 Fixed Angle Coated Rotor with Lid ○ Fiberlite™ F9-6 x 1000 LEX Fixed Angle Rotor ○ Fiberlite™ F21-8 x 50y Fixed-Angle Rotor with Auto-Lock ○ M10 Microplate Swinging Bucket Rotor	○ Eppendorf ○ Eppendorf ○ Thermo Fisher Scientific ○ Thermo Fisher Scientific ○ Thermo Fisher Scientific/Fisher Scientific
Centrifuges	○ Eppendorf™ MiniSpin™ ○ MiniStar Microcentrifuge ○ Sorvall LYNX 6000 Superspeed Centrifuge ○ Centrifuge 5430/ 5430 R - High-Speed Centrifuge	○ Thermo Fisher Scientific/Fisher Scientific ○ VWR ○ Thermo Fisher Scientific ○ Eppendorf
Cuvettes	Hellma® absorption cuvettes, semi-Micro	Merck
Eppendorf™ tubes	○ 200 µL ○ 1.5 mL ○ 2 mL	Eppendorf
Filters	MF-Millipore™ 0.45 µm MCE Membrane 25 Filters, 47 mm	Merck
Freezer	○ -20℃ ○ -80℃	○ Whirlpool ○ Sanyo
Fridge	4℃	Whirlpool
GelDoc Go Gel Imaging System	System for UV imaging of gels	Bio-Rad
Gel Loading Dye Purple (6x)	Dye to color samples for DNA gel electrophoresis	New England Biolabs Inc.

Glass- or plasticware in different sizes	○ Baffled culture flasks ○ Beakers ○ Erlenmeyer flasks ○ Graduated cylinders ○ Volumetric flasks	○ Thermo Fisher Scientific ○ VWR
HPLC vials and caps	200 µL	VWR
Ice container	KF 145	PORKKA, VWR
Incubators	○ Multitron Standard ○ T100™ Thermal Cycler ○ ThermoMixer C	○ Infors HT ○ Bio-Rad ○ Eppendorf
Magnets	Spinbar® magnetic stirring fleas	Merck
Magnetic stirrer with hotplate	Fisherbrand Magnetic stirrer hotplate 230V 50Hz 630W metal topup to 15L	Thermo Fisher Scientific/Fisher Scientific
Microtiter Microplate	Corning™ 96 well-plate, 200 µL	Thermo Fisher Scientific/Fisher Scientific
Milli-Q® Direct water purification system	Ultrapure water system directly from tap producing RiOs™ and Milli-Q® water	Merck
Mini-PROTEAN Tetra Vertical Electrophoresis Cell	Chamber for SDS-PAGE gel electrophoresis	Bio-Rad
Mini-PROTEAN Tetra Vertical Electrophoresis for Handcast Gels	Supply for the Electrophoresis Cell to make SDS-PAGE gels	Bio-Rad
Mini-PROTEAN TGX Stain-FreePrecast Gel	10 or 15 wells	Bio-Rad
Mini-Sub Cell GT Horizontal Electrophoresis System	UV transparent trays ○ 7 x 10 cm ○ 7 x 7 cm 10-well and 20-well combs	Bio-Rad
Parafilm	5 cm x 76 m	Merck
Petri dishes	9 cm	Merck
pH meter	FiveEasy Plus pH	METTLER TOLEDO
Pipette tips	Next Generation Tip Refill • 10 and 20 µL • 100, 200 and 250 µL	VWR

	• 1000 and 1250 µL	
Plastic pipettes	Disposable pipettes, 1 mL	VWR
Polypropylene Deep Well Plate	96 well-plate, 2 mL	Thermo Fisher Scientific
PowerPac™ Basic Power Supply	SDS-PAGE electrophoresis power supply	Bio-Rad
Scales	-	VWR
Sonicator system	Sonics 130-Watt Ultrasonic Processors	Sonics (VWR)
Syringes	Different sizes (1 mL-50 mL)	Merck
UV trays for SDS-PAGE	○ Blue Tray ○ UV/Stain-Free tray	Bio-Rad
Vortex	IKA™ Lab Dancer Vortex Mixer	Thermo Fisher Scientific/Fisher Scientific
Water bath	42℃	Merck

Table 2.3. Columns and kits. The columns utilized in purification, plus the kits used in PCR clean-up and plasmid extraction. Both columns and kits are listed with specification and their supplier.

COMPONENT	SPECIFICATION	SUPPLIER
E.Z.N.A.® Plasmid DNA Mini Kit I	Kit used for plasmid extraction	omega, BIO-TEK
DNA Clean & Concentrator ™-5	Kit used to clean DNA after PCR	ZYMO RESEARCH
HiTrap® Q HP (High Performance) column	5 mL Q-column	Cytiva

2.2 Software for Analysis

Table 2.4. Software for analysis. In this master's thesis, it was operated two different softwares. Their application and supplier are listed in the table below.

SOFTWARE	APPLICATION	SUPPLIER
ImageJ	Java-based software for analyzing, among other areas of use, images (here; SDS-PAGE results)	The National Institutes of Health and the Laboratory for Optical and Computational Instrumentation

LTQ Series Thermo Tune Plus	MS analysis	Thermo Fisher Scientific
Microsoft Office Excel	Spreadsheet used for analyzing data and making graphs	Microsoft
PyMOL	System for 3D visualization of everything from small molecules to proteins	Schrödinger Inc
SnapGene	Software used as a tool for molecular cloning procedures	Dotmatics
Unicorn 7.6	AEX	Cytiva
Xcalibur 4.5 (Thermo Scientific)	MS analysis	Thermo Fisher Scientific

2.3 Proteins, Enzymes, Primers, and Plasmids

Table 2.5. Proteins and enzymes. Specifications and suppliers for the proteins and enzymes used in this thesis are presented in this table.

NAME	SPECIFICATION	SUPPLIER
DNase I	Digestion of single and double-stranded DNA	Merck
DnpI	Restriction enzyme used for specific cutting of vectors	Merck
GeneRuler	1 kb DNA Ladder	Thermo Fisher Scientific
Lysozyme	From chicken egg white	Merck
Unstained Protein Standard	Ladder for SDS-PAGE	New England Biolabs Inc.

Table 2.6. Plasmids and primers. In this thesis, there were several primers utilized, plus one plasmid. The primers marked in red are the primers used to make the 11 mutants made for this project. They are listed with their respective sequences from 5' end to 3' end, but the plasmid is presented with its number of base pairs.

NAME	SEQUENCE (5' – 3')
Plasmids	
Pet_28b	5206 bp
Primers	
CYPBM3_A184F_fwd	TGTTCATAAATTCATCCAGTGCACGGACCATACTTGTAATAAA

CYPBM3_A184F_rev	TGGATGAATTTATGAACAAGCTGCAGCGAGCAAATCCAGACGA
CYPBM3_A328L_fwd	AACGCAGGCAGAGTTGGCCATAAGCGCAGCGCTTCGTTTAAGA
CYPBM3_A328L_rev	GCCAACTCTGCCTGCGTTTTCCCTATATGCAAAAGAAGATACG
CYPBM3_A330P_fwd	GGGAAAACGGAGGAGCAGTTGGCCATAAGCGCAGCGCTTC
CYPBM3_A330P_rev	CTGCTCCTCCGTTTTCCCTATATGCAAAAGAAGATACGGTGCT
CYPBM3_A74F_fwd	AAATTTAAGAAATTGACTTAAGTTTTTATCAAAGCGTGATTCATC
CYPBM3_A74F_rev	AAGTCAATTTCTTAAATTTGTACGTGATTTTGCAGGAGACGGG
CYPBM3_A74G_fwd	AATTTAAGGCCTTGACTTAAGTTTTTATCAAAGCGTGATTCAT
CYPBM3_A74G_rev	AAGTCAAGGCCTTAAATTTGTACGTGATTTTGCAGGAGACGGG
CYPBM3_A82L_fwd	CGTCTCCCAGAAAATCACGTACAAATTTAAGCGCTTGACTTAA
CYPBM3_A82L_rev	GTGATTTTCTGGGAGACGGGTTATTTACAAGCTGGACGCATGA
CYPBM3_D251G_fwd	AATGTTCTCGCCATCAAGCGGCTCACCCGTTTCTGGATCTTTT
CYPBM3_D251G_rev	CTTGATGGCGAGAACATTCGCTATCAAATTATTACATTCTTAA
CYPBM3_F87A_fwd	CAGCTTGTAGCTAACCCGTCTCCTGCAAAATCACGTACAAATT
CYPBM3_F87A_rev	CGGGTTAGCTACAAGCTGGACGCATGAAAAAAATTGGAAAAAA
CYPBM3_L188C_fwd	CTCGCTGGCACTTGTTCATTGCTTCATCCAGTGCACGGACCAT
CYPBM3_L188C_rev	TGAACAAGTGCCAGCGAGCAAATCCAGACGACCCAGCTTATGA
CYPBM3_L437F_fwd	TTAACGTAAAAGTTTCTTTAATATCCAGCTCGTAGTTTGTATG
CYPBM3_L437F_rev	AAGAAACTTTTACGTTAAAACCTGAAGGCTTTGTGGTAAAAGC
CYPBM3_L75T_fwd	ACAAATTTGGTCGCTTGACTTAAGTTTTTATCAAAGCGTGATT
CYPBM3_L75T_rev	TCAAGCGACCAAATTTGTACGTGATTTTGCAGGAGACGGGTTA
Middle_CYPBM3_fwd	TGAAGCTCCACGTATTGCAGAAGCT
Middle_CYPBM3_rev	AAAAGATCCAGAAACGGGTGAGCC
pET28b_amplify_fwd	GGTATATCTCCTTCTTAAAGTTAAAC
pET28b_amplify_rev	GATCCGGCTGCTAACAAAGCCCGAAA
T7 promoter (fwd)	TAATACGACTCACTATAG
T7 terminator (rev)	GCTAGTTATTGCTCAGCGG

2.4 Chemicals

Table 2.7. Chemical reagents. All chemical reagents, their formula or specification, and supplier used in this experimental work are presented in this table.

CHEMICAL	SPECIFICATION	SUPPLIER
4-propyl syringol	$C_{11}H_{16}O_3$	Enamine
4-propyl guaiacol	$C_{10}H_{14}O_2$	Merck

4-propyl phenol	$C_9H_{12}O$	Sigma-Aldrich
Acetonitrile (ACN)	C_2H_3N	Merck
Aminolevulinic acid (5-ALA)	$C_5H_9NO_3$	Merck
Bradford reagent (Bio-Rad Protein Assay Dye Reagent Concentrate)	Colorimetric assay dye, concentrate	Bio-Rad
Dithionite	$O_4S_2^{-2}$	Merck
Ethanol	C_2H_6O	VWR
Etylendiamintetraacetat (EDTA)	$C_{10}H_{16}N_2O_8$	Merck
Glycerol	$C_3H_8O_3$	Merck
Indole	C_8H_7N	Merck
Isopropyl β-D-1-thiogalactopyranoside (IPTG)	$C_9H_{18}O_5S$	Thermo Fisher Scientific
Kanamycin	$C_{18}H_{36}N_4O_{11}$	Sigma-Aldrich
Methanol	CH_3OH	VWR
Nicotinamide adenine dinucleotide phosphate (NADPH)	$C_{21}H_{29}N_7O_{17}P_3$	Merck
Palmitic acid	$C_{16}H_{32}O_2$	Merck
Phenylmethylsulfonyl fluoride (PMSF)	$C_7H_7FO_2S$	Thermo Fisher Scientific
SYBR™ Safe DNA Gel Stain	10 000 × in DMSO	Invitrogen by Thermo Fisher Scientific
Tris	$C_4H_{11}NO_3$	Merck
Tryptone	C_3H_5NO	Gibco by Thermo Fisher Scientific
UltraPure™ Agarose gel	$(C_{12}H_{18}O_9)_n$	Invitrogen by Thermo Fisher Scientific

Table 2.8. Buffers, solutions, and media for growth. This table is divided into three main groups, and all groups are presented with each component's application and specification.

COMPONENT	APPLICATION	SPECIFICATION
Buffers		
Loading buffer	Preparation and loading of protein samples onto gel for SDS-PAGE analysis	▪ 500 µL LDS Sample buffer ▪ 200 µL Reducing Agent ▪ 300 µL Milli-Q water
Tris, acetate, EDTA (TAE) buffer [1x]	DNA electrophoresis buffer for PCR screening	▪ 40 mM Tris ▪ 20 mM acetic acid ▪ 1 mM EDTA
Tris, glycine, SDS buffer [1x]	SDS-PAGE running buffer used for SDS-PAGE	- 25 mM Tris - 192 mM glycine - 0.1% SDS (w/v)
Tris/HCl pH = 8 [1 M stock]	Stock solution ○ Equilibration buffer for HIC (AEX) ○ Storage buffer	▪ 121.1 g Tris ▪ HCl until wanted pH ▪ Milli-Q water until 1 L
Tris/HCl pH = 8 [50 M stock] with 1 M NaCl	Stock solution ○ Elution buffer for HIC (AEX)	▪ 50 mL Tris/HCl pH [1 M stock] ▪ 58.44 g NaCl ▪ HCl until wanted pH ▪ Milli-Q water until 1 L
Phosphate buffer pH = 7/8 [100 mM]	Stock solution ○ Addition to TB media ○ Storage buffer	▪ 0.17 M KH_2PO_4 ▪ 0.72 M K_2HPO_4
Media for growth		
Luria-Bertani (LB) broth	-	▪ 5 g/L tryptone ▪ 5 g/L sodium chloride (NaCl) ▪ 2.5 g/L yeast extract ▪ Distilled water (500 mL) ▪ LB agar: 15 g/L agar for solid media
Terrific broth (TB)	-	▪ 20 g/L tryptone ▪ 24 g/L yeast extract ▪ 4 mL glycerol ▪ Distilled water (900 mL)
Solutions		
Super Optimal broth with Catabolite repression (SOC media)	Addition to transform competent cells (*E. coli* TOP10)	▪ 2% (w/v) Bacto-tryptone ▪ 0.5% (w/v) Bacto-yeast extract ▪ 10 mM Sodium chloride ▪ 2.5 mM Potassium chloride (KCl)

		▪ 10 mM Magnesium sulfate (MgSO4) ▪ 10 mM Magnesium chloride (MgCl2) ▪ 20 mM Glucose Not self-made (https://www.laboratorynotes.com/preparation-of-soc-super-optimal-broth-with-catabolite-repression-medium/)
Taq Master Mix	Red Taq DNA Polymerase Master Mix used in colony-study by plasmid PCR	▪ Tris-HCl pH 8.5, (NH4)2S04, 3.0 or 4.0 mM MgCl2*, 0.2 % Tween® 20 ▪ 0.4 mM of each dNTP ▪ 0.2 units/µl VWR Taq polymerase ▪ Inert red dye and a stabilizer Bought from VWR, not self-made (https://no.vwr.com/assetsvc/asset/no_NO/id/21936874/contents)
Trace element solution	Catalyst in enzyme systems	▪ 1100 mg/L FeCl3 x6H2O ▪ 50 mg/L CuSO4 x5H2O ▪ 200 mg/L HBO3 ▪ 200 mg/L MnSO4 xH2O ▪ 80 mg/L Na2MoO4 x2H2O ▪ 60 mg/L CoCl2 x6H2O ▪ 90 mg/L ZnSO4 x7H2O ▪ 10 mg/L Na2SeO4 Not self-made (https://protocols.scienceexchange.com/protocols/msm-trace-element-te-solution)
Q5® High-Fidelity Master Mix	Q5® High-Fidelity Master Mix used for high-fidelity amplification	Bought from New England Biolabs Inc., not self-made (https://international.neb.com/products/m0492-q5-high-fidelity-2x-master-mix#Product%20Information)

3 METHODS

3.1 Site-directed Mutagenesis

Site-directed mutagenesis was performed together with Dr. Gabriela Schröder, Dr. Kelsi Hall and Ph.D. candidate Marta Barros to determine amino acids involved in the region-selectivity and kinetics of derived-monolignol oxidations. For that, 11 single mutations were selected based on structural and chemical properties and on similar activities reported in previous papers:

1. Ala184Phe: Alanine 184 to Phenylalanine (Ellis *et al.*, 2021; Wolf *et al.*, 2022)
2. Phe87Ala: Phenylalanine 87 to Alanine (Li *et al.*, 2001)
3. Ala82Leu: Alanine 82 to Leucine (based on structural and chemical enzyme properties)
4. Leu75Thr: Leucine 75 to Threonine (based on structural and chemical enzyme properties)
5. Ala74Gly: Alanine 74 to Glycine (Appel *et al.*, 2001)
6. Leu437Phe: Leucine 437 to Phenylalanine (Klaus *et al.*, 2019; Seifert *et al.*, 2011)
7. Ala328Leu: Alanine 328 to Leucine (Klaus *et al.*, 2019; Seifert *et al.*, 2011)
8. Ala330Pro: Alanine 330 to Proline (Munday *et al.*, 2017)
9. Asp251Gly: Aspartic Acid 251 to Glycine (Tsotsou *et al.*, 2012)
10. Leu188Cys: Leucine 188 to Cysteine (Appel *et al.*, 2001; Neufeld *et al.*, 2013)
11. Ala74Phe: Alanine 74 to Phenylalanine (Appel *et al.*, 2001)

3.1.1 Building the Vector

Plasmid pET28b (5206 bp) containing CYPBM3 wild type (3150 bp) was employed as a cloning vector. A one-step PCR-based method was performed for substitution mutagenesis based on the procedure from Qi et al., (2008). For that, primers containing the nucleotide substitution were designed and eleven different plasmids were built for each single amino acid mutation (Table 3.1).

Table 3.1. CYPBM3 primers with nucleotide substitution. All the 11 primers designed by using rational design and their respective sequences are listed in this table.

Primer	**Sequence (5' – 3')**
CYPBM3_A184F_fwd	TGTTCATAAATTCATCCAGTGCACGGACCATACTTGTAATAAA
CYPBM3_A184F_rev	TGGATGAATTTATGAACAAGCTGCAGCGAGCAAATCCAGACGA
CYPBM3_A328L_fwd	AACGCAGGCAGAGTTGGCCATAAGCGCAGCGCTTCGTTTAAGA
CYPBM3_A328L_rev	GCCAACTCTGCCTGCGTTTTCCCTATATGCAAAAGAAGATACG
CYPBM3_A330P_fwd	GGGAAAACGGAGGAGCAGTTGGCCATAAGCGCAGCGCTTC
CYPBM3_A330P_rev	CTGCTCCTCCGTTTTCCCTATATGCAAAAGAAGATACGGTGCT

CYPBM3_A74F_fwd	AAATTTAAGAAATTGACTTAAGTTTTTATCAAAGCGTGATTCATC
CYPBM3_A74F_rev	AAGTCAATTTCTTAAATTTGTACGTGATTTTGCAGGAGACGGG
CYPBM3_A74G_fwd	AATTTAAGGCCTTGACTTAAGTTTTTATCAAAGCGTGATTCAT
CYPBM3_A74G_rev	AAGTCAAGGCCTTAAATTTGTACGTGATTTTGCAGGAGACGGG
CYPBM3_A82L_fwd	CGTCTCCCAGAAAATCACGTACAAATTTAAGCGCTTGACTTAA
CYPBM3_A82L_rev	GTGATTTTCTGGGAGACGGGTTATTTACAAGCTGGACGCATGA
CYPBM3_D251G_fwd	AATGTTCTCGCCATCAAGCGGCTCACCCGTTTCTGGATCTTTT
CYPBM3_D251G_rev	CTTGATGGCGAGAACATTCGCTATCAAATTATTACATTCTTAA
CYPBM3_F87A_fwd	CAGCTTGTAGCTAACCCGTCTCCTGCAAAATCACGTACAAATT
CYPBM3_F87A_rev	CGGGTTAGCTACAAGCTGGACGCATGAAAAAAATTGGAAAAAA
CYPBM3_L188C_fwd	CTCGCTGGCACTTGTTCATTGCTTCATCCAGTGCACGGACCAT
CYPBM3_L188C_rev	TGAACAAGTGCCAGCGAGCAAATCCAGACGACCCAGCTTATGA
CYPBM3_L437F_fwd	TTAACGTAAAAGTTTCTTTAATATCCAGCTCGTAGTTTGTATG
CYPBM3_L437F_rev	AAGAAACTTTTACGTTAAAACCTGAAGGCTTTGTGGTAAAAGC
CYPBM3_L75T_fwd	ACAAATTTGGTCGCTTGACTTAAGTTTTTATCAAAGCGTGATT
CYPBM3_L75T_rev	TCAAGCGACCAAATTTGTACGTGATTTTGCAGGAGACGGGTTA

Primers were purchased from Thermo Fisher Scientific and were resuspended to have a stock concentration of 100 µM. PCR was performed using Q5® High-Fidelity 2X Master Mix (New England, Biolabs Inc.) which contains Q5 High-Fidelity DNA Polymerase, dNTPs, and Mg++ in a broad-use buffer. The reaction mix was prepared using the concentrations specified in Table 3.2. Eleven different reaction mixes were performed containing forward and reverse primers (for mutagenesis), Q5® High-Fidelity 2X Master Mix, and as a template the plasmid pET28b_CYPBM3wt was used. A negative control without the template was also included to look for possible DNA contaminations.

Table 3.2. Reaction mix. Specification of the materials utilized to make this reaction mix and their respective concentration. The CYP primers marked in red are the 11 different primers presented in Table 3.1.

Component	**Final Concentration**
CYPBM3_fwd for mutagenesis	10 µM
CYPBM3_rev for mutagenesis	10 µM
Q5 High-Fidelity master mix 2x	1x
Plasmid pET28b_CYPBM3wt	1 ng
mQ-water	-

PCR was performed with the conditions listed in Table 3.3. The annealing temperature for each pair of primers was determined according to nucleotide length and %GC using the NEB TmCalculator (New England, Biolabs Inc.).

Table 3.3. Polymerase Chain Reaction (PCR) conditions. The temperature (°C) and the number and duration of each cycle are specified for the different PCR steps. For the annealing step, two different temperatures were set up according to length and %GC of the primer.

PCR steps	Temperature (°C)	Number of cycles and duration of each cycle	
1. Initial denaturation	98	1	30 sec
2. Denaturation	98	1	10 sec
3. Annealing	57/63	1	30 sec
4. Extension	72	28	6 min
5. Final extension	72	1	2 min

Unspecific annealing of the primers could result in undesired products. To confirm the size of the amplified products, agarose gel electrophoresis was run after PCR. Electrophoresis allows the separation of DNA by size, where smaller molecules travel faster than large ones. A voltage is applied and negatively charged molecules move along the gel according to the number of base pairs.

An agarose gel was prepared with 0.8% UltraPure™ Agarose powder and TAE buffer [1x] by heating in the microwave until the powder was dissolved. SYBR™ Safe DNA Gel Stain (Thermo Fischer Scientific) (10 000x) was added (1x) in order to visualize DNA by UV-excitation. Once the agarose matrix was solidified, samples (previously mixed 1:1 with Gel Loading Dye (6x)) were loaded in the wells. GeneRuler DNA ladder (Thermo Fisher Scientific) was also loaded in one of the wells to be able to determine the DNA size. MiniSub Cell GT system was run at 110 V for 20 min. DNA bands were visualized using GelDoc Go Gel Imaging System as presented in Figure 3.1.

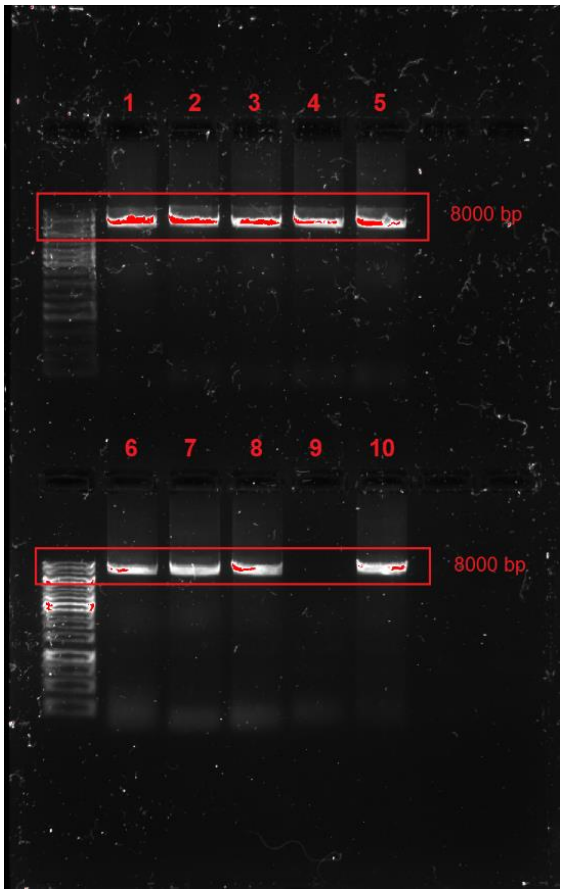

Figure 3.1: Building the vector of CYPBM3 with site-specific mutagenesis in plasmid pET28b. *The gel is showing the primers after the first PCR run, where the wish was to check if the DNA had the size of 8356 bp. All the primers are marked with a number from 1 to 10, a ladder is included in the well on the left for every gel. Primer 9 had no visible band in the first run and was therefore run on another gel with primer 11 and a negative control.*

Once the correct size of DNA products was verified, the DNA was cleaned from small DNA fragments and nucleotides and concentrated using the DNA Clean & Concentrator™-5 kit (ZYMO RESEARCH). DNA Binding Buffer was applied to each DNA sample, and the mixture was transferred to a Zymo-Spin™ Column in a Collection tube. The tubes were centrifuged for 30 seconds, flow-through was discarded and DNA Wash Buffer was then added to the column. The tubes were centrifuged for another 30 seconds, and the washing step with the DNA Wash Buffer was repeated twice. To dry the filter the tubes were spun for 2 min, and prewarmed mQ-water was applied to the columns to elute the DNA. After 1 min of incubation at room temperature, columns were spun one last time for 30 seconds and the DNA was eluted and collected in microcentrifuge tubes. DNA concentration was then measured by the absorbance at 260 nm (A260) wavelength using the NanoDrop™ One.

3.2 Transformation of Chemically Competent Cells: *E. coli* TOP10 and *E. coli* BL21

3.2.1 *E. coli* TOP10 Transformation

OneShot TOP10 chemically competent cells (Thermo Fisher Scientific) were employed to obtain high transformation efficiency. Initially, the linear plasmid was centrifuged and kept on ice together with the vial containing the *E. coli* TOP10 strain that was thawed on ice. Then 2 µL of the linear plasmid was added and mixed by tapping gently. After the vial had been kept on ice for 30 minutes, it was incubated at 42°C in a water bath for 30 seconds, and then, it was kept on ice again for 1 minute. Under sterile conditions, 250 µL of prewarmed SOC media (Super Optimal broth with Catabolite repression) was added to the cells and then incubated at 37° for 1 hour and at 225 rpm. Each transformant was spread on LB agar plates with 50 µg/mL kanamycin and incubated at 37° overnight.

3.2.2 Colony Study by Plasmid PCR

To verify that the transformation was successful and that the colonies contained the plasmid with the gene of interest, PCR was performed. Two-three colonies were picked from each of the eleven transformants, and a negative control was also included. Selected colonies were labeled for further plasmid isolation. Taq 2X Master Mix (New England, Biolabs Inc.) containing Taq DNA Polymerase, dNTPs, $MgCl_2$, KCI, and stabilizers was employed. A reaction mix was prepared using the concentrations specified in Table 3.4. To amplify only the gene of interest, T7 promotor, and terminator primers were employed since they are surrounding the gene. Reactions were performed with PCR conditions listed in Table 3.5. Annealing temperatures were selected in accordance with the T7 primers, and for the extension step, duration was set based on the length of the gene (3147 bp). The PCR products were run on a 1% agarose gel to confirm the presence of the gene.

Table 3.4. Reaction mix. Specification of the materials utilized to make this reaction mix and their respective concentration.

Component	**Final Concentration**
T7 promoter (fwd)	0.5 µM
T7 terminator (rev)	0.5 µM
Taq master mix 2x	1x
mQ-water	-

Table 3.5. Polymerase Chain Reaction (PCR) conditions. The five steps of the PCR are also specified with temperature in Celsius, number of cycles + duration of each cycle. The temperature in the annealing step is the temperature for the T7-primers.

PCR steps	Temperature (°C)	Number of cycles and duration of each cycle	
1. Initial denaturation	95	1	30 sec
2. Denaturation	95	1	10 sec
3. Annealing	50	1	30 sec
4. Extension	72	30	3 min, 20 sec
5. Final extension	72	1	5 min

3.2.3 MiniPrep Plasmid Extraction

Once gene length was confirmed, corresponding colonies were grown overnight in 5 mL LB media and kanamycin (50 µg/mL) at 37°C and 200 rpm. 500 µL of the culture was employed for glycerol stocks (50% glycerol), which were kept at -80°C.

From the rest of the culture, the plasmid was extracted. For this the E.Z.N.A.® Plasmid DNA Mini Kit I was employed. The culture was centrifuged for 1 minute, at 10 000 xg and room temperature with the Centrifuge 5430/5430 R - High-Speed Centrifuge and the Eppendorf F-35-6-30 Rotor. For the other centrifugations performed in this plasmid extraction, the Eppendorf™ MiniSpin™ centrifuge was employed. Culture media was discarded after centrifugation and Solution I with RNase A was added and vortexed. The suspensions were then transferred into new microcentrifuge tubes, and Solution II was applied to all the samples. To mix the liquids the tubes were gently inverted and incubated for 2-3 minutes (maximum 5 minutes) to obtain a clear lysate. After the addition of Solution III to all the samples, the tubes were inverted immediately until the solutions formed flocculent white precipitates. The tubes were centrifuged at maximum speed for 10 minutes to form a compact white pellet. The supernatants were transferred to HiBind® DNA Mini Columns that were placed into collection tubes. These tubes, with columns, were centrifuged at maximum speed for 1 minute, the filtrates were discarded, and the collection tubes were reused. To wash the samples HBC Buffer diluted with 100% isopropanol was added to each tube. The tubes were centrifugated at maximum speed for 1 minute, the filtrates were discarded, and the collection tubes were once again reused. DNA Wash Buffer diluted with 100% ethanol was now added to the samples, which were centrifuged at maximum speed for 30 seconds, and the filtrates were discarded. The collection tubes were reused for another repetition of the washing step with DNA Wash Buffer. To dry

the columns and get rid of trace ethanol that could interfere with downstream applications, they were centrifuged at maximum speed for 2 minutes. The columns were placed in clean, nuclease-free microcentrifuge tubes, and the DNA was eluted with prewarmed mQ-water by first letting the tubes sit at room temperature for 1 minute and then centrifuging them at maximum speed for 2 minutes.

The plasmids were sent to eurofins Genomics for sequencing. For that, the concentration of the plasmids was measured with NanoDrop™ One. The final plasmid concentration required for sequencing was 50-100 ng/µL. The following primers (5 µM) were used in order to cover all of the gene sequence: Middle_CYPBM3_rev, Middle_CYPBM3_fwd, T7_promoter, and T7_terminator.

3.2.4 *E. coli* BL21 Transformation

BL21 (DE3) Competent Cells (Thermo Fisher Scientific) was transformed to be used for protein expression. The transformation was performed following the commercial guidelines from Thermo Fisher Scientific. The PCR screening was repeated under the same conditions as in 3.2.2 “Colony Study by Plasmid PCR”.

3.2.5 Expression Test

To confirm that transformation was performed correctly, and that the protein is expressed, an expression test was performed at a smaller scale for CYPBM3wt. For that, cells were precultured in 5 mL LB media with kanamycin (50 µg/mL) and incubated overnight at 37°C and 200 rpm in the Multitron Standard incubator.

Preculture (1:100) was used to inoculate 150 mL of Terrific Broth (TB) media with kanamycin (50 µg/mL) and trace elements. The culture was incubated at 37°C and 200 rpm until absorbance (OD600) reached a value between 0.7-1. Right after, induction was initiated. For that, 1 mM Isopropyl β-D-1-thiogalactopyranoside (IPTG) and 0.5 mM Aminolevulinic acid (5-ALA) were added to the culture. IPTG mimics allolactose, a lactose metabolite that triggers transcription of the lac operon, and 5-ALA serves as a precursor for the heme cofactor. The temperature was decreased to 25°C to induce growth arrest and ensure a more efficient protein expression. Protein expression was conducted overnight.

Cells were harvested by centrifugation, and for that, the culture was transferred to 1 L Nalgene™ Super-Speed Centrifuge Bottles, and centrifugation was performed at 5000 xg for 20 minutes at 4°C operating the Sorvall LYNX 6000 Superspeed Centrifuge. After

centrifugation, the supernatant was discarded and cells were resuspended in 25 mL buffer lysis (25 mM Tris-HCl buffer (pH 8), 0.5 mg/mL lysozyme, and 31.25 µM PMSF). Cells were lysed by sonication using Sonics 130-Watt Ultrasonic Processors at 30% amplitude, for 5 min, with cycles of 30 seconds. During sonication, cells were kept in ice to alleviate the heat denaturation of proteins. Subsequently, to remove cell debris, the lysate was transferred to 50 mL Nalgene™ High-Speed Centrifuge Tubes and centrifuged at 20 000 xg for 30 minutes at 4°C with the LYNX 6000 centrifuge.

To confirm protein expression, the cell lysate was run on an SDS-PAGE Electrophoresis gel. For that, the Mini-PROTEAN Tetra Vertical Electrophoresis Cell, the Mini-PROTEAN Tetra Vertical Electrophoresis for Handcast Gels, and the Mini-PROTEAN TGX Stain-Free Precast Gel were employed. The lysate was mixed with a Loading buffer (1:1) containing LDS Sample buffer, Reducing Agent, and mQ-water, and incubated on the T100™ Thermal Cycler at 95°C for 5 minutes. After centrifugation, using the MiniStar Microcentrifuge, samples were loaded into the wells of the gel, and SDS buffer (1x) containing 25 mM Tris, 192 mM acetic acid, and 1 mM EDTA was applied to the Electrophoresis Cell. An Unstained Protein Standard ladder (New England Biolabs Inc.) was loaded to determine the size of proteins. The cell was coupled to a PowerPac™ Basic Power supply, and the gel was run at 200 V for 30 min. The results were analyzed using the GelDoc Go Gel Imaging System.

3.3 Initial Screening Assays on Cell Lysate and Selection of Best Candidates

3.3.1. Protein Expression in 96 well-plates

This protocol was designed based on the paper from Lewis *et al.*, (2009) with slight changes. *E. coli* BL21 transformants for WT and the 11 mutants were grown in Corning™ 96 well Microtiter Microplates (200 µL) on LB media with kanamycin (50 µg/mL). Incubation was performed overnight at 37°C and 500 rpm. Preculture (50 µL) was utilized to inoculate 600 µL TB-media with kanamycin (50 µg/mL) and trace element solution – for that, a Polypropylene 2 mL Deep 96 Well Plate was employed. Cells were grown for 4 hours at 37°C and 700 rpm. Protein expression was induced with IPTG (1 mM) and 5-ALA (0.5 mM). Expression was conducted overnight at 25°C and 800 rpm.

Cells were collected by centrifugation using the M10 Microplate Swinging Bucket Rotor and the 5430/ 5430 R - High-Speed Centrifuge at 4°C and 3000 xg for 15 minutes. To facilitate cell

lysis, pellets were kept at -20℃ for 2 hours. For protein extraction, the pellets were thawed at room temperature for 30 minutes, and the cells were resuspended in lysis buffer (50 mM phosphate buffer pH 7, 1.5 mg/mL lysozyme, 31.25 µM PMSF and 0.02 mg/mL DNase) and incubated at 37℃ for 1 hour. Cell debris was removed by centrifugation, and supernatants were transferred to 200 µL 96 well microtiter microplates. Finally, to confirm protein expression and extraction, cell lysates were run on an SDS-PAGE gel, as explained in 3.2.5 “Expression Test”.

3.3.2. NADPH Depletion Assay

CYPs require electrons from an electron donor to catalyze oxidation (Behrendorff, 2021). NADPH works as an electron donor for CYBM3, and in its reduced form absorbs light at 340 nm. Measuring the absorbance makes it possible to follow electron consumption by observing the decrease in absorbance at 340 nm. Electron depletion could be related to the oxidation of monolignols. For that, with this assay, a preliminary screen could be done to check for possible activities of the different mutants with the three different monolignols.

The conditions employed in this assay were 50 mM Phosphate buffer (pH 8), 5 mM substrate, and 0.2 mM NADPH in addition to 25 µL cell lysate with a final volume of 100 µL per well. NADPH consumption was measured by operating the Varioskan LUX Multimode Microplate Reader, for 10 minutes with intervals of 10 seconds. The three different monolignols; 4-propyl phenol (4-PP), 4-propyl guaiacol (4-PG), and 4-propyl syringol (4-PS) were tested. Palmitic acid, which is a fatty acid that works as a natural substrate for CYPBM3, was used as a positive control. As a negative control, 70% ethanol was employed instead of the substrates since stock substrates are dissolved in 70% ethanol, leaving the final concentration of the assay at 3.5%. Cell lysate for a transformant with an “empty” plasmid (without CYPMB3 gene) was also employed as a negative control.

Three parallels of the 11 mutants, WT, and empty plasmid were analyzed, together with three wells without supernatant, which served as a third negative control. One microtiter microplate was utilized for each of the four substrates (4-PP, 4-PG, 4-PS, and palmitic acid) and for the negative control (70% ethanol). The plate design is presented in Figure 3.2.

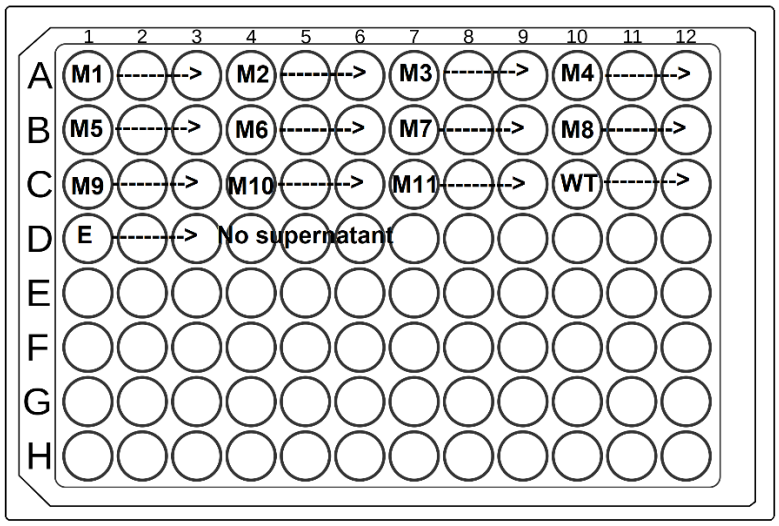

Figure 3.2: Plate design for NADPH depletion assay with CYPBM3 mutants, WT, and empty plasmid. *This plate design was used when measuring the NADPH depletion for the mutants and the WT. Each mutant was measured in three parallels, and so was the WT. Row D contains three parallels of the "empty" supernatant – the supernatant with no CYPBM3, and three parallels of samples without the supernatant at all.*

The same samples were also used for the initial MS analysis and indole oxidation of the mutants.

3.3.3 Indole Oxidation

Indigo formation via indole oxidation has been widely used to screen for oxidations in CYP mutagenesis studies. It has also extensively been used as a surrogate molecule for phenolic compounds in CYPs (Whitehouse *et al.*, 2008). The oxidation of indole makes the products indigo and indirubin (Lamb *et al.*, 2007). While the indole itself is colorless/slightly yellow, the indigo product is purple and can be determined both by the naked eye and by measuring the absorbance at 620 nm.

The same plate design as Figure 3.2 was employed when performing the indole oxidation. In this assay, one plate with 50 mM phosphate buffer (pH 8), 25 µL cell lysis, 0.5 mM NADPH, and 0.2 mM indole with a final volume of 100 µL was utilized. The plate was measured using the same microplate reader as mentioned in paragraph 3.3.1, and absorbance was measured at 620 nm for 30 min to track the formation of the indigo product.

3.3.4 MS Analysis

To determine CYPs activity on monolignols, reactions with the different mutants and substrates were set up. Possible product formation was determined by mass spectrometry. Reaction conditions are listed in Table 3.6. Samples were incubated in the ThermoMixer C at 20℃, 750 rpm overnight.

Before running the MS system, samples were filtered using 0.45 µM filters and transferred to high-performance liquid chromatography (HPLC) vials with caps. Table 3.6 presents the concentrations of each component utilized in the MS analysis.

Table 3.6. Concentrations of reagents used in reactions for MS analysis. This table presents all the components used in the samples for the MS analysis together with the concentration of each component. For the lysate of CYPBM3wt and mutants, the concentrations were not measured and are therefore not represented in this table.

Reagents	**Concentration (mM)**
CYPBM3 lysate	25 µL
NADPH	2
Substrate (PA, 4-PP, 4-PG and 4-PS)	1
Phosphate buffer (pH 7)	50
mQ-water	To reach a final volume of 200 µL

The Thermo LTQ Velos Pro MS/MS system with an ESI source working in the negative mode was used for the mass spectrometric analysis. Nitrogen was used as a nebulizer and collision gas. The optimal mass spectrometer parameters were determined experimentally, and these parameters were Heater Temp (°C) 200.00, Sheath Gas Flow Rate 12, Aux Gas Flow Rate 5, Sweep Gas Flow Rate 0, I Spray Voltage (kV) 3.00, Spray Current (µA) 0.46, Capillary Temp. (°C) 275.00, and S-Lens RF Level (%) 69.2. As a solvent, a 1:1 acetonitrile:water solution with ammonium hydroxide (NH_4OH), pH 9 was employed with a flow rate of 0.3 mL/min.

To determine the reaction products, FullScan spectra (MS) were employed, with a Scan Rate of m/z 60-260. The Thermo Scientific Xcalibur 4.5 software was used to set the sequence. For data acquisition and analysis Thermo Xcalibur Qual Browser 4.5 was employed.

3.3.5 Selection of Best Candidates

Cell lysates for all 11 mutants and the wild type were run on an electrophoresis gel. ImageJ was employed to quantify the protein bands' intensity from the electrophoresis gel to determine which mutants showed better expression efficiency (OpenWetWare, n.d.).

Initially, the band with the lowest concentration of body surface area (BSA) was decided. When the bands had been numbered from lowest to highest concentration of BSA, the results were plotted into histograms as inverted peaks. After defining the areas of the peaks, the results presented in a table were transferred to Microsoft Office Excel. The area of the wild type was set as the standard, and the other mutants' peak percentages were calculated from this standard.

The bands that were stronger than the wild type got a percentage higher than 100%, but the reasoning behind using ImageJ was to check if the band intensity indicated high expression of protein or just a high amount of protein. For the next step, the slopes of each monolignol (palmitic acid, 4-PP, 4-PG, and 4-PS) observed in the NADPH depletion assay for each mutant were calculated from the decrease in absorbance. Finally, the rates between the peak area of each mutant compared to the wild type were calculated using the values from ImageJ's band-intensity results and dividing them by the slopes of each monolignol.

The mutants that showed high rates from the ImageJ-quantification, or at least 50% expression of the wild type, and that additionally showed good results in the other experiments done measuring the initial activity with the monolignols (NADPH depletion assay and MS analysis), were chosen for further analysis. These mutants were M1, M5, and M7.

3.4 Expression and Purification of CYPBM3

3.4.1 Expression of CYPBM3

After the screening test, three mutants were chosen for further purification and characterization. For that, selected mutants and wild type were expressed using *E. coli* BL21 transformants. The procedure was performed as in 3.2.5 "Expression Test" with slight differences. Higher culture volumes were employed (400 mL) to obtain the desired amount of protein. After protein extraction, CYPBM3 was purified.

3.4.2 Purification of CYPBM3 Wild Type and Mutants

To separate the protein of interest from the rest of the proteins, anion exchange chromatography (AEX) was employed. AEX uses an exchange resin with a positive charge that has an affinity for molecules with a negative charge (Bio-Rad, n.d.). When the pH is above the isoelectric point (pI) of the protein, the latter will have a net negative charge (Bio-Rad, n.d.). The positively charged resin and the proteins' pIs will determine the different protein binding strengths. A salt gradient is employed to elute proteins based on their net surface charge; therefore, proteins will be separated based on different salt concentrations (Bio-Rad, n.d.).

The purification system operated was the NGC Chromatography System (ÄKTA). The column employed was the HiTrap® Q HP (High Performance) column, 5 mL (Cytiva), which is a strong anion exchanger that remains fully charged during the purification process, giving an effective

protein separation (McSweeney, 2021). The column was equilibrated with 50 mM Tris-HCl (pH 8) buffer. The isoelectric point of CYPBM3 is 5.22, therefore, at the chosen pH buffer of 8, CYPBM3 will have a negative net charge. For the salt gradient, 1M NaCl in 50 mM Tris-HCl buffer (pH 8) was used.

Before loading in the column, cell lysate and buffers were filtered through 0.45 µM filters. The salt gradient was, first, set to 0-8% of 1M NaCl to remove unwanted proteins. Then, the gradient was increased to 25% and the collection of fractions started, whereas CYPBM3 was eluted around 35% (35 mM NaCl). Finally, the gradient was increased to 100% NaCl to regenerate the column and remove any molecules still bound.

Figure 3.3 presents a visualization of the purification of mutant 5 (M5). The salt gradient is represented with the orange line and the UV peaks are represented with the blue line. The fractions collected are marked with grey vertical lines.

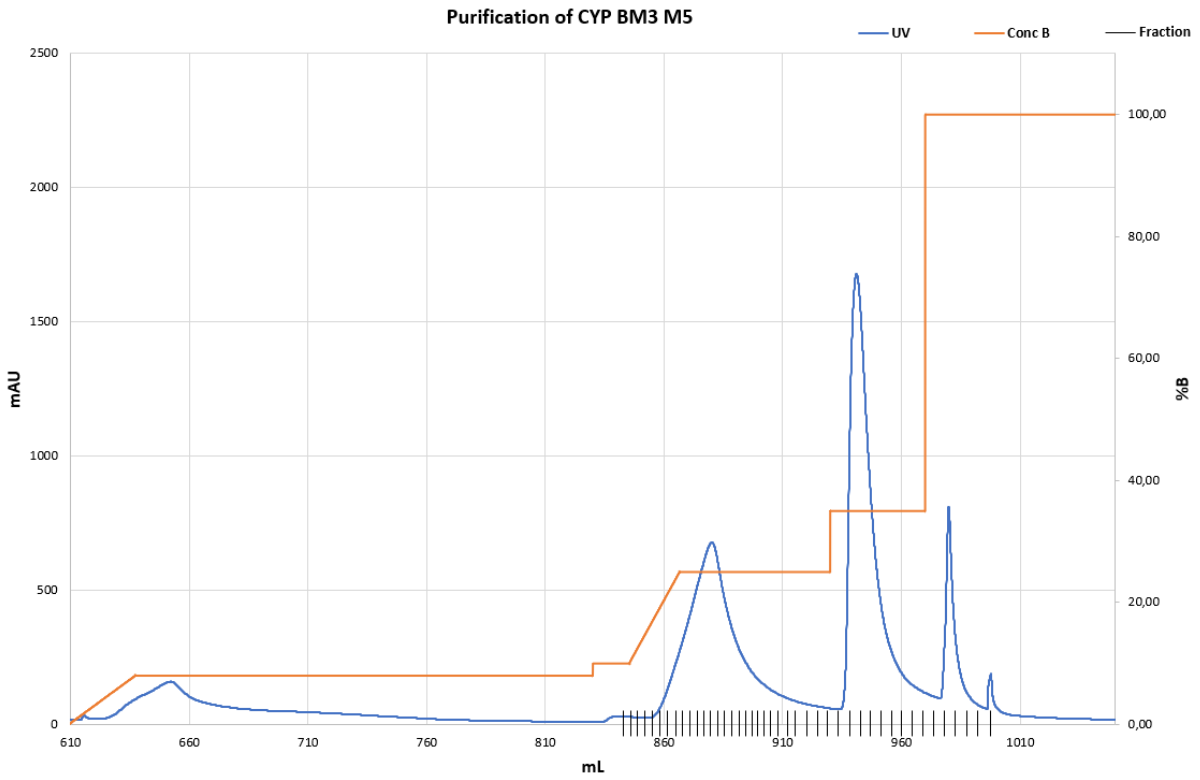

Figure 3.3: Purification of CYPBM3 M5 with stepwise gradient. *Mutant 5 was purified using a stepwise gradient. When the gradient – orange – is increased, the UV – blue – increases in the form of peaks. These peaks indicate the elution of protein. Fractions (grey) were collected from the gradients 25%, 35%, and 100%.*

SDS-PAGE Electrophoresis was employed to determine the presence and purity of the protein at the different stages of the purification. For that, fractions from the three different peaks

(Figure 3.3) observed in the chromatogram were selected. Results were analyzed with the GelDoc Go Gel Imaging System to determine which fractions to keep and concentrate.

The different fractions with pure protein were concentrated with Amicon™ Centrifugal Filter Units (30 kDa cutoff). Filters were washed with mQ-water before the proteins were concentrated to remove traces of glycerin. Centrifugation was performed at 4°C, 5000 xg for approximately 2 hours. Centrifuge 5430/ 5430 R - High-Speed with an Eppendorf F-35-6-30 Rotor was employed. Concentrated proteins were kept in the fridge for further use.

3.5 Characterization of Pure Wild Type and Mutants

3.5.1 NADPH Depletion Assay

Electron consumption could be related to monolignol oxidation by CYP. For that, NADPH depletion was measured along the time by tracking the absorbance at 340 nm. The NADPH depletion was measured in two parallels for each of the three mutants and WT, with each of the three monolignols and Palmitic acid as a positive control. As a negative control, 70% ethanol was added instead of substrate. Concentrations used can be found in section 3.3.2 "NADPH Depletion Assay", however, in this instance, 2.5 µM of pure protein was added instead of cell lysate. Pure mutants and WT concentrations were measured using the NanoPhotometer® C40. The wavelength utilized was 418 nm (heme group absorbance at the soret band). Concentrations were calculated using The Beer-Lambert Law: $\mathbf{A = \varepsilon * l * c}$. **A** equals the absorbance at the wavelength (418 nm), **l** equals the path length of the light through the cuvette (1 cm), and **ε** equals the extinction coefficient (105 $mM^{-1}cm^{-1}$). Using this formula, the concentrations (**c**) were determined.

3.5.2 Binding Assay

To determine possible binding of the different substrates to the catalytic center, the absorbance of the heme group was measured. When no substrate is present, the heme group has a low spin state at 390 nm (G. Schröder, personal communication, 21st of March 2023). When the substrate binds to the active site water is removed, and the heme group will go from a low spin state to a high spin state. In this high spin state, the absorbance will have increased to 418 nm.

NanoPhotometer® C40 and Hellma® absorption cuvettes were employed. The shift could vary, but the absorbance after the substrate binding should be around 418 nm. For the binding assay,

a solution mix was made consisting of the four components: CYPBM3 (WT and mutants), 50 mM phosphate buffer (pH 8), mQ-water, and substrate (4-PP, 4-PG, 4-PS, and PA).

Initially, the absorbance of the enzyme (without substrate) was measured. The protein concentration employed was around 7 µM for all enzymes.

By adding 1 µL of substrate to each measurement, a concentration of 246 µM was incrementally achieved. After the addition of the substrates, a spectrum was recorded. The addition of 1 µL of substrate was repeated until a shift in the soret band was observed.

3.5.3 MS Analysis

For this MS analysis, two replicates of each sample were made to check if the results were valid. Reactions were set with the three selected mutants (M1, M5, M7) and wild-type for each of the substrates (4-PP, 4-PG, and 4-PS) and 70% ethanol as a negative control. Another negative control was tested, where phosphate buffer was added instead of the enzymes. There was a total of 40 reactions, including replicates. The concentrations of the reactants used in each reaction are listed in Table 3.7.

Table 3.7. Concentrations of reactants used in samples for MS analysis. This table presents concentrations of the reactants used in the reactions for the MS analysis.

Component	**Concentration (mM)**
CYPBM3 (M1, M5, M7 and WT)	5 µM
NADPH	2 mM
Substrate (PA, 4-PP, 4-PG and 4-PS)	1 mM
Phosphate buffer (pH 7)	50 mM
mQ-water	To reach a final volume of 200 µL

All the reactions were incubated overnight and filtered as described in 3.3.4 “MS Analysis”. This MS analysis was also run similarly to the MS analysis described in paragraph 3.3.4, but this time there was also performed a fragmentation analysis. To determine the reaction product, FullScan (m/z 60-260) was employed. To do the MSMS fragmentation analysis, a Normalized Collision Energy of 26.0 was utilized together with the conditions: Parent Mass (m/z) 151.00, Act. Type CID, Iso. Width (m/z) 0.5, Act. Q 0.250, and Act. Time (ms) 30.00.

Depending on the MS of the product, standards corresponding to that mass were employed. Since hydroxylation of 4-PP was observed, the 5 different isomers (Figure 3.4) for the hydroxylation of 4-PP (4-(3-hydroxypropyl)phenol, 4-(2-hydroxypropyl)phenol, 4-1-hydroxy

propyl phenol, 4-propylbenzene-1,3-diol, and 4-propylbenzene-1,2-diol) were run in the MS and fragmentation pattern was obtained in order to be able to determine which isomer it was obtained in the enzymatic reaction.

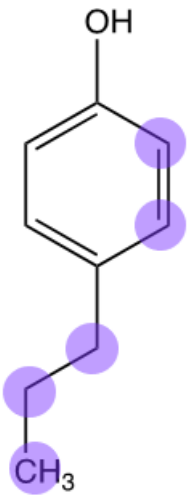

4-propyl phenol

Figure 3.4: Hydroxylation sites of 4-PP. *The 5 hydroxylation sites of 4-PP that can result in different isomers in the MS scan are presented in this figure.*

4 RESULTS

4.1 Site-directed Mutagenesis

4.1.1 Selected Mutations

To alter the substrate specificity of CYPBM3 P450, rational site-specific mutagenesis was chosen as a strategy. The mutations that were performed in this project were based on sites that showed successful applications in other studies and were, therefore, used as a precedent for this study. These previous works were mutagenesis studies where the substrate utilized was substituted benzene similar in structure to the monolignols of interest. The rationale used was that if the mutations utilized in previous studies successfully altered the regioselectivity of substrates with a similar chemical structure, the same achievement may be possible with the chosen monolignols. Presented in Table 4.1 are the 11 different residues targeted for mutations and the role these residues play in CYPBM3 to reshape the specificity of the enzyme to fit the three monolignols. The mutations are split into three main groups according to their location: channel access, binding pocket, and long range.

Table 4.1. The CYPBM3 residues with their mutations and their roles. The 11 mutations, their respective BM3 residues, and their role in this study are presented in this table. The three main groups that the mutations are divided into in this paragraph are marked in pink (channel access), blue (binding pocket), and yellow (long range).

BM3 residue	Mutation	Role
Leu188	Cys	Entrance channel
Ala328	Leu	Hydrophobic binding pocket
Leu437	Phe	Active site hydrophobic pocket (β4-sheet)
Ala330	Pro	Opens active site
Phe87	Ala	Active site mediates substrate specificity
Ala74	Gly	Hydrophobic pocket near the entrance
Ala184	Phe	Active site hydrophobic pocket
Ala82	Leu	Active site hydrophobic pocket
Ala74	Phe	Active site hydrophobic pocket
Leu75	Thr	Hydrogen bond with and orientate the substrate
Asp251	Gly	Conformational change destabilizes open conformation

In Figure 4.1 the active site (heme group) of CYPBM3 is shown together with the positions of all the residues used in this site-directed mutagenesis study.

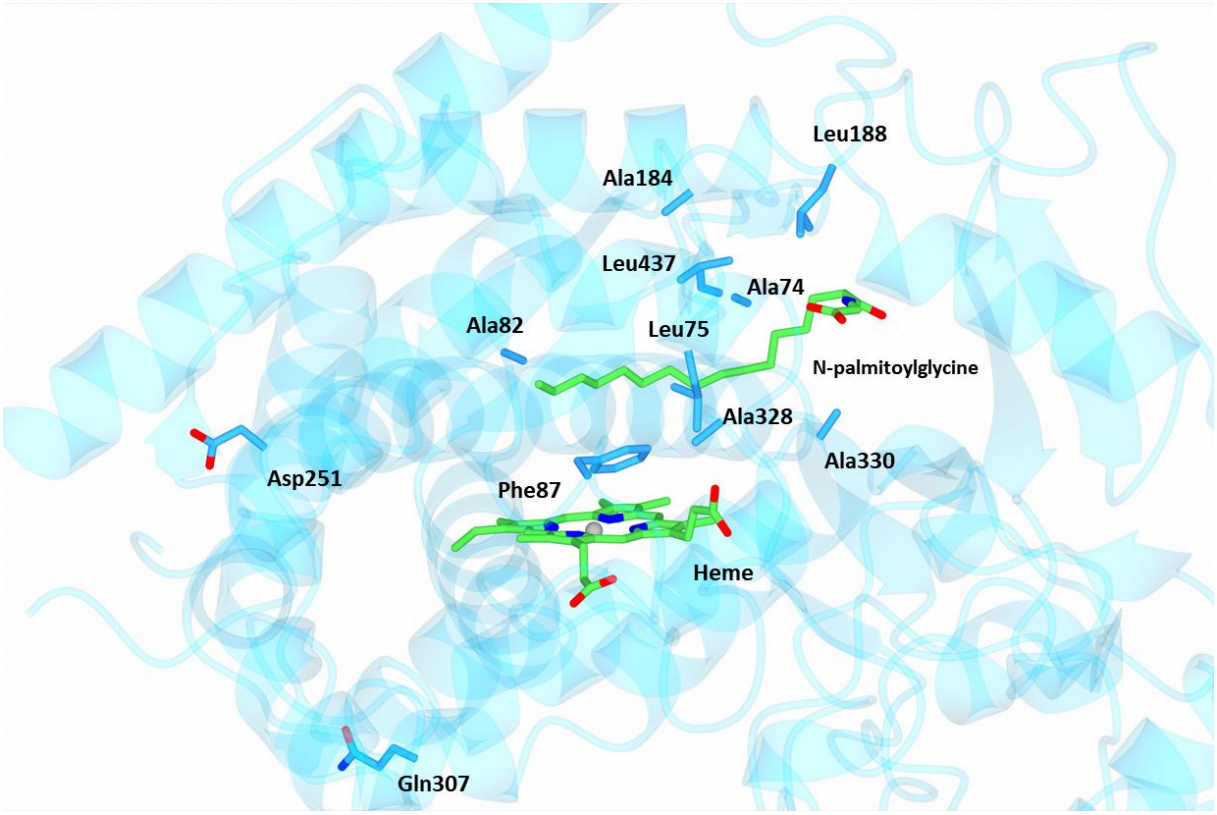

Figure 4.1: Mutant positions. *The mutants used in this thesis at their respective positions in CYPBM3. The active site – with the heme group – and its position in the enzyme are also presented in this figure.*

The mutations in the active site cavity of CYPBM3 are hydrophobic due to the hydrophobic nature of the native fatty acid substrate tail, while the residues closer to the binding channel are hydrophilic to interact with the fatty acid carboxyl.

Channel Access – *Leu188Cys*

The vast majority of enzymes have active sites that are buried within their structure, but that can be reached through multiple access channels (Pravada *et al.*, 2014). These channels can control the access of a substrate and its ability to bind to the enzyme's active site. Mutations in an enzyme's active site access channels can therefore be used in rational design to broaden the substrate specificity. CYP450s are diverse biocatalysts, and the flexibility of their access channels contributes to the broad spectrum of substrate specificity that these enzymes show. P450 BM3, on the other hand, has a rather narrow specificity for substrates whereas there has only been reported fatty acids or an indolyl-fatty acid derivative as working substrates for the

native enzyme (Appel *et al*., 2001). In a study done by Li *et al*., 2000, it was shown that a triple mutant of CYPBM3 (Leu188Gln, Phe87Val, Ala74Gly) was able to hydroxylate indole which led to the production of indirubin and indigo. This observation made Appel *et al*. to perform a study in 2001 to see if the triple BM3 mutant could be capable of hydroxylating other substrates of a broad range and of no resemblance to the usual substrates (i.e., long fatty acids) of the wild type, and this proved to be successful. A study done by Neufeld *et al*. in 2013 showed that the double BM3 mutant (Phe87Ala, Leu188Cys) was able to hydroxylate, especially in the presence of carboxyl- or carbonyl functional groups directly attached to the aromatic ring, a number of toluene derivates. This revealed that this kind of mutant possesses the ability to be a catalyst for substrates with benzylic hydroxyl groups, such as monolignols (Neufeld *et al*., 2013).

Binding Pocket – *Phe87Ala, Ala330Pro, Leu75Thr, Ala82Leu, Ala184Phe, Ala328Leu, Ala74Gly, Ala74Phe, Leu437Phe*

The channel in CYPBM3 P450 for substrate binding is long and narrow. This limits other substrates besides long-chain fatty acids. Li *et al*., 2001 discovered that replacing the Phe87 residue with Ala would increase the hydroxylation of the carbons in aromatic compounds, such as propylbenzene. The removal of the large Phe87 side chain and insertion of Ala would leave more space in the active binding site, making it possible for larger substrates to bind to the enzyme (Li *et al*., 2001). This residue points directly into the heme active site and is also reported to be the most commonly mutated residue in mutagenesis studies.

Active-site mutations such as Ala330Pro open the possibility for an altered selectivity of the substrate oxidations, as observed in a study done by Munday *et al*. in 2017. They detected that this mutation had a major impact on the regioselectivity of oxidation of substituted benzenes (Munday *et al*., 2017). This resulted in a significant improvement in product formation activity and a higher yield in metabolite generation.

In 2019 Klaus *et al*. did a study where they discovered that enzymes with different mutations, among others the mutations Ala328Leu and Leu437Phe, were able to oxidize 3-methylanisole to vanillyl alcohol, which is an important precursor of vanillin. The hydrophobic amino acids Ala and Leu in the 328 position are identified as a “hotspot” for specificity and selectivity in the CYP enzyme. This is because they are located above the heme group and therefore anticipated to have an influence on the ability of substrates to access the heme group in the active site from the opposite sides of the heme access channel (Klaus *et al*., 2019). It was also determined that amino acids in position 437 could have an effect on the orientation of the

substrate to the heme group in the active substrate binding site. This mutation was observed to have the highest activity in the formation of 3-methylanisole. The oxidation of 3-methylanisole, which is a substituted aromatic compound, made room for the idea that these kinds of mutations had the potential to hydroxylate aromatic substrates, such as monolignols.

As discussed earlier, Appel *et al*. were able to prove in 2001 that a triple BM3 mutant, where one of the mutations was Ala74Gly, was capable of hydroxylating a broad spectrum of substrates by mutation of a hydrophobic binding channel near the entrance of the active site. The same study also paved the way for other similar mutations, such as Ala74Phe, which were able to broaden the CYPBM3 substrate specificity through modification of a hydrophobic pocket near the heme group in the active site.

The mutation Leu75Thr was designed to potentially form a hydrogen bond with the hydroxyl group of the monolignol, which would reorientate the propyl chain to point to the active site of CYPBM3 (G. Schröder, personal communication, 21st of March 2023). A further mutation made was Ala82Leu, which potentially could create a more restricted hydrophobic binding pocket to try to push the monolignol substrate closer to the heme group in the active site. The Ala184Phe mutation was designed using CYP199A – another CYP450, which is natively active on monolignols. This mutation is also present in the hydrophobic pocket mentioned earlier and is located in the same position as the phenylalanine triad of CYP199A (Wolf *et al.*, 2022).

Long range – *Asp251Gly*

In a study performed by Tsotsou *et al*. in 2012, error-prone PCR was used to make CYPBM3 P450 mutants that could target drugs. One of the mutants made was the double mutant (Asp251Gly, Gln307His) that showed activity toward several drugs. It was found that *E. coli* cells heterologously expressed the mutants in the presence of the targeted substrates (Tsoutsou *et al*., 2012). This observation was based on the observation of oxidation of NADPH during enzymatic turnover on the cells in the bacteria. Even though the mutations in the double mutant were not involved directly in the enzymatic turnover or substrate binding because of their location on the surface of the enzyme, they contributed to a conformational change of the structure which led to the destabilization of the open conformation and increased substrate promiscuity.

4.2 Initial Screening Assays on Cell Lysate and Selection of Best Candidates

Results for the initial screening of the activity of the mutants, compared to the wild type, were performed with cell lysates and the monolignol obtained from RCF. This allowed the selection of a few candidates for initial characterization. For this, these different assays were performed: NADPH depletion assay, indole oxidation, MS analysis for product detection, and ImageJ for protein expression.

4.2.1 NADPH Depletion Assay

To screen for NADPH consumption, 11 mutants, and wild type were tested (Figure 4.2). Empty plasmid (no CYPBM3) was used as a negative control. Buffer instead of supernatant was also employed as a negative control. Three different monolignols were tested: 4-PP, 4-PG, and 4-PS. Palmitic acid (natural substrate) was used as a positive control, and 70% ethanol was used as a negative control.

For **4-propyl phenol** (Figure 4.2 A)), mutant 9 (M9) and mutant 10 (M10) showed the highest consumption rate, followed by wild type (WT), mutant 7 (M7), mutant 5 (M5), and mutant 11 (M11). Mutants with the lowest NADPH consumption rate were mutant 3 (M3), mutant 4 (M4), and mutant 6 (M6). Supernatant for empty plasmid (Empty) did not show consumption, and neither did the negative control with buffer (No lysate). The standard deviation was low for all the candidates, except for M5, M9, and M10.

For **4-propyl guaiacol** (Figure 4.2 B)), mutant 9 (M9), mutant 8 (M8), and mutant 10 (M10) showed the highest consumption rate, followed by mutant 1 (M1), mutant 2 (M2), and mutant 7 (M7). The wild type (WT), mutant 5 (M5), and mutant 11 (M11) showed some consumption. Mutants with the lowest NADPH consumption rate were mutant 3 (M3), mutant 4 (M4), and mutant 6 (M6). The empty plasmid (Empty) showed close to no consumption, while the negative control with buffer (No lysate) showed no consumption at all. The standard deviation was pretty low for most of the candidates, except M1, M9, and M10 which had a higher std. deviation than the others.

For **4-propyl syringol** (Figure 4.2 C)), many of the candidates showed close to a similar NADPH consumption rate. The highest rate was seen in mutant 1 (M1) and mutant 7 (M7), with the wild type (WT) and mutant 8 (M8) following close by. Mutant 2 (M2), mutant 5 (M5), and mutant 11 (M11) also showed a noticeable consumption rate. The lowest NADPH consumption rate was measured for mutant 3 (M3) and mutant 4 (M4). The empty plasmid

(Empty) showed close to no consumption, while the negative control with buffer (No lysate) showed no consumption at all. The standard deviation was low for most of the candidates, except M6 and M9.

For **palmitic acid** (Figure 4.2 D)), mutant 1 (M1) showed the highest NADPH consumption rate of all the mutants. Mutant 9 (M9) also showed a noticeable consumption rate. For mutant 5 (M5), mutant 7 (M7), and mutant 10 (M10) the rate was similar to the wild type (WT). Mutants with the lowest, and almost no NADPH consumption, were mutant 4 (M4), mutant 6 (M6), and mutant 11 (M11). Most of the mutants had a low standard deviation, except M9 where it was a little higher than the others. Empty plasmid (Empty) and negative control (No lysate) showed no NADPH consumption at all.

The **negative control** (Figure 4.2 E)) with 70% ethanol instead of substrate had no considerable amount of NADPH consumption for any of the candidates.

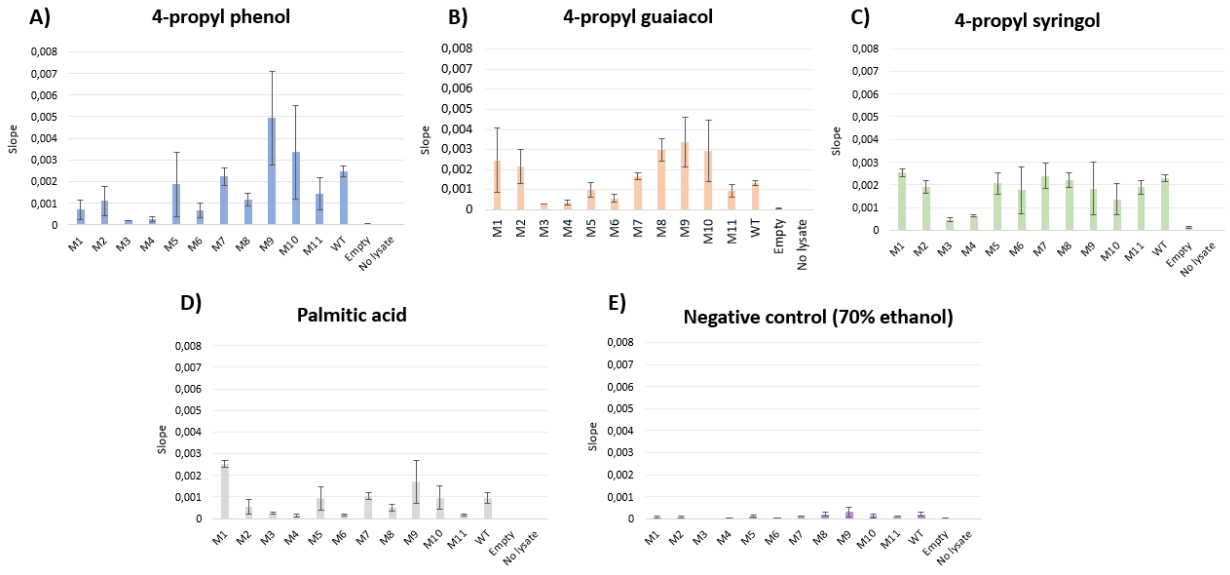

Figure 4.2: NADPH depletion for all 11 mutants and wild type. *Empty plasmid (no CYPBM3) and buffer instead of lysate were tested as negative controls.* ***A-C.*** *The three different monolignols were tested (**A)** 4-PP, **B)** 4-PG, and **C)** 4-PS).* ***D)*** *Palmitic acid was used as a positive control, and* ***E)*** *70% ethanol was used as a negative control*

It can be concluded that M9 and M10 showed a high NADPH depletion rate for all the substrates. M3 and M4 showed the lowest consumption rates for all the substrates. Empty plasmid and negative control with buffer (No lysate) did not show any considerable amount of NADPH consumption.

These results together with the ImageJ analysis to correct for protein expression, were used to decide the mutants chosen for further experiments.

4.2.2 Indole Oxidation

The oxidation of indole, which is commonly used for detection of CYP activity, makes an indigo product that is purple and can be determined both by the naked eye and by measuring the absorbance at 620 nm. No indole oxidation was observed for any of the mutants nor for the wild type CYPBM3.

4.2.3 MS Analysis

To determine CYP activity on monolignols, reactions with the different mutants and substrates were set up. Possible product formation was observed by mass spectrometry. Reaction conditions are listed in Table 3.6.

For **4-propyl phenol**, hydroxylation was observed in the full scan spectra (m/z +16) for the 11 mutants and wild type CYPBM3. Figure 4.3 shows an example of the full scan for one of the mutants. The substrate corresponds to the m/z 135 ion and the possible product (hydroxylation) with to m/z 151 ion. For the negative control (supernatant for the empty plasmid transformant), no m/z 151 ion was observed in the spectra.

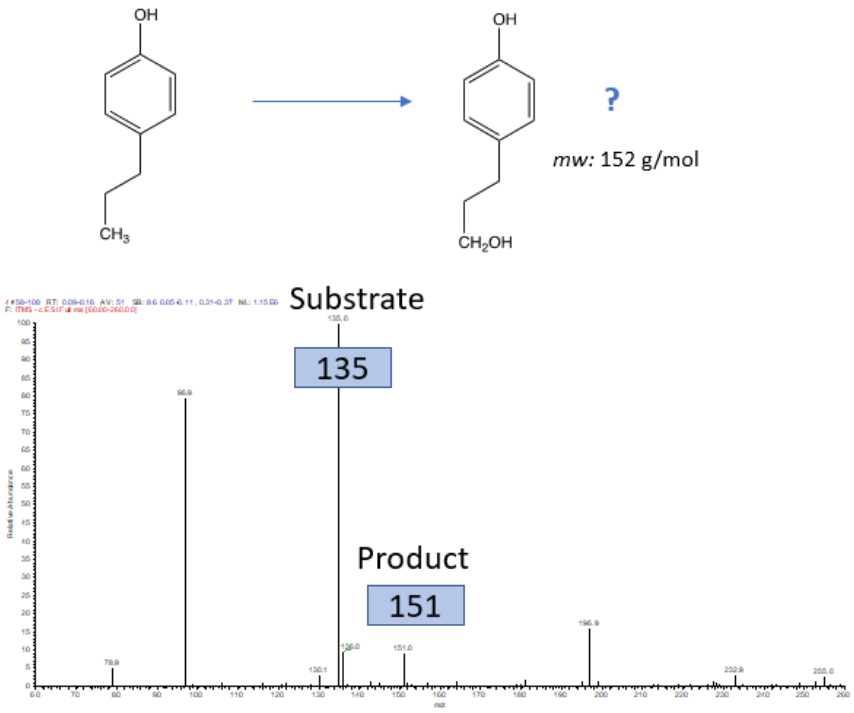

Figure 4.3: MS analysis of activity with 4-PP. *4-PP has a structure as shown above, and after an enzyme-substrate connection with CYPBM3, it may produce the product of interest with a mass of 152 g/mol. Both the substrate itself and the products will appear on the MS with a mass of one gram less than their original weight.*

For **4-propyl guaiacol**, Figure 4.4 shows an example of the full scan for one of the mutants. The substrate corresponds to the m/z 166 ion and, a peak at m/z 181 was observed that may be the result of a single hydroxylation. However, this peak was also observed in the full scan spectra (m/z +16) in the negative control (supernatant for the empty plasmid transformant). Therefore, it cannot be concluded that hydroxylation is happening for the mutants and wild type. The utilization of pure enzyme could assist in clarifying this matter.

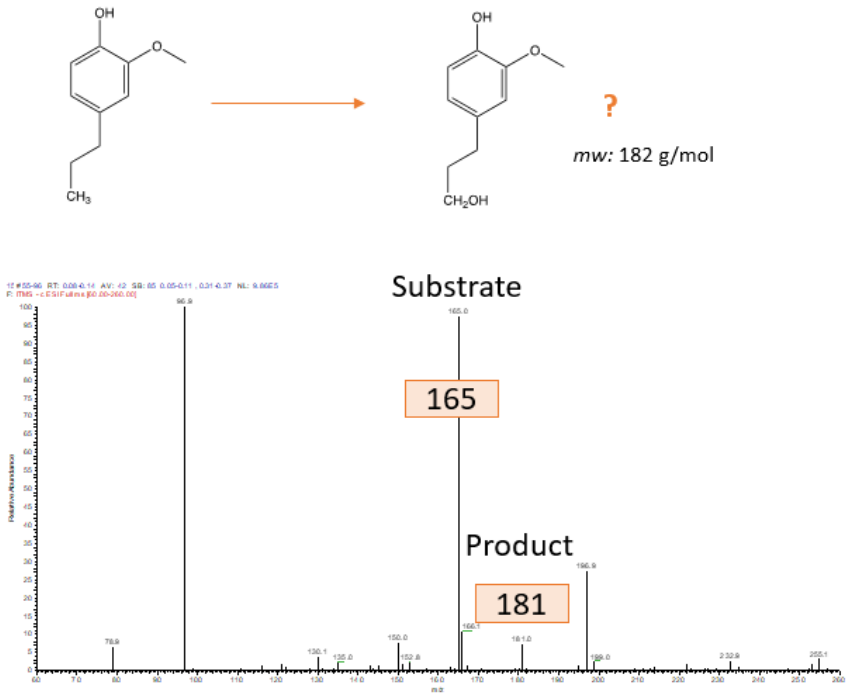

Figure 4.4: MS analysis of activity with 4-PG. *One of the possible products of interest 4-PGl may produce together with CYPBM3 has a mass of 182 g/mol. This product will appear on the MS with a mass of 181 g/mol. All the mutants, plus the wild type and the negative control, showed a peak on the MS with a mass of 181 g/mol together with 4-PG.*

For **4-propyl syringol**, hydroxylation was not observed in the full scan spectra (m/z +16). Figure 4.5 shows an example of the full scan for one of the mutants. Substrate corresponds to the m/z 196 ion, and it can be observed that m/z 211 peak is negligible. For the negative control (supernatant for the empty plasmid transformant), same spectra were observed.

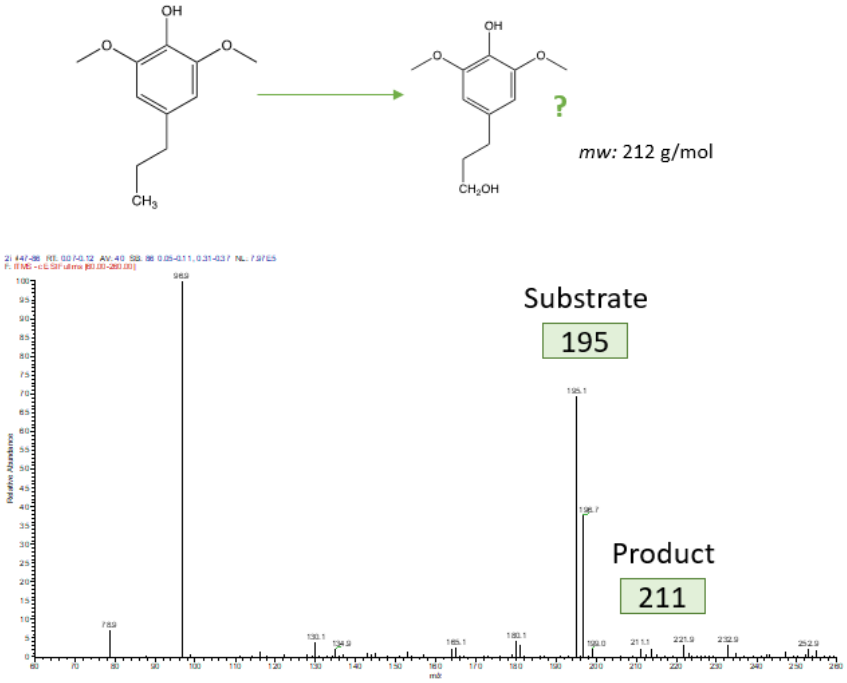

Figure 4.5: MS analysis of activity with 4-PS. *This substrate with a mass of 196 g/mol can together with CYPBM3 create a product with a mass of 212 g/mol. On the MS analysis done with the different mutants of CYPBM3 and the CYPBM3 WT, there were only two samples that showed a possible product of interest. The negative control did not show any product with 4-PS.*

The conclusion of the MS analysis is that 4-PP substrate hydroxylation occurs for all the mutants and the wild type. For 4-PG, m/z 181 peak was observed for all the mutants, the wild type, and the negative control (empty), therefore further analysis with pure enzyme would clarify if the actual hydroxylation is happening. For 4-PS, m/z 211 peak was negligible for all mutants and wild type, indicating no product formation.

4.2.4 Expression Quantification with ImageJ

ImageJ software was utilized to choose three mutants by normalizing NADPH consumption rates with protein concentration for further characterization with the three monolignols. For that, cell lysate for every mutant and wild type was analyzed using SDS-PAGE Gel electrophoresis, and the intensity of the protein band on the resulting gel (presented in Figure 4.6) was utilized to quantify the relative protein expression (band around 117 kDa). Intensity values were relativized with respect to the WT value. NADPH depletion rates were normalized using relative protein concentration values, then, fold change in percentage was calculated with respect to WT.

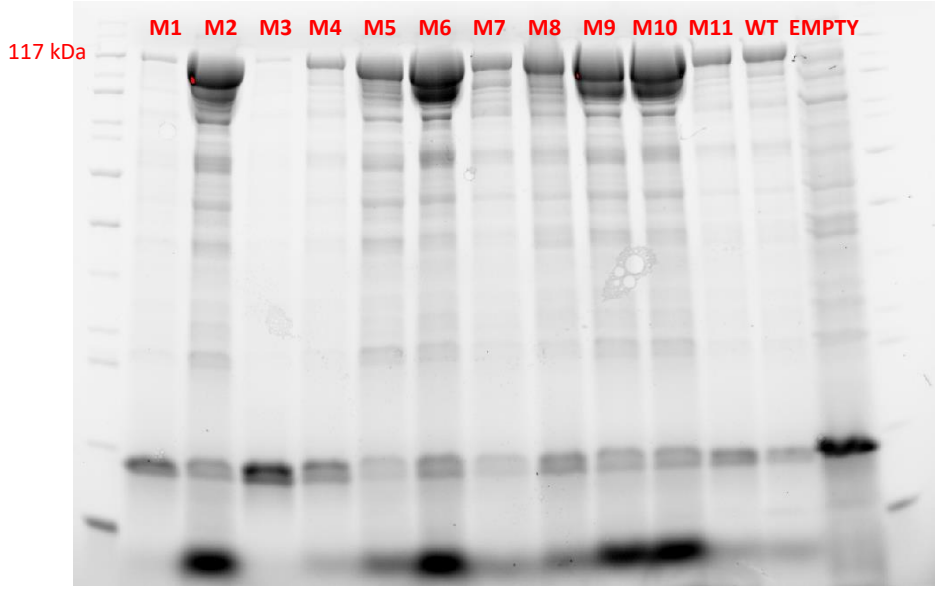

Figure 4.6: The expression levels of each mutant and wild type. *This image presents the expression levels of each mutant and wild type on an SDS-PAGE gel. Each well is presented with the mutant which it's containing. There was also included a sample without the CYPBM3, which is marked with "EMPTY". The respective bands of interest had a size of 117 kDa.*

The ImageJ software transformed the band intensities of each mutant and wild type into peaks proportional to the abundance, and the area of each peak was measured. These values are presented in Figure 4.7, where the peak area corresponds with band intensity – this means that bigger peak area means higher band intensity.

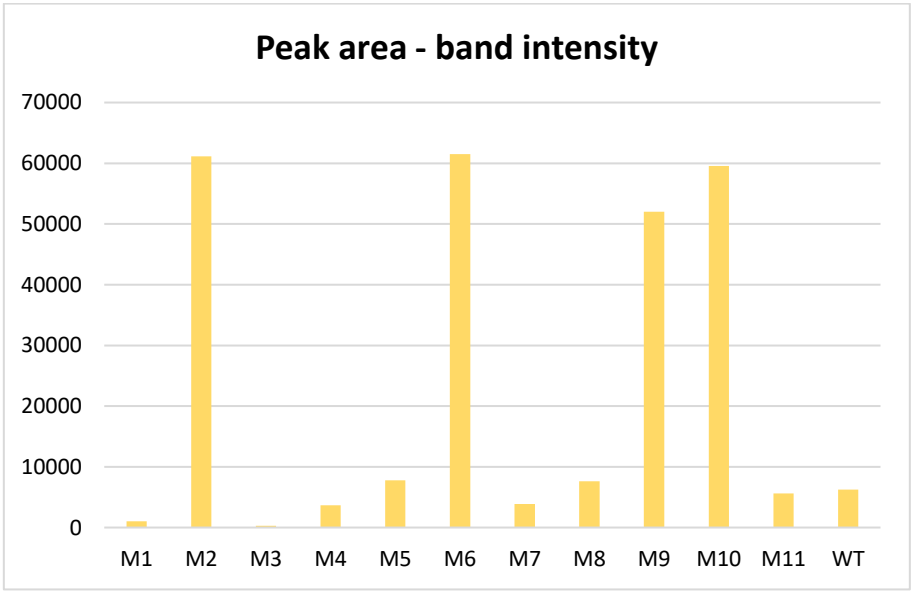

Figure 4.7: Band intensity of each mutant analyzed with ImageJ. *The band intensity of each mutant + wild type was calculated with ImageJ. The different intensities came in the shape of peaks, and this figure presents the peak area of each mutant and wild type.*

For **4-propyl phenol** (Figure 4.8), mutant 3 (M3), mutant 1 (M1), and mutant 7 (M7) had the highest values, while mutant 2 (M2) and mutant 6 (M6) had the lowest values.

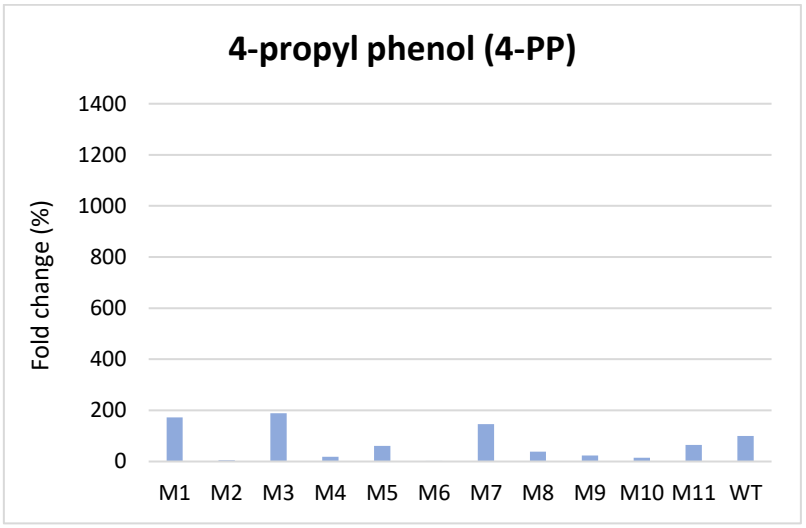

Figure 4.8: Fold change for 11 mutants compared to wild type with 4-PP. *The fold change of each mutant was calculated compared to the wild type (WT). The mutants with a higher percentage than WT had an expression level higher than 100%.*

For **4-propyl guaiacol** (Figure 4.9), mutant 1 (M1) showed the highest fold change of all the candidates. Mutant 3 (M3) also had high values compared to the others. The lowest percentage was shown by mutant 2 (M2) and mutant 6 (M6). Mutant 7 (M7) and mutant 8 (M8) had higher values than the wild type, with fold changes over 100%.

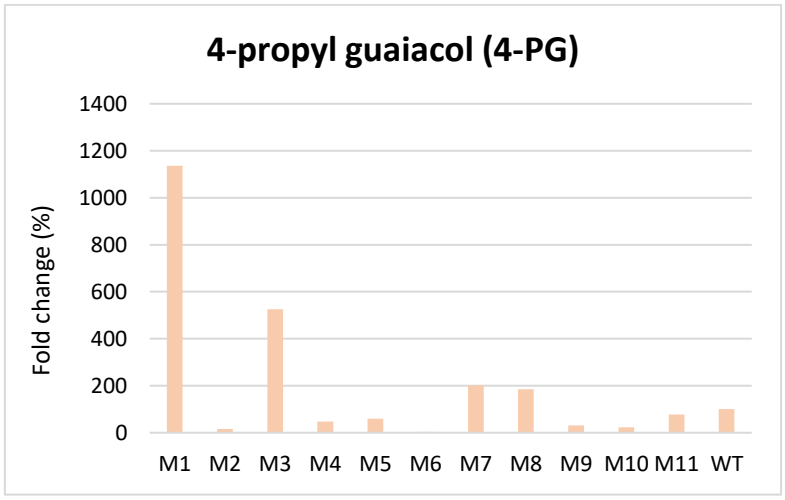

Figure 4.9: Fold change for 11 mutants compared to wild type with 4-PG. *The fold change of the mutants in percent compared to the wild type (100%) with this monolignol is presented in this figure. The values were calculated using the software ImageJ.*

For **4-propyl syringol** (Figure 4.10), mutant 1 (M1) showed the absolute highest fold change, with mutant 3 (M3) following close by. The lowest values were shown by mutant 9 (M9), mutant 2 (M2), mutant 10 (M10), and mutant 6 (M6) which were the mutants with the lowest band intensities.

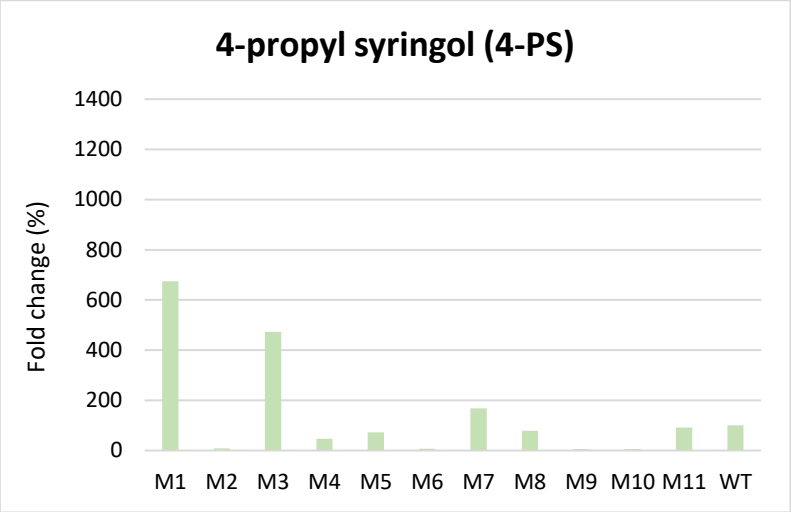

Figure 4.10: Fold change for 11 mutants compared to wild type with 4-PS. *In this figure, the fold change (in percent) of the mutants compared to the wild type is presented with 4-PS. The calculation of the values was done by employing the software ImageJ.*

For **palmitic acid** (Figure 4.11), mutant 1 (M1) showed the highest percentage of fold change, followed by M3. Mutant 7 (M7) showed higher fold than the wild type. Other candidates showed low values. The lowest rate was found for mutant 2 (M2) and mutant 6 (M6) which showed insignificant consumption.

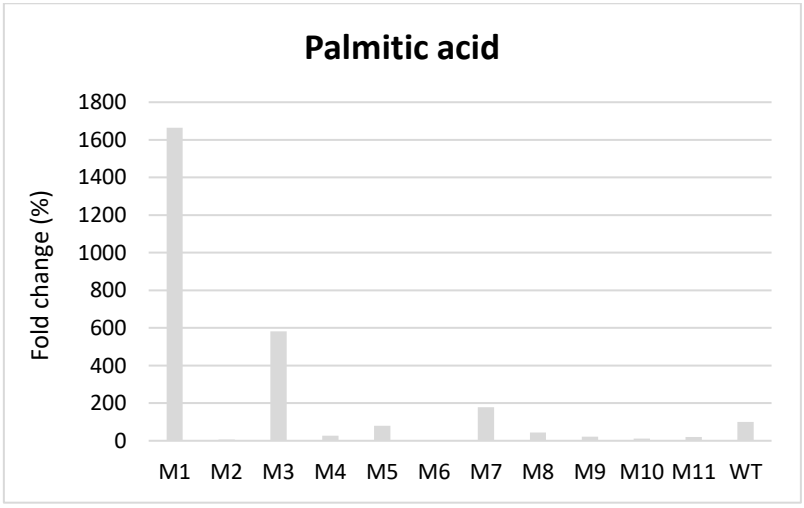

Figure 4.11: Fold change for 11 mutants compared to wild type with palmitic acid. *The natural substrate of CYPBM3 and fold change values for 11 mutants and wild type are presented in this figure. ImageJ was used to calculate the different percentages.*

It can be concluded that M1 showed the highest values with most of the substrates, and products with 4-PP and 4-PS in the MS analysis. M1 was therefore selected as the first candidate for further characterization. M3 showed high values with all the substrates but had the lowest rates of all the mutants in the initial NADPH depletion screening. This mutant was therefore excluded. M7 had a higher percentage of fold change than the wild type (WT) and had the third-highest values with all the substrates, despite having a low band intensity as presented in Figure 4.6. This mutant was chosen as the second candidate for further analysis. The last mutant chosen for expression, purification, and characterization was a mutant that had at least 50% of the expression of WT. M11 had similar values as M5 in this selection as well as the NADPH assay, but M5 had higher values with palmitic acid for both screenings. M5 showed good values with especially 4-PP and 4-PS, despite having a low band intensity. This indicates a good performance of this mutant, and for that, M5 was chosen as the third and last candidate.

The three mutants M1, M5, and M7 were selected as the best candidates for further characterization.

4.3 Characterization of Wild Type and Mutants' Activity on Monolignols

4.3.1 NADPH Depletion Assay

An NADPH depletion assay was done for the selected mutants (M1, M5, and M7) and WT, using the three monolignols as substrates. Palmitic acid was used as a positive control, and 70% ethanol was used as a negative control. The conditions used were the same as in section 3.5.1. Two replicates were done for each reaction. NADPH depletion was also measured before adding the substrate to ensure NADPH stability before measuring reaction rates. NADPH depletion rates were determined by calculating the reaction slopes. The average slopes and std. deviation for the mutants and wild type were put into the graphs presented in Figure 4.12.

For **4-propyl phenol** (Figure 4.12 A)), the wild type (WT) showed the highest consumption rate. Mutant 5 (M5) and mutant 7 (M7) showed some NADPH consumption, while mutant 1 (M1) showed close to no consumption. The standard deviation was low for all the candidates.

For **4-propyl guaiacol** (Figure 4.12 B)), the wild type (WT) also showed the highest NADPH consumption. The three mutants (M1, M5, and M7) showed similar rates, with M5 having a little higher rate than the other two. The standard deviation was low for all the mutants and the wild type.

For **4-propyl syringol** (Figure 4.12 C)), the wild type (WT) showed the highest consumption rate, as the other monolignols. Mutant 1 (M1) had the lowest rate, and mutant 5 (M5) had the highest NADPH consumption. The standard deviation was low for all the candidates, but for M1 it was a little higher.

For **palmitic acid** (Figure 4.12 D)), mutant 7 (M7) showed the absolute highest NADPH consumption rate of the candidates. Mutant 5 (M5) had the lowest consumption of NADPH. The standard deviation was high for M1 and M7, but low for the others. The **negative control** with 70% ethanol (Figure 4.12 E)) did not show any NADPH consumption.

It can be concluded that WT measured the highest consumption of NADPH with most of the substrates, except with palmitic acid where M7 had the highest rate. As preferred, the negative control did not show any consumption rate with any substrate.

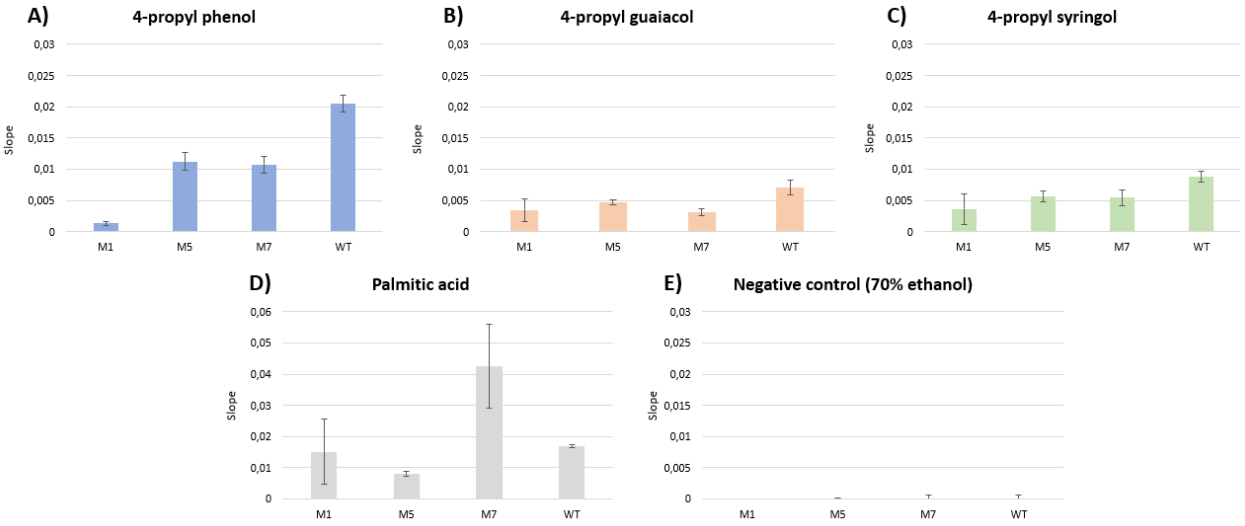

Figure 4.12: NADPH depletion assay with purified CYPBM3 selected mutants and wild type. *The NADPH depletion was measured for M1, M5, M7, and WT with the substrates:* ***A)*** *4-PP,* ***B)*** *4-PG,* ***C)*** *4-PS, and* ***D)*** *Palmitic acid. A negative control* ***E)*** *with 70% ethanol was also included.*

4.3.2 Binding Assay

As described in paragraph 3.5.2, the binding assay was performed on the enzymes WT, M1, M5, and M7 with the monolignols 4-PP, 4-PG, and 4-PS as well as the native substrate palmitic acid. The results presented are the ones that showed a trend with a clear shift in absorbance, and the other results are therefore not included.

4-propyl phenol

For this monolignol, only the wild type displayed a shift in absorbance when performing the binding assay, as shown in Figure 4.13. There is a slight shift at a monolignol concentration of 246 µM, but the shift is more apparent at 484 µM. At 714 µM the peak has fully shifted from approximately 390 nm to approximately 418 nm.

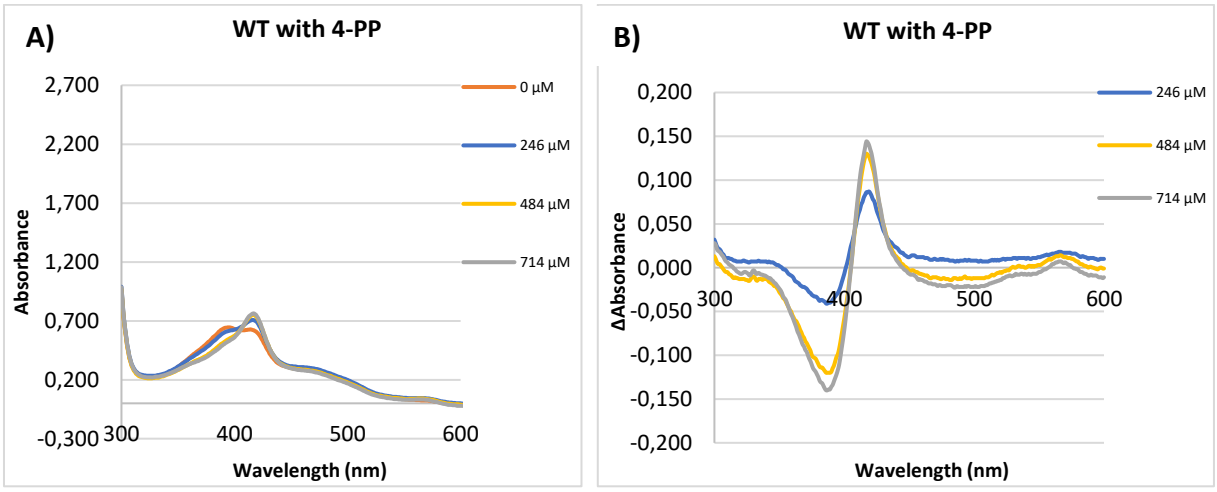

Figure 4.13: CYPBM3 wild type with 4-PP. *The binding assay of the CYPBM3 WT and monolignol 4-PP shows a shift in absorbance from 390 nm to 418 nm at increasing substrate concentration (A). A difference spectrum generated by subtracting the substrate-free spectrum from the substrate-bound BM3 confirms the shift in spectra upon substrate addition (B).*

4-propyl guaiacol

4-PG had a successful binding assay with both the wild type and M5, displaying a peak shift for both. The wild type, as presented in Figure 4.14, indicates that the increase in absorbance begins at a substrate concentration of 246 µM and that the peak has fully shifted to 418 nm at 714 µM

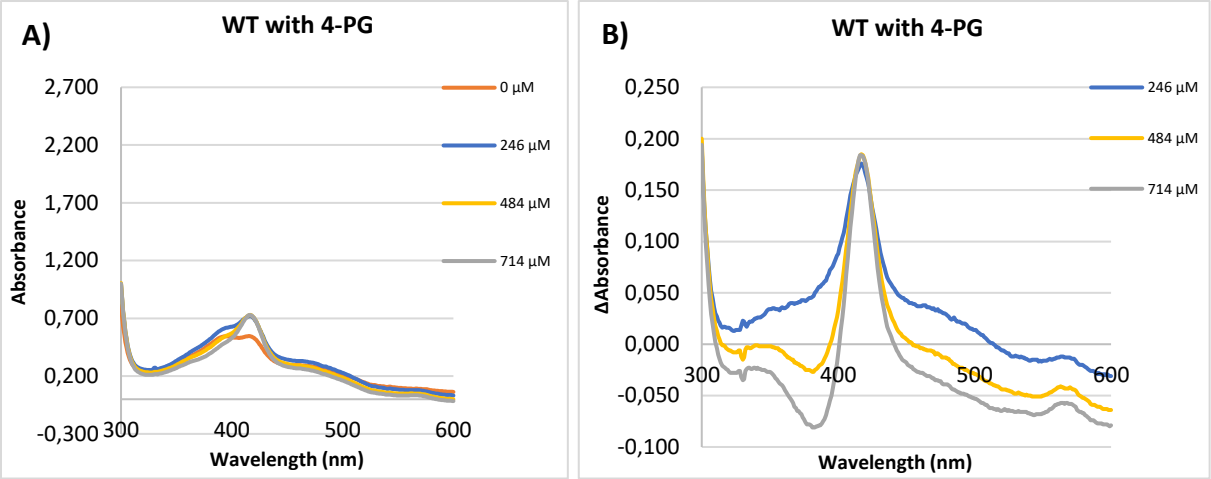

Figure 4.14: CYPBM3 wild type with 4-PG. *The change in absorbance shown in this binding assay with WT and 4-PG can be seen from a substrate concentration of 246 µM with the peak fully shifted to wavelength 418 nm at 714 µM (A). A difference spectrum generated by subtracting the substrate-free spectrum from the substrate-bound BM3 confirms the shift in spectra upon substrate addition with a fully shifted peak at 714 µM. (B).*

For M5 the shift is in the form of a slight decrease in the absorbance from wavelength 419 nm to 417 nm when 246 µM of substrate was added, as seen in Figure 4.15 (A). The change in absorbance was complete at 938 µM when the wavelength reached 415 nm.

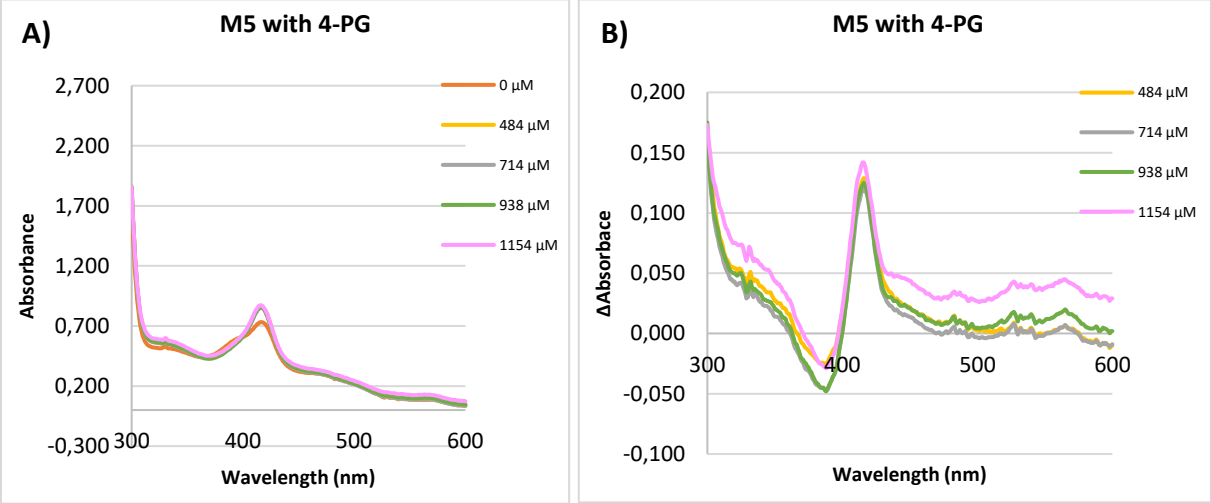

Figure 4.15: CYPBM3 M5 with 4-PG. *In this binding assay between M5 and 4-PG, a slight decrease in absorbance can be seen from 419 nm to 417 nm when 246 µM of substrate was added (A). A difference spectrum generated by subtracting the substrate-free spectrum from the substrate-bound BM3. The change is fully visible at wavelength 415 nm with the substrate concentration 938 µM (B).*

4-propyl syringol

As observed for 4-PG, 4-PS displayed a shift in the binding assay with both CYPBM3 WT and M5. The wild type (Figure 4.16) revealed a shift in the absorbance peak starting at a monolignol

concentration of 246 µM. A slight change can be seen at 418 nm with a concentration of 484 µM in the difference spectrum (B), but it is almost not visible in the absorbance spectrum (A).

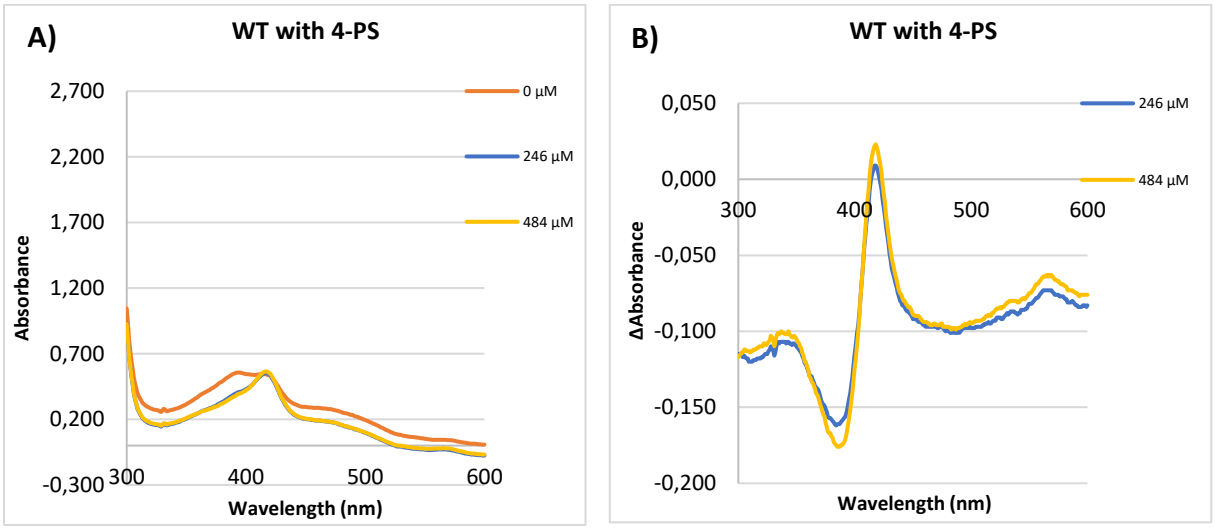

Figure 4.16: CYPBM3 wild type with 4-PS. *For this binding assay between the WT and 4-PS, the peak of absorbance exhibits a clear shift in absorbance at the substrate concentration of 246 µM (A). With the substrate concentration of 484 µM and a wavelength of 418 nm, a slight increase in absorbance can be spotted in a difference spectrum generated by subtracting the substrate-free spectrum from the substrate-bound BM3 (B).*

For the mutant, M5, the absorbance showed a slight decrease in the peak maxima at 418 nm with a substrate concentration of 484 µM, but the full shift happened at 938 µM (417 nm) as shown in Figure 4.17.

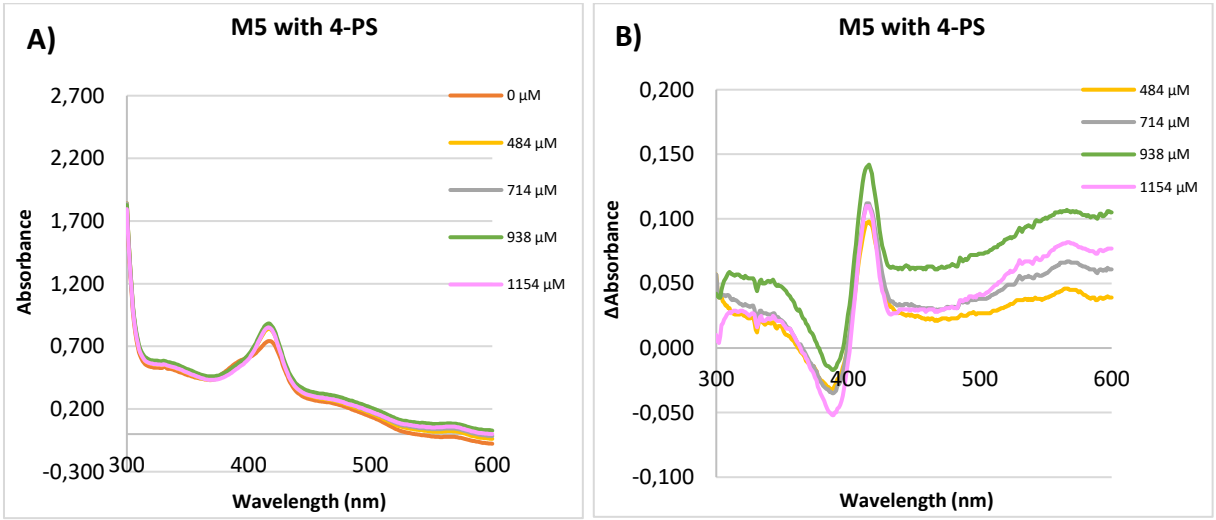

Figure 4.17: CYPBM3 M5 with 4-PS. *For 4-PS binding assay to M5, the peak shift happened at the monolignol concentration of 484 µM (A). A difference spectrum generated by subtracting the substrate-free spectrum from the substrate-bound BM3 (B). An increase in the absorbance can be observed at wavelength 417 nm and concentration 938 µM, so the full shift likely happened at this concentration.*

Palmitic acid

The palmitic acid was the substrate that had successful binding assays with the most enzymes, displaying a peak shift. The only enzyme that did not have a successful binding assay with this substrate was M7. Firstly, the CYPBM3 wild type showed a good trend with palmitic acid as seen in Figure 4.18. The shift in absorbance is seen to start at 484 µM, with a complete peak shift to 418 nm at a substrate concentration of 1364 µM. The shift was shown to gradually increase at higher substrate concentrations.

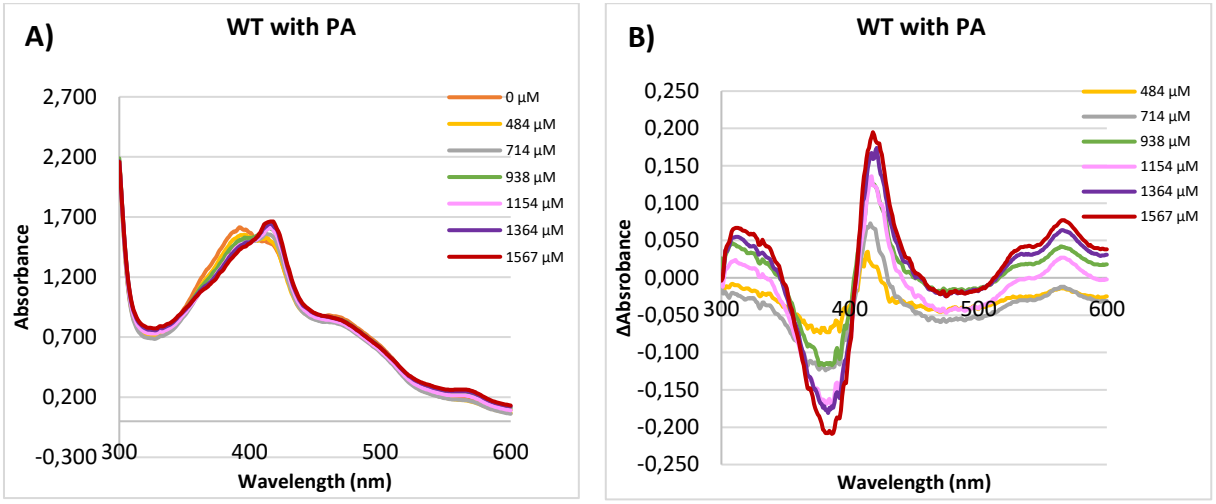

Figure 4.18: CYPBM3 wild type with palmitic acid. *A slight shift of the peak in this binding assay between WT and the palmitic assay can be seen already at 484 µM with a complete shift apparent at 1364 µM (A). A difference spectrum generated by subtracting the substrate-free spectrum from the substrate-bound BM3. The peak has fully shifted from approximately 390 nm to 418 nm when the substrate concentration is 1364 µM (B).*

Mutant M1 also displayed a slight shift of absorbance upon palmitic acid-binding. As presented in Figure 4.19, the peak is seen to have a small alteration at a substrate concentration of 484 µM from 420 nm to 416 nm (A). The change in absorbance can be seen more clearly in the difference spectrum (B).

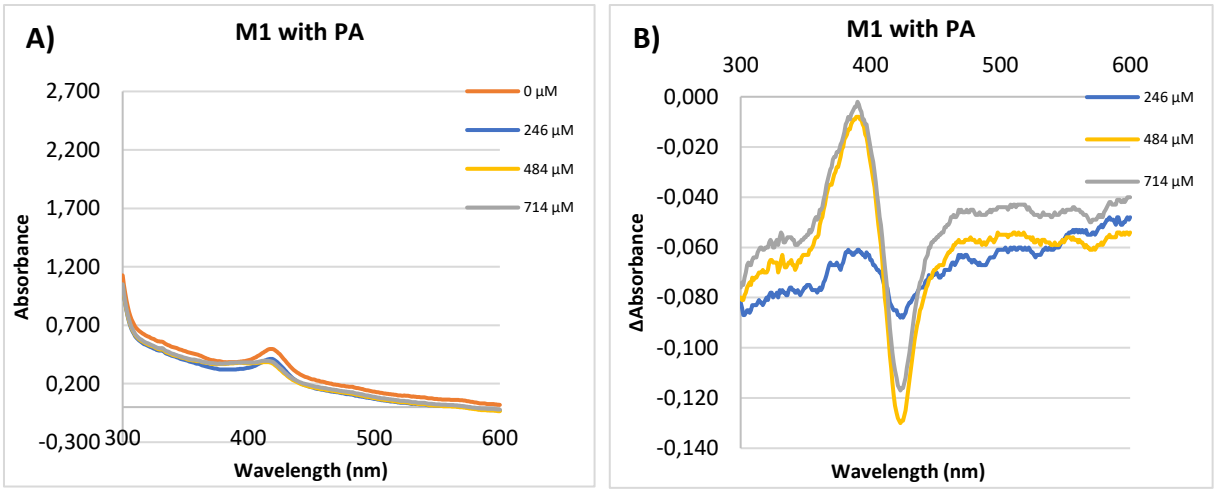

Figure 4.19: CYPBM3 M1 with palmitic acid. *For M1 the change in absorbance happens at 484 µM from 420 nm to 416 nm (A). The shift in the peak at 246 µM and 484 µM is more noticeable in the difference spectrum generated by subtracting the substrate-free spectrum from the substrate-bound BM3 (B).*

The binding assay with M5 and palmitic acid, as presented in Figure 4.20, showed a change in absorbance at 246 µM. In this instance, the absorbance decreased as the substrate concentration was increased, with the peak maximum shifting from 418 nm to 414 nm.

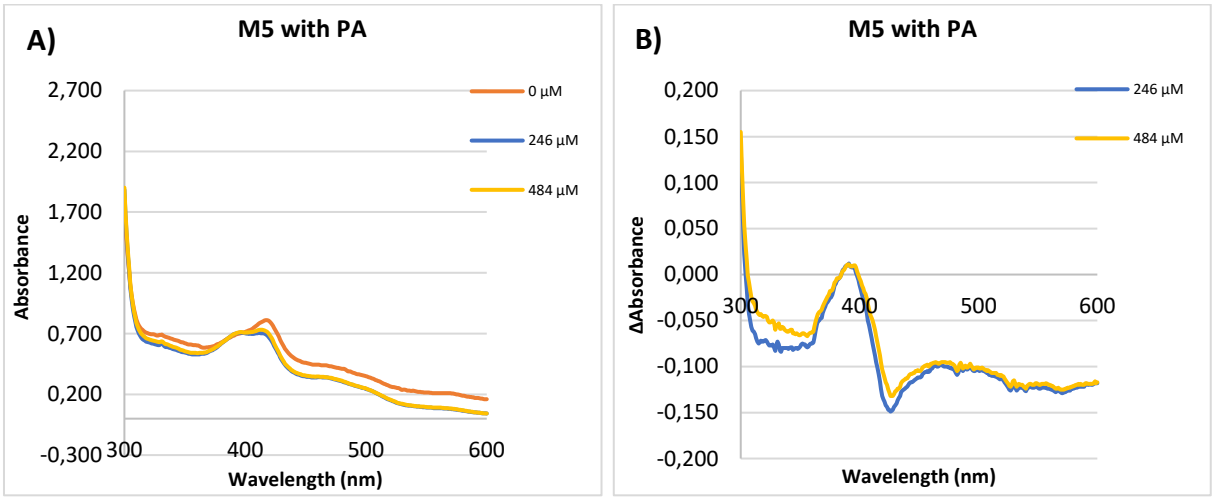

Figure 4.20: CYPBM3 M5 with palmitic acid. *Mutant M5 showed a decrease in absorbance from 418 nm to 414 nm when 246 µM of palmitic acid was added(A). There was little to no change when the substrate concentration was increased to 484 µM in the difference spectrum generated by subtracting the substrate-free spectrum from the substrate-bound BM3 (B).*

4.3.3 MS Analysis

Reactions with the different mutants and substrates were set up to determine CYP activity on monolignols. To identify the products, fragmentation patterns from MS/MS were employed. Reaction conditions are listed in Table 3.7.

For **4-propyl phenol**, mutant 1 (M1) had a product with a mass of 151 (Figure 4.21 A). The fragmentation analysis results showed that the product was a combination of two isomers (**1: 4-propylbenzene-1,2-diol** and **2: 4-propylbenzene-1,3-diol**).

For **4-propyl phenol**, hydroxylation of the substrate was observed in the full scan spectra (m/z +16) for the 3 mutants (M1, M5, M7) and wild type CYPBM3 (Figure 4.21 A). Fragmentation patterns (MS/MS) suggest that hydroxylation happen in the ortho (**1**) and meta (**2**) position on the benzene ring: 4-propylbenzene-1,2-diol (**1**) and 4-propylbenzene-1,3-diol (**2**). For all the candidates, a mix of these two isomers was observed. However, fragmentation patterns were different between M1 (Figure 4.21 A) and mutants 5 and 7 (Figure 4.22), probably because the abundance of the isomer is different.

For **4-propyl guaiacol**, there was also a product with a mass of 181 (Figure 4.21 B). This indicates that hydroxylation has happened. The same hydroxylation happened for all the mutants and the wild type. However, standards for the different isomers were not purchased, therefore, it cannot be determined where the hydroxylation takes place.

For **4-propyl syringol**, no product formation was detected for any mutant or wild type, and the product of 211 was background "noise" since this peak was also present on the negative control (Figure 4.21 C).

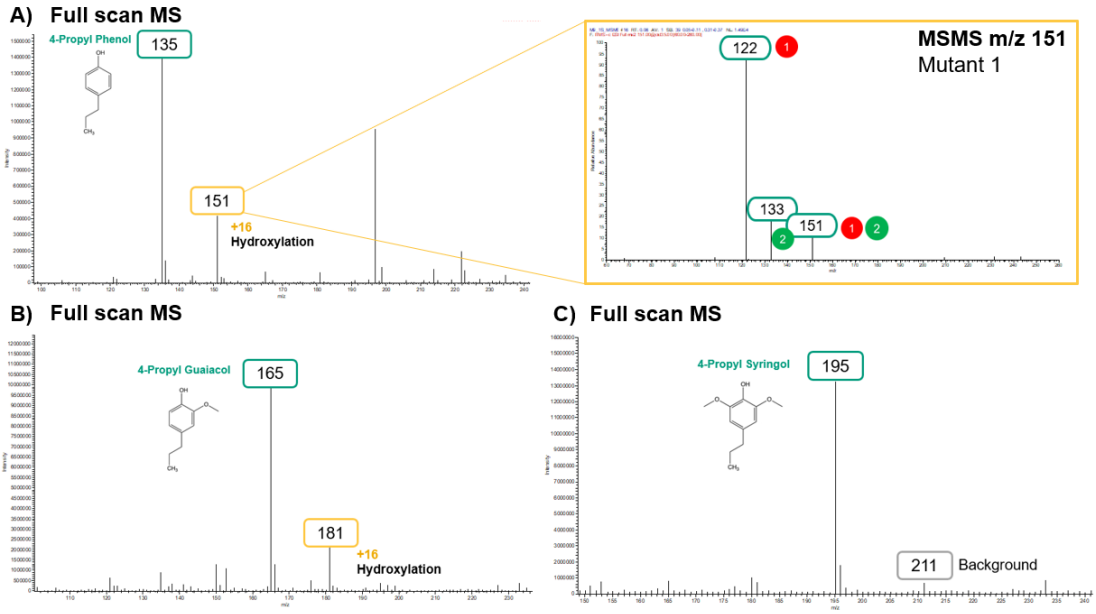

Figure 4.21: Full scan MS for all mutants and MSMS for mutant 1. *The MSMS fragmentation analysis showed a product combined of two isomers with 4-PP for mutant 1 (A). There was some product formation with 4-PG, but in an unknown position (B). 4-PS had no activity with any mutants or wild type (C).*

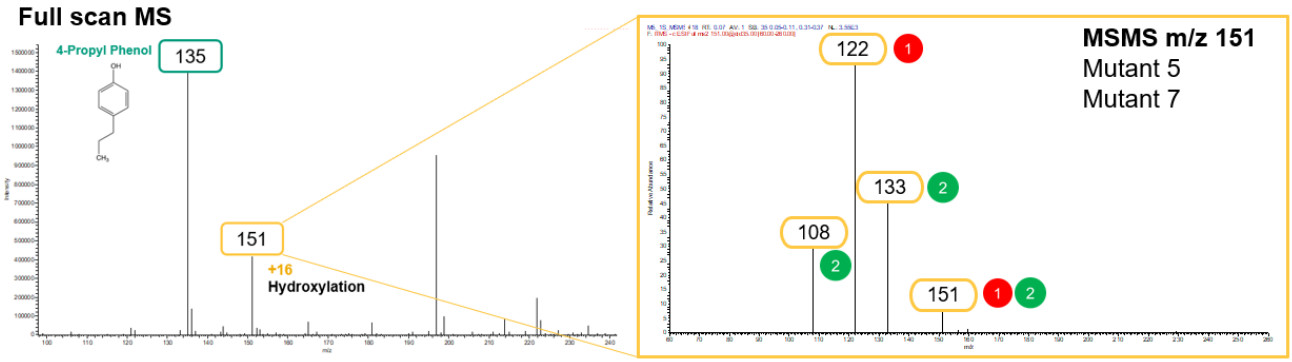

Figure 4.22: Full scan MS with 4-PP and MSMS for mutants 5 and 7. *The MSMS fragmentation analysis showed a product combined of isomers with 4-PP for mutants 5 and 7.*

5 DISCUSSION

The topic of CYPBM3 P450's activity with lignin-derived monolignols lacks knowledge. Previous studies done to improve CYPs (P450) by mutagenesis have shown that mutations of specific residues are able to affect the ability of these enzymes to bind to substrates with different, and bulkier structures than CYPs native substrates (Li *et al.*, 2000; Munday *et al.*, 2017; Tsoutsou *et al.*, 2012).

In this study, 11 single mutations of CYPBM3 were selected based on previous studies, and initial assays were performed to evaluate the activity of the mutants on the three monolignols 4-PP, 4-PG, and 4-PS.

5.1 Initial Screening on Cell Lysate

5.1.1 NADPH Depletion Assay with Cell Lysate

The initial NADPH depletion screening utilizing cell lysate in 96 well-plates showed that most of the mutants had electron transfer with all three monolignols.

For **4-propyl phenol**, mutant 9 (M9) and mutant 10 (M10) exhibited the highest NADPH consumption rate, with higher rates than for the wild type. M9 corresponds to the mutation Asp251Gly which leads to a conformational change in the enzyme, resulting in the destabilization of its open conformation (Tsoutsou *et al*., 2012). This destabilization could increase the substrate promiscuity, making possible for the monolignol to bind to the active site. M10 corresponds to the mutation Leu188Cys that can control the access of the substrate and its ability to bind to the enzyme's active site (Neufeld *et al*., 2013). This mutation increases the polarity of the access channel, and this could make the interaction between the benzylic hydroxyl group and Cys188 possible.

For **4-propyl guaiacol**, mutant 8 (M8), mutant 9 (M9), and mutant 10 (M10) had the highest NADPH consumption rates exceeding the wild type. M8 corresponds to the mutation Ala330Pro which opens the active heme site for the substrate (Munday *et al*., 2017), and could favor the entrance of 4-PG.

For **4-propyl syringol**, mutant 1 (M1) and mutant 7 (M7) showed the highest NADPH consumption rate, also exceeding the wild type. M1 corresponds to the mutation Ala184Phe

while M7 corresponds to the mutation Ala328Leu, and both mutations affect the active site hydrophobic pocket which may increase the interaction with the propyl chain of the monolignol (Wolf *et al.*, 2022; Klaus *et al*., 2019).

Mutant 3 (M3) and mutant 4 (M4) showed the lowest NADPH consumption rates with all the monolignols, and they were excluded for further analysis. M3 corresponds to the mutation Ala82Leu which could potentially create a more restricted hydrophobic binding pocket, aiming to bring the monolignol substrate closer to the heme group in the active site (G. Schröder, personal communication, 21st of March 2023). M4 corresponds to the mutation Leu75Thr and was designed to potentially form a hydrogen bond with the hydroxyl group of the monolignol, this interaction aims to reposition the propyl chain towards the active site of CYPBM3. These two mutants may have limited capability to interact with the monolignols, or/and because of interference with the uptake of electrons.

Comparing monolignol performance, 4-PP, and 4-PG showed a faster NADPH depletion rate than 4-PS. In contrast, the empty plasmid (Empty) and the sample without lysate demonstrated negligible NADPH depletion with the substrates, as did the negative control with 70% ethanol. This indicates that NADPH is not unstable in the presence of cell debris and is not being oxidized to $NADP^+$ by other proteins present in the assay, which makes these results more dependable. The use of pure enzymes in this assay is still important to get more reliable results.

The results from the initial NADPH depletion assay may suggest improved catalytic performance in the mutants mentioned above. There are however uncoupling reactions that may occur within the catalytic cycle of CYPs. The interaction between molecular oxygen and the reduced intermediates (FAD and FMN of CPR) can lead to these uncoupling reactions (Ebrecht *et al.,* 2019). This causes a significant challenge in the electron transfer between CPRs and CYPs resulting in the loss of electrons derived from NADPH. In these reactions, the electrons are consumed, and substrate oxidation does not happen. This implies that the method may not be trustworthy. Another crucial factor is the significant variations in protein expression levels, which becomes challenging when comparing between mutants. To address this issue, ImageJ analysis was conducted to normalize NADPH consumption rates.

5.1.2 Indole Assay

In the previous study done by Li *et al.* in 2000, they observed that the triple mutant Phe87Val, Leu188Gln, Ala74Gly incorporated into a single CYPBM3 enzyme were able to hydroxylate indole. However, in this study, it was employed individual mutations (i.e., Ala74Gly) which

could have affected the enzyme's ability to hydroxylate indole to indigo and indirubin and therefore made this assay unsuccessful.

5.1.3 MS Analysis

To determine product formation and be able to confirm NADPH assay results, reactions for all the mutants and monolignols were analyzed by MS.

For the reaction with **4-propyl phenol,** MS analysis showed hydroxylation for all mutants and the wild type, indicating that results from the NADPH assay are in accordance with these results. Formation of acids or aldehydes was not observed.

For **4-propyl guaiacol**, m/z 181 peak (corresponding to hydroxylation) was observed for all the mutants, the wild type, and the negative control (Empty), therefore, further analysis with pure enzyme was necessary to clarify if the actual hydroxylation is happening. Neither formation of acids nor aldehydes was observed.

For **4-propyl syringol,** m/z 211 peak (corresponding to hydroxylation) was negligible for all mutants and wild type, and neither formation of acids nor aldehydes was observed indicating no product formation. The NADPH depletion assay showed an overall high NADPH consumption rate with most of the mutants and wild type. These MS results are therefore not in accordance with the NADPH depletion results, indicating that the NADPH consumption rates observed are a result of uncoupling reactions.

This concludes that the NADPH assay with cell lysate is not reliable whereas cell debris can interfere with the enzyme activity. Therefore, further analysis with pure enzyme is necessary to confirm the MS results.

5.1.4 Expression Quantification with ImageJ

By employing the software ImageJ, the fold change in NADPH rates for each mutant compared to the wild type was determined. ImageJ allows the estimation of CYPBM3 concentration in the cell lysate through the utilization of the SDS-PAGE gel image. NADPH ratios are normalized with the protein concentration, and then in percentage (fold change) with respect to the CYPBM3 wild type.

M9 and M10 showed the highest NADPH consumption rates in the initial screening with cell lysate, but after protein normalization, these mutants showed low rates. From the graph presenting band intensities, M9 and M10 had some of the strongest bands (Figure 4.7). This

indicates that the highest rations observed in the NAPDH assay are probably linked to the high protein levels rather than being a result of better performance by these two candidates.

The three mutants with the highest fold change with respect to the wild type (FC-WT) for all the substrates were M1, M3, and M7. The fold change values for these three mutants with each substrate are presented in Figure 4.8, Figure 4.9, Figure 4.10, and Figure 4.11. However, NADPH depletion ratios for M3 were almost insignificant, indicating that the normalization of the protein concentration could lead to misinterpretation of the results. For that, this mutant was not preferable to use in further analysis.

It is important to notice that when normalizing NADPH ratios based on protein concentration from the gel image, there could be significant deviations in the results. These deviations may arise from the lack of sample homogeneity, variations in the volume loaded in the gel among mutants, and the saturation threshold of pixels in the gel image. To ensure more reliable results, the best option would be to compare all the mutants after purification. This allows more accurate quantification of each mutant by measuring the absorbance on the soret band of the heme group.

5.1.5 Chosen Candidates with Respective Mutations

After evaluating the performance of the mutants based on NADPH consumptions rates and protein expression levels, three mutants were selected for further analysis: M1, M5, and M7.

M1 had the highest % FC-WT for all the substrates, except with 4-PP, but M1 showed still the second better performance after M3. Despite low expression levels, M1 performed significant NAPH depletion rates. Therefore, this mutant was chosen for further analysis. M1 corresponds, as mentioned, to the mutation Ala184Phe which affects the active site hydrophobic pocket. The intention behind introducing this mutation was to create a narrower hydrophobic binding pocket. The objective was to facilitate the positioning of the monolignol substrate in closer proximity to the heme group within the active site. This mutation provides bulkier side chains involved in enantio-preference in the F-helix and was designed using CYP199A which is natively active on monolignols (Wolf *et al.*, 2022).

M5 had at least 50% FC-WT for all the monolignols. The expression level was considerable, as well as NADPH depletion rates it was therefore chosen for further analysis. M5 corresponds to the mutation Ala74Gly, which is located within the hydrophobic pocket adjacent to the entrance channel of the heme active site. In previous studies, this specific mutation influenced

the hydrophobic pocket, resulting in the capability to hydroxylate a wide range of substrates (Appel *et al.*, 2001).

The third mutant chosen for further analysis was M7. It had the third highest % FC-WT, after M3 which was discarded due to insignificant NADPH depletion ratios. For M7, despite low expression levels of protein, NADPH depletion rates were significant. Therefore, this mutant was a highly valued candidate chosen for further characterization. M7 corresponds, as mentioned, to the mutation Ala328Leu, which similarly impacts the hydrophobic binding pocket like the previously mentioned mutants. The amino acid substitution at position 328, where the hydrophobic Ala residue is replaced by Leu, is considered a crucial "hotspot" for specificity and selectivity in the CYP enzyme. This is due to its positioning above the heme group, enabling it to exert influence over the substrate's access to the heme active site. The mutation affects the substrate's accessibility from the opposite side of the heme access channel (Klaus *et al.*, 2019).

As observed in previous studies, and mentioned above, all three chosen candidates have shown to have a big influence on the hydrophobic binding pocket near the heme active site. For that, we considered the selection of the three mutants to be a suitable option for conducting further characterization.

5.2 Characterization of Wild Type and Mutants

5.2.1 NADPH Depletion Assay

NADPH assay was repeated with the three selected pure mutants (M1, M5, and M7) in order to obtain more reliable results with known enzyme concentrations, as well as avoid interferences from cell debris.

Pure CYPBM3 wild type showed the highest NADPH consumption rate with all the monolignols in this assay. It does not mean that the wild type is showing a better performance than the mutants since it could be the result of uncoupling electrons. The results for the wild type were different when using cell lysate in the initial NADPH depletion assay, suggesting that cell debris is interfering in the assay.

Regarding the mutants, M1 showed the lowest NADPH consumption rates with 4-PP and 4-PS. M5 showed the highest NADPH consumption rates with the three monolignols. M5 corresponds

to the mutation Ala74Gly, and the high rates may correlate with the studies performed before where this mutant was capable of hydroxylating a broad spectrum of substrates. M7 showed the highest NADPH consumption rate for palmitic acid, exceeding CYPBM3wt, which can be the result of the uncoupling of electrons.

Despite the wild type showing the highest NADPH consumption rate with all the monolignols in this assay, it cannot be concluded that this enzyme has a better performance than the mutants. It can neither be concluded that any of the mutants were better than the others in correlation to substrate-enzyme binding. Product quantification and LC-MS analysis are required to determine the performance value of these enzymes.

5.2.2 Binding Assay

To verify if the activity ascertained from the NADPH assays and MS analysis was related to substrates binding to the active heme site of the enzyme, a binding assay was performed. In this assay, several concentrations of the monolignols were added to each mutant with the aspiration of observing a peak shift. Additionally, the aim was to determine minimum monolignol concentration needed for the shift to occur.

4-propyl phenol

For this monolignol, the shift in absorbance peak was only observed for the wild type. This may suggest that the other mutants had undergone conformational changes, as well as changes in the active site, which may have decreased their binding affinity with 4-PP. When utilizing pure enzyme in the NADPH depletion assay, the wild type had a higher activity with 4-PP than the other mutants, as well as the observation of hydroxylation of CYPBM3wt in the initial MS analysis. This may imply that there is a relationship between activity and binding, and this suggests that the substrate's affinity to the CYPBM3 may correlate with higher rates.

An apparent shift was not detectable for the mutants, however, NADPH depletion at a low level was observed. Hence, the mutants having lower NADPH consumption rates may have a lower or not detectable binding affinity to the substrate.

4-propyl guaiacol

For 4-PG, the wild type and M5 showed a binding shift. The shift for CYPBM3wt happened at 714 µM, while for M5 it happened at 938 µM which means that a higher concentration of 4-PG for M5 was needed in the binding assay than for the wild type. In the NADPH depletion assay with pure enzyme, M5 had a lower consumption rate than the wild type. On the contrary, M5

had a higher consumption rate than the other mutants in that NADPH depletion assay. The activity observed was still lower than the rates shown with 4-PP, and this may suggest that M5 binds better to 4-PG, but the low activity may imply that the binding is non-productive.

As the mutation in M5 affects the hydrophobic binding pocket (Ala74Gly) and creates a bigger space for the substrate to bind. This may suggest that this mutation has a bigger impact on a bulkier substrate, such as 4-PG. In the study by Appel *et al*. in 2001 a mutant with the Ala74Gly mutation was able to hydroxylate a bulky hydrophobic substrate (indole). This may imply that binding of 4-PG is favored in the larger active site due to fewer steric clashes.

4-propyl syringol

For 4-PS, M5 and wild type also showed a shift. Here the differences in concentration needed were higher than for 4-PG. M5 showed a slight shift at 484 µM, but the full shift was observed at 938 µM, while for the wild type, the full shift happened immediately with the lowest monolignol concentration added (246 µM). This indicates that the wild type has greater affinity for 4-PS compared to M5.

This assay shows a trend where binding is present only for M5 among the mutants. As discussed for 4-PG, this may correlate with the bulkier structure of 4-PS. Pure CYPBM3wt had the highest NADPH consumption rate of all the enzymes with 4-PS, while M5 had the highest NADPH consumption rate of the three mutants with this monolignol. M7 had a close to similar NADPH consumption rate compared to M5 with pure enzyme. Therefore, it is difficult to correlate the activity observed in the NADPH depletion assay to the actual binding of substrate to the heme group. Both WT and M5 show binding affinity to 4-PS. Residue 74 in the wild type is occupied by a small and hydrophobic alanine residue, while M5 contains a small, hydrophobic glycine residue. This may suggest that small hydrophobic amino acids have a higher affinity binding to this substrate due to increased space in the active site. M1 (Ala184Phe) and M7 (Ala328Leu) have bulkier amino acids introduced, and this may have an impact on steric hindrance. For M1, the entrance channel may have become too narrow due to the bulky Phe-residue, and for M7 the volume of the hydrophobic binding pocket has decreased due to a bulkier Leu-residue.

Palmitic acid

For palmitic acid, it can be expected that there is a peak shift for the CYPBM3wt since it is the native substrate. For M1 the shift was observed at 484 µM, for M5 it was observed at 246 µM and for the wild type the shift started at 484 µM but was fully saturated at 1364 µM. This

suggests that M5 has improved affinity for the substrate since M5 needed the lowest substrate concentration for binding. The shift for M5 and WT was better and more observable than for M1. All these mutations affect the hydrophobic binding pocket close to the heme group, and this should affect the binding of the substrate to the active site.

An important observation made was that M7 did not bind with palmitic acid since no shift was observed. This mutant had the highest NADPH consumption with palmitic acid, however since no binding shift is observed this may be due to reaction uncoupling. This suggests that the mutation (Ala328Leu) may cause steric hindrance, decreasing its affinity to bind with the native substrate, or resulting in non-productive binding.

In conclusion, CYPBM3wt bound with all substrates. This correlates with results observed on NADPH assay and also with MS results (discussed in next section 5.2.3) for 4-PP and 4-PG, however, for 4-PS the results suggest that the binding is non-productive since product formation was not observed on MS results. For M5, binding was observed with all substrates except 4-PP, which again is not linked with NADPH assay, neither MS results where product formation was observed for 4-PP. This may suggest that the conformational changes which the mutants had undergone caused their binding affinity with 4-PP to decrease. M5 showed a higher binding affinity with bulkier substrates, such as 4-PG and 4-PS, which is not in concordance with MS results, where there was product formation for 4-PS. M1 only bound with palmitic acid, while M7 did not bind with any of the substrates. These results are neither in concordance with MS results, since M1and M7 showed product formation for both 4-PP and 4-PG. Ultimately, the results observed in the binding assay are unreliable due to lack of correlation with NADPH assay and MS analysis results (e.g., non-productive binding), and further analysis is necessary to compare binding affinity between the mutants.

5.2.3 MS Analysis

MS analysis with pure enzyme was important to determine the actual presence of product (avoiding possible interferences by cell debris) and be able to identify the isomers by MSMS.

The hydroxylation of **4-propyl phenol** in the ortho- and meta positions of the benzene ring was observed in all three mutants and the wild type, resulting in a mix of 4-propylbenzene-1,3-diol (meta) and 4-propylbenzene-1,2-diol (ortho). Interestingly, distinctive fragmentation patterns were observed among the mutants, suggesting differences in the abundance of each isomer. These variations in isomer production seem to be influenced by the positioning of 4-PP within the active heme site. Notably, the presence of these isomers indicates that the propyl chain of

the monolignol is not situated in the catalytic center. To compare performance between mutants and WT, an LC-MS method is needed, allowing separation of the isomers and subsequent quantification using a calibration curve specific to each isomer.

For **4-propyl guaiacol,** there was also observed a peak at m/z 181 for the three mutants and wild type, which indicates that hydroxylation has occurred. However, the resulting isomers were not identified due to a lack of standards.

For **4-propyl syringol** there was no observed product formation, indicating that hydroxylation did not happen.

In summary of the findings, we noticed that 4-PP undergoes hydroxylation in the benzene ring, whereas no product formation was observed for 4-PS. This lack of product formation could be attributed to steric hindrance caused by the methoxy groups in the benzene ring. This observation suggests that the propyl chains of the monolignols may not be favorably positioned for interaction with the catalytic center. Although the specific positioning of hydroxylation in 4-PG was not determined, it can be inferred that it likely occurs within the benzene ring. In conclusion, product formation was observed for 4-PP and 4-PG, confirming that these two monolignols are interacting with the catalytic center. 4-PS had no product formation, which may indicate that the results of the NADPH depletion assay with pure enzyme and binding assay were due to uncoupling of electrons and non-productive binding, respectively.

6 CONCLUSION & FURTHER PERSPECTIVES

In conclusion, this thesis showed that the utilization of lignin-derived monolignols in CYPBM3 P450 biocatalysis is possible. However, there is difficult to conclude whether the single mutants produced by rational design had an impact on CYPBM3's ability for improved catalysis.

Cell lysate of 11 CYPBM3 mutants and wild type was screened in an initial NADPH depletion assay. This screening aimed to select candidates with enhanced activity to perform oxyfunctionalization of the three chosen monolignols. For that NADPH assay and MS analysis were performed.

After the screening, the three mutants, M1 (Ala184Phe), M5 (Ala74Gly), and M7 (Ala328Leu) were chosen for further characterization with pure enzyme. M5 showed the highest NADPH consumption rate with all three monolignols. A binding assay was also performed. M5 implied binding with the bulkier monolignols (4-PG and 4-PS), while for M1 binding was only observed with palmitic acid.

MS analysis was employed to determine product formation. 4-PP was the only monolignol with identified products with hydroxylation in the meta- and ortho positions of the benzene ring. 4-PG also showed hydroxylation but in unknown positions. 4-PS had no product formation indicating that the NADPH depletion assay and binding assay results were due to uncoupling of electrons and non-productive binding, respectively.

Regarding the mutants, the NADPH depletion assay and binding assay were inconclusive because of a lack of correlation, and this is also the case for the MS analysis. There cannot be drawn any conclusion of which candidate showed a better performance.

Further perspectives of this study are to employ LC-MC for quantification for a better understanding of which candidates that have a better performance. This was a preliminary study to map the performance of mutants with single mutations, and a combination of single mutations in the same CYPBM3 enzyme will be necessary to obtain information on improved activity. Lastly, this study has provided a foundation in the form of guidelines for further research on CYPBM3 P450's biocatalysis of lignin-derived monolignols to achieve target properties and more valuable products in future lignin industry.

7 REFERENCES

Abdel-Hamid, A.M., Solbiati, J.O., & Cann, I.K.O. (2013). Chapter One - Insights into Lignin Degradation and its Potential Industrial Applications. *Advances in Applied Microbiology, Academic Press, 82,* 1-28. https://doi.org/10.1016/B978-0-12-407679-2.00001-6

Argyropoulos, D.S., & Menachem, S. B. (1997). Lignin. *Biotechnology in the Pulp and Paper Industry, Advances in Biochemical Engineering/Biotechnology, 57,* 127-158. https://doi.org/10.1007/BFb0102073

Appel, D., Lutz-Wahl, S., Fischer, P., Schwaneberg, U., & Schmid, R.D. (2001). A P450 BM-3 mutant hydroxylates alkanes, cycloalkanes, arenes and heteroarenes. *Journal of Biotechnology, 88*(2), 167–171. https://doi.org/10.1016/S0168-1656(01)00249-8

Arts, W., Ruijten, D., Van Aelst, K., Trullemans, L., & Sels, B. (2021). Chapter eight- The RCF biorefinery: Building on a chemical platform from lignin. *Advances in Inorganic Chemistry, 77*, 241–297. https://doi.org/10.1016/bs.adioch.2021.02.006

Battistuzzi, G., Bellei, M., Bortolotti, C.A., & Sola, M. (2010). Redox properties of heme peroxidases. *Archives of Biochemistry and Biophysics, 500*(1), 21-36. https://doi.org/10.1016/j.abb.2010.03.002

Behrendorff, J.B.Y.H. (2021). Reductive Cytochrome P450 Reactions and Their Potential Role in Bioremediation. *Frontiers in Microbiology, 12*. https://doi.org/10.3389/fmicb.2021.649273

Biocompare. (n.d.). T7 primers [Online]. Available: https://www.biocompare.com/paragraphs/564970-T7-primers/ [Accessed 22nd of March 2023].

Bio-Rad. (n.d.). Anion Exchange Chromatography [Online]. Available: https://www.bio-rad.com/en-no/applications-technologies/anion-exchange-chromatography?ID=MWHAZ4C4S [Accessed 23rd of March 2023].

Bomon, J., Bal, M., Achar, T.K., Sergeyev, S., Wu, X., Wambacq, B., Lemière, F., Sels, B.F. & Maes, B.U.W. (2021). Efficient demethylation of aromatic methyl ethers with HCl in water. *Green Chemistry, 23*(5), 1995–2009. https://doi.org/10.1039/d0gc04268d

Carmichael, A.B., & Wong, L.L. (2001). Protein engineering of Bacillus megaterium CYP102. *European Journal of Biochemistry, 268*(10), 3117–3125. https://doi.org/10.1046/j.1432-1327.2001.02212.x

del Río, J.C., Rencoret, J., Gutiérrez, A., Elder, T., Kim, H., & Ralph, J. (2020). Lignin Monomers from beyond the Canonical Monolignol Biosynthetic Pathway: Another Brick in the Wall. *ACS Sustainable Chemistry & Engineering*, *8*(13), 4997–5012. https://doi.org/10.1021/acssuschemeng.0c01109

Denisov, I.G., Makris, T.M., Sligar, S.G. & Schlichting, I. (2005). Structure and Chemistry of Cytochrome P450. *Chemical Reviews, 105*(6), 2253–2278. https://doi.org/10.1021/cr0307143

Ebrecht, A.C., van der Bergh, N., Harrison, S.T.L., Smit, M.S., Sewell, B.T., & Opperman, D.J. (2019). Biochemical and structural insights into the cytochrome P450 reductase from Candida tropicalis. *Scientific Reports, 9*(1). https://doi.org/10.1038/s41598-019-56516-6

Ellis, E.S., Hinchen, D.J., Bleem, A., Bu, L., Mallinson, S.J.B., Allen, M.D., Streit, B.R., Machovina, M.M., Doolin, Q.V., Michener, W.E., Johnson, C.W., Knott, B.C., Beckham, G.T., McGeehan, J.E., & DuBois, J.L. (2021). Engineering a Cytochrome P450 for Demethylation of Lignin-Derived Aromatic Aldehydes. *Journal of the American Chemical Society (JACS Au), 1*(3), 252-261. https://doi.org/10.1021/jacsau.0c00103

Eser, B.E., Zhang, Y., Zong, L., & Guo, Z. (2021). Self-sufficient Cytochrome P450s and their potential applications in biotechnology. *Chinese Journal of Chemical Engineering, 30*, 121-135. https://doi.org/10.1016/j.cjche.2020.12.002

Gianfreda, L., Xu, F., & Bollag, J.M. (1999). Laccases: A Useful Group of Oxidoreductive Enzymes. *Bioremediation Journal, 3*(1), 1-26. https://doi.org/10.1080/10889869991219163

Goring, D.A.I. (1977). A Speculative Picture of the Delignification Process. *Cellulose Chemistry and Technology, ACS Symposium Series, 48*, 273-277. https://doi.org/10.1021/bk-1977-0048.ch019

Guan, M., Li, C., Shan, X., Chen, F., Wang, S., Dixon, R.A., Zhao, Q. Dual Mechanisms of Coniferyl Alcohol in Phenylpropanoid Pathway Regulation. *Frontiers in Plant Science, 13*. https://doi.org/10.3389/fpls.2022.896540

Guengerich, F.P. (2018). Mechanisms of Cytochrome P450-Catalyzed Oxidations. *ACS Catalysis, 8*(12), 10964-10976. https://doi.org/10.1021/acscatal.8b03401

Hannemann, F., Bichet, A., Ewen, K.M., & Bernhardt, R. (2006). Cytochrome P450 systems—biological variations of electron transport chains. *Biochimica et Biophysica Acta (BBA) - General Subjects, 1770*(3), 330–344. https://doi.org/10.1016/j.bbagen.2006.07.017

Jeffreys, L.N., Girvan, H.M., McLean, K.J., Munro, A.W., & Laura N. (2018). Chapter Eight - Characterization of Cytochrome P450 Enzymes and Their Applications in Synthetic Biology. *Methods in Enzymology, Academic Press, 608*, 189-261. https://doi.org/10.1016/bs.mie.2018.06.013

Karunarathna, M.S., & Smith, R.C. (2020). Valorization of Lignin as a Sustainable Component of Structural Materials and Composites: Advances from 2011 to 2019. *Sustainability, 12*(2), 734. https://doi.org/10.3390/su12020734

Klaus, T., Seifert, A., Häbe, T., Nestl, B.M., & Hauer, B. (2019). An enzyme cascade synthesis of vanillin. *Catalysts, 9*(3), 252. https://doi.org/10.3390/catal9030252

Kunkel, T.A. (1985). Rapid and efficient site-specific mutagenesis without phenotypic selection. *Proceedings of the National Academy of Sciences, 82*(2), 488–492. https://doi.org/10.1073/pnas.82.2.488

Lamb, D.C., Waterman, M.R., Kelly, S.L., & Guengerich, F.P. (2007). Cytochromes P450 and drug discovery. *Current Opinion in Biotechnology, 18*(6), 504-512. https://doi.org/10.1016/j.copbio.2007.09.010

Lewis, J.C., Bastian, S., Bennett, C.S., Fu, Y., Mitsuda, Y., Chen, M.M., Greenberg, W.A., Wong, C.H., & Arnold, F.H. (2009). Chemoenzymatic elaboration of monosaccharides using engineered cytochrome P450BM3 demethylases. *Proceedings of the National Academy of Sciences, 106*(39), 16550-16555. https://doi.org/10.1073/pnas.0908954106

Li, Q.S., Ogawa, J., Schmid, R.D., & Shimizu, S. (2001). Residue size at position 87 of cytochrome P450 BM-3 determines its stereoselectivity in propylbenzene and 3-chlorostyrene oxidation. *FEBS Letters, 508*(2), 249–252. https://doi.org/10.1016/S0014-5793(01)03074-5

Li, Q.S., Schwaneberg, U., Fischer, P., & Schmid, R.D. (2000). Directed evolution of the fatty-acid hydroxylase P450BM-3 into an indole-hydroxylating catalyst. *Chemistry – A European Journal, 6*(9), 1531-153. https://doi.org/10.1002/(sici)1521-3765(20000502)6:9<1531::aid-chem1531>3.3.co;2-4

McSweeney, E. (2021). All Charged Up: The Basics of Ion-Exchange Chromatography, Analytical Chemistry and Chromatography Techniques [Online]. Available: https://bitesizebio.com/31744/basics-ion-exchange-chromatography/ [Accessed 24th of March 2023].

Moody, P.C.E., & Raven, E.L. (2018). The Nature and Reactivity of Ferryl Heme in Compounds I and II. *Accounts of Chemical Research, 51*(2), 427–435. https://doi.org/10.1021/acs.accounts.7b00463

Munday, S.D., Dezvarei, S., Lau, I.C.K., & Bell S.G. (2017). Examination of Selectivity in the Oxidation of ortho- and meta-Disubstituted Benzenes by CYP102A1 (P450 Bm3) Variants. *ChemCatChem, 9*(13), 2512–2522. https://doi.org/10.1002/cctc.201700116

Munro, A.W., Leys, D.G., McLean, K.J., Marshall, K.R., Ost, T.W.B., Daff, S., Miles, C.S., Chapman, S.K., Lysek, D.A., Moser, C.C., Page, C.C., & Dutton, P.L. (2002). P450 BM3: the very model of a modern flavocytochrome. *Trends in Biochemical Sciences, 27*(5), 250-257. https://doi.org/10.1016/S0968-0004(02)02086-8

Neufeld, K., Marienhagen, J., Schwaneberg, U., & Pietruszka, J. (2013). Benzylic hydroxylation of aromatic compounds by P450 BM3. *Green Chemistry, 15*(9), 2408–2421. https://doi.org/10.1039/c3gc40838h

OpenWetWare. (n.d.). Protein Quantification Using ImageJ [Online]. Available: https://openwetware.org/wiki/Protein_Quantification_Using_ImageJ [Accessed 6th of February 2023].

PCR Biosystems. (n.d.). Long Range PCR. [Online]. Available: https://pcrbio.com/row/applications/pcr/long-range-pcr/ [Accessed 21st of April 2023].

Pravda, L., Berka, K., Svobodová Vařeková, R.S., Sehnal, D., Banáš, P., Laskowski, R.A., Koča, J., & Otyepka, M. (2014). Anatomy of enzyme channels. *BMC Bioinformatics, 15*(1), 379. https://doi.org/10.1186/s12859-014-0379-x

Qian, E.W. (2014). Chapter 7 - Pretreatment and Saccharification of Lignocellulosic Biomass. *Research Approaches to Sustainable Biomass Systems, Academic Press,* 181-204. https://doi.org/10.1016/B978-0-12-404609-2.00007-6

Qi, D., & Scholthof, K.B.G. (2008). A one-step PCR-based method for rapid and efficient site-directed fragment deletion, insertion, and substitution mutagenesis. *Journal of Virological Methods, 149*(1), 85-90. https://doi.org/10.1016/j.jviromet.2008.01.002

Renders, T., Van den Bossche, G., Vangeel, T., Van Aelst, K., & Sels, B. (2019). Reductive catalytic fractionation: state of the art of the lignin-first biorefinery. *Current Opinion in Biotechnology, 56*, 193-201. https://doi.org/10.1016/j.copbio.2018.12.005

Rinaldi, R., Jastrzebski, R., Clough, M.T., Ralph, J., Kennema, M., Bruijnincx, P.C.A., & Weckhuysen, B.M. (2016). Paving the Way for Lignin Valorisation: Recent Advances in Bioengineering, Biorefining and Catalysis. *Angewandte Chemie International Edition, 55*(29), 8164–8215. https://doi.org/10.1002/anie.201510351

Schröder, G.C., Smit, M.S., & Opperman, D.J. (2023). Harnessing heme chemistry: Recent advances in the biocatalytic applications of cytochrome P450 monooxgenases. *Current Opinion in Green and Sustainable Chemistry, 39*. https://doi.org/10.1016/j.cogsc.2022.100734

Seifert, A., Antonovici, M., Hauer, B., & Pleiss, J. (2011). An Efficient Route to Selective Bio-oxidation Catalysts: an Iterative Approach Comprising Modeling, Diversification, and Screening, Based on CYP102A1. *ChemBioChem, 12*(9), 1346–1351. https://doi.org/10.1002/cbic.201100067

Sevrioukova, I.F., Li, H., Zhang, H., Peterson, J.A., & Poulos, T. L. (1999). Structure of a cytochrome P450–redox partner electron-transfer complex. *Proceedings of the National Academy of Sciences, 96*(5), 1863-1868. https://doi.org/10.1073/pnas.96.5.1863

Sun, J., Li, H., Xiao, L.P., Guo, X., Fang, Y., Sun, R.C., & Song, G. (2019). Fragmentation of Woody Lignocellulose into Primary Monolignols and their Derivatives. *ACS Sustainable Chemistry & Engineering, 7*(5), 4666–4674. https://.doi.org/10.1021/acssuschemeng.8b04032

Takahama, U., Oniki, T., Shimokawa, H. (1996). A Possible Mechanism for the Oxidation of Sinapyl Alcohol by Peroxidase-Dependent Reactions in the Apoplast: Enhancement of the Oxidation by Hydroxycinnamic Acids and Components of the Apoplast. *Plant and Cell Physiology, 37*(4), 499–504. https://doi.org/10.1093/oxfordjournals.pcp.a028972

Thermo Fisher Scientific. (n.d.). Protocols for Oligonucleotides [Online]. Available: https://www.thermofisher.com/no/en/home/life-science/oligonucleotides-primers-probes-genes/custom-dna-oligos/oligo-technical-resources/oligo-protocols.html#2 [Accessed 14th of March 2023].

Tsotsou, G.E., Sideri, A., Goyal, A., Di Nardo, G., & Gilardi, G. (2012). Identification of Mutant Asp251Gly/Gln307His of Cytochrome P450 BM3 for the Generation of Metabolites of Diclofenac, Ibuprofen and Tolbutamide. *Chemistry - A European Journal, 18*(12), 3582–3588. https://doi.org/10.1002/chem.201102470

Urlacher, V.B., & Girhard, M. (2012). Cytochrome P450 monooxygenases: an update on perspectives for synthetic application. *Trends in Biotechnology, 30*(1), 26–36. https://doi.org/10.1016/j.tibtech.2011.06.012

Vanholme, R., Demedts, B., Morreel, K., Ralph, J., & Boerjan, W. (2010). Lignin biosynthesis and structure. *Plant Physiology, 153*(3), 895–905. https://doi.org/10.1104/pp.110.155119

Wang, Y., Xue, P., Cao, M., Yu, T., Lane, S.T. & Zhao, H. (2021). Directed Evolution: Methodologies and Applications. *Chemical Reviews, 121*(20), 12384–12444. https://doi.org/10.1021/acs.chemrev.1c00260

Whitehouse, C.J.C., Bell, S.G., Tufton, H.G., Kenny, R.J.P., Ogilvie L.C.I., & Wong, L. (2008). Evolved CYP102A1 ($P450_{BM3}$) variants oxidise a range of non-natural substrates and offer new selectivity options. *Chemical Communications*, (8), 966–968. https://doi.org/10.1039/B718124H

Wolf, M.E., Hinchen, D.J., DuBois, J.L., McGeehan, J.E., & Eltis, L.D. (2022). Cytochromes P450 in the biocatalytic valorization of lignin. *Current Opinion in Biotechnology, 73*, 43-50. https://doi.org/10.1016/j.copbio.2021.06.022

YouTube. (2014). Using ImageJ to quantify protein bands on a PAGE gel. Available: https://www.youtube.com/watch?v=JlR5v-DsTds&ab_channel=MCBiology [Accessed 6th of February 2023]

Zabel, R.A., & Morrell, J.J. (2020). Chapter Eight - Chemical changes in wood caused by decay fungi. *Wood Microbiology (Second Edition), Academic Press*, 215-244. https://doi.org/10.1016/B978-0-12-819465-2.00008-5

Norges miljø- og biovitenskapelige universitet
Noregs miljø- og biovitskapelege universitet
Norwegian University of Life Sciences

Postboks 5003
NO-1432 Ås
Norway